KYAMBOGO UNIVERSITY

GRADUATE SCHOOL

DEPARTMENT OF MECHANICAL AND PRODUCTION ENGINEERING

PERFORMANCE ANALYSIS OF THE TOP ROLLERS IN A SUGAR MILL USING FINITE ELEMENT METHOD

KASAMBULA VICENT

18/U/GMSE/19355/PD

SUPERVISORS:

Dr. Catherine Wandera

Dr. Titus Bitek Watmon

A Dissertation submitted to the Graduate School in fulfilment of the Requirements for the Award of the degree of Master of Science in Advanced Manufacturing Systems Engineering of Kyambogo University

AUGUST 2022

DECLARATION

I, Kasambula Vicent, a student of the Master of Science in Advanced Manufacturing Systems Engineering do declare that this work on "Performance Analysis of Top Rollers in a Sugar Mill" is my original work and has never been submitted for any degree award in any other university or higher education institution and is not subject to plagiarism.

Name: Kasambula Vicent

Registration No.: 18/U/GMSE/19355/PD

Sign: ..... Date: 09/09/2022.....

APPROVAL

This is to certify that this Research work titled "Performance Analysis of Top Rollers in a Sugar Mill" was carried out by KASAMBULA VICENT with Registration number 18/U/GMSE/19355/PD under our supervision.

First Supervisor

Sign: ..... Date: 12TH SEPTEMBER 2022

Dr. Catherine Wandera

Second Supervisor

Sign: ..... Date: 15/09/22

Dr. Titus Bitek Watmon

DEDICATION

To my daddy Mr. Ssimbwa John Augustine, mummy Mrs. Nabankema Edith and my siblings Ssimbwa Paul, Wamala Joseph and Kaaya Jacob.

ACKNOWLEDGMENT

I would like to take this opportunity to express my sincere gratitude to my supervisors Dr. Catherine Wandera and Dr. Titus Bitek Watmon for their excellent guidance, invaluable support and considerable encouragement throughout my study

I am also grateful to Mr. Vincent Obbo, Head of Research and Training department, SCOUL and Mr. Brian Kazimoto, Human Resource Sugar and Allied industries for granting me access to the facility especially in the COVID period.

Thanks to my colleague, Mr. Peter Obeli of Kyambogo University Department of Mechanical & Production Engineering and my former works supervisor Mr. Peter Manyala with whom, I worked with in the investigation of insurance related mechanical breakdowns. I trust that the findings in this research work will lay a foundation for future risk improvement relating top roller breakdowns in sugar mills.

Finally, I earnestly congratulate my father Mr. Ssimbwa John Augustine, mummy Mrs. Ssimbwa Nabankema Edith for their continued financial support and encouragement and my siblings Ssimbwa Paul, Wamala Joseph and Kaaya Jacob for bearing with me when I had to keep myself in the library working on this study. MAY God bless you all!

All in all Thanks be to God for the wisdom, life and protection granted to me in the entire period of the programme and research.

ABSTRACT

Sugar milling is the process of extracting juice from crushed sugarcane fibres for production of sugar crystals. The three-shaft sugar mill set consists of the top roller and two bottom rollers to crush the sugarcane. The top roller shaft is the main crushing shaft of the sugar mill which is directly attached to the prime mover so it rotates and is loaded. Therefore, the top roller shaft in the mill set is subjected to more torsion and bending stresses. This study examined the mechanical performance of four top rollers under dynamic loading in four mill sets 1-4 of the sugar plant. To achieve this, firstly, the forces on the top rollers were determined and stresses on the top rollers were analysed using the maximum shear stress method to determine the unsafe loaded zones of the top rollers. Secondly, camera photos were obtained for visual inspection, detailed micrographs of the failed surfaces were obtained for microstructural examination; and the chemical composition and hardness of the failed components were determined and compared with known material standards for the top roller bare shafts, roller shells and couplings. Thirdly, geometrical models of the top roller were generated using solid works and transferred to ANSYS workbench which was used to analyse the maximum displacement, fatigue sensitivity, safety factor and equivalent alternating stress for the subjected dynamic loading in sugar milling; monotonic and cyclic parameters of forged steel were used for the bare shaft and parameters of ductile cast iron were used for the roller shell. The results of the shear stress analysis, microstructural characterization, and chemical composition and hardness of the failed top rollers showed that material non-conformance contributed to shaft failures. Maximum displacement, fatigue sensitivity and equivalent alternating stress showed that failure occurs at shoulders, keyway and shaft square ends; and top rollers in mill sets 3 and 4 are more susceptible to failure than top rollers in mill sets 1 and 2. The study evaluated the fatigue performance of top rollers in sugar mills.

Keywords: Top Roller Shafts, Dynamic loading, Shear Stress, Alternating Stress, Mechanical Performance.

TABLE OF CONTENT

LIST OF TABLES

LIST OF FIGURES

ABBREVIATIONS/ ACRONYMS

AGG	-	Ageing at 923K for 2 hours after SHTWC
IS	-	Indian Standards
MTBF	-	Mean Time Between Failure
MTTF	-	Mean Time To Failure
PCD	-	Pitch Centre Diameter
SHTFC	-	Furnace Cooling after Solution Heat Treatment
SHTWC	-	Solution Heat treatment at 1323K for 1 hour and Water Cooled
UDL	-	Uniformly Distributed Load
AFFDL	-	Air Force Flight Dynamics Laboratory
AM1	-	Macrostructure for specimen 1 from Sugar miller A,
AMi1	-	Microstructure for speciment1 from Sugar miller A,
AC1	-	Chemical composition for specimen 1 from Sugar miller A,
AH1	-	Hardness of specimen 1 from Sugar miller A,
AM2	-	Macrostructure for specimen 2 from Sugar miller A,
AMi2	-	Microstructure for specimen 2 from Sugar miller A,
AC2	-	Chemical composition for specimen 2 from Sugar miller A,
AH2	-	Hardness of specimen 2 from Sugar miller A,
AM3	-	Macrostructure for specimen 3 from Sugar miller A,
AMi3	-	Microstructure for speciment3 from Sugar miller A,
AC3	-	Chemical composition for specimen 3 from Sugar miller A,
AH3	-	Hardness of specimen 3 from Sugar miller A,
BM4	-	Macrostructure for specimen 4 from Sugar miller B,
BMi4	-	Microstructure for speciment4 from Sugar miller B,
BC4	-	Chemical composition for specimen 4 from Sugar miller B,
BH4	-	Hardness of specimen 4 from Sugar miller B.

CHAPTER ONE

INTRODUCTION

1.0 Introduction

This chapter introduces the background to the sugar mills and the current research done in regards to the performance and associated top roller failure, lays a problem statement based on Ugandan based mills, states the general and specific objectives, research questions, develops a conceptual framework, significance and justification of the research, research scope and limitations.

1.1 Background to the study

Sugar millers have contributed to Uganda's economic growth through the production of sugar consumed in the country. There are over 11 sugar milling companies in various parts of the country employing both skilled and unskilled/semi-skilled workers (Ministry of Trade, Tourism & Industry [MTTI], 2010). Sugar processing begins with harvesting sugarcanes and transporting them to the sugar mill for chopping into sugarcane fibres which are crushed between rollers to extract sugarcane juice (Anderson and Loughran, 1998). Rollers are laid out in a three or four-shaft configuration mill set comprising the discharge, feed and top rollers; attached to the top roller is the torque driving system by coupling through the tail bars and box couplings or hydraulic drives as prime movers (Anderson and Loughran, 1998).

The sugarcane crushing rollers are subject to loads during the milling process designed to operate for a specified period without failure (Bloch, 1998). Shaft failures originate from faulty designs, stress concentration points on shafts around corners, fillets and holes that raise localized stress at such regions, residual stresses and surface defects due to inclusions and centreline shrinkages (Reid, 2009). Roller shaft failure could result from operator error, inadequate maintenance of the roller shafts, worn-out shells, faulty bearing and inadequate lubrication (Cornelius and Jean, 2018). Roller shaft failures can also be due to corrosion, wear, fatigue and creep failures whilst in operation (Neville, 2012).

Marin (2005) investigated the stress distribution on a top roller shaft in a sugar mill and reported that stress was more in the drive shaft shoulder reflected by 30% cracks in that region. Casanova (2010) found out that a simple geometrical change at the change of section zone significantly varies the shaft reliability; Implying that there is a significant stress concentration at change of section zones. According to Giordani *et al.* (2004), non-metallic inclusions reflected by geometric discontinuities increases with the early fatigue crack growth for a stainless steel. Babakr *et al.* (2009) reported that a combination of small fillet radius and welding defects accelerate fatigue failures in shafts; Welding defects at the keyways weaken the shaft causing it to fail early due to fatigue. Marin (2005) found out that the welded shaft reliability reduced to about 63% due to inadequate stress-relieving process at the stress concentration points. Khangar and Jaju (2012) reported improper maintenance as a cause of shaft failure and recommended proper stress relieving of shafts during welding repair works to prevent unexpected shaft failure. Reid (2009) reported that improving the mill design, the tail bar coupling improvement and limiting the hydraulic loading can reduce shaft failures. Padhal and Meshram (2013) agreed with Reid's recommendation of redesigning the shaft with

modified material and diameter to eliminate unexpected shaft failure. Reid (2009) reported that most shaft failures originate from the surface. The fracture surface condition indicates whether shaft failure is due to overload or fatigue (Neville, 2012). Marudachalam *et al.* (2011) reported torsional-bending fatigue as the cause of shaft failure. Pérez-Mora *et al*. (2015) found out that the pit size on the shaft surface is related to corrosion-fatigue stress and are related in that crack initiation at very low-stress amplitudes correspond to the interaction between corrosion pitting and fatigue damage. Ebara (2010) reported that cracks initiated at the corroded pits of the welded joint of stainless steel subjected to fatigue loading.

Suhas *et al*. (2016) reviewed the influence of surface cracks on shafts and reported a relationship between the crack depth and a known natural frequency. Puskar and Varkoly (1986) reported that the specimen width increased with the crack growth time. The fatigue-based crack growth rate was proportional to temperature rise for the range between 250℃ and 500℃ except CSN 415313 steel which showed no significant temperature effect on its crack growth rate (Puskar and Varkoly, 1986). Fatigue tests in a sugar cane juice environment for quenched and tempered SAE 1045 steel showed better fatigue strength for a temperature of 300℃ than 600℃ but lower in sugarcane juice than air environment (Muñoz Cubillos *et al.*, 2016). Evins (2004) corroborates the findings of May *et al*. (2013) that corrosion fatigue strength reduces more in an aqueous environment than in air. Heavily loaded roller shafts took less time to develop maximum allowable crack size but can be retained in a running mill for low positions at a specific crack size and crack growth rate (Arzola *et al*., 2005). Khot & Mandale (2015) analysed the static structural performance of a three-roller sugar mill and reported that all the shafts were safe under the given loading generating nearly the same shear

stress by analytical and finite element method. Analysis of the dynamic structural performance of the top roller has not been found out which is the basis of this study.

Focusing on the transient-structural mechanical performance of the top roller from mill set 1 through 4, the present study is intended to determine the stresses and forces subject to the top rollers in the four mills, characterize the structural properties of the failed components with the known material standards and use of ANSYS finite element modeller to examine the structural transient stress distribution on the top roller.

1.2 Statement of the Problem

Roller shafts used in sugarcane mills to crush the fiberized sugarcane are composed of a set of three rollers; namely the top roller, feed roller and discharge roller that extract the juice in either 4 or 6 stages. In the three-roller mill set, driving power from the prime mover is transmitted to the top roller through a gear reduction system and a coupling. The top roller moves in the anticlockwise direction which forces the other two roller shafts (the feed and discharge rollers) to move in the clockwise direction to enable the sugarcane crushing action. The crushed sugarcane fibres are transferred from the feed roller to the discharge roller crushing points with the help of a trash plate. Therefore, the top roller is more subject to torsion and bending stresses than the feed and discharge rollers in the mill set. Failures of the square couplings and bare shafts at different sugar mills in Uganda have caused frequent mill complete stoppage to replace the entire top roller. This leads to loss of sugar production time, high sugar production and plant maintenance overheads. Literature has shown that the low sugar production in Uganda is mainly due to technical inefficiencies and failures causing mill

shutdowns. Subsequently, sugar millers in Uganda often increase the final sugar price level compared to the fair sugar prices on imported sugar. No information is available on top roller failures in Ugandan sugar mills but between 5 to 10 breakdowns associated with top rollers occur annually (MTTI, 2010). This study focused on establishing the mechanical performance of the top rollers in 4 mills under structural transient stress using the finite element method.

1.3 Objectives of the Study

1.3.2 General Objective

To establish the mechanical performance of the top roller in Uganda based sugar mills.

1.3.2 Specific Objectives

The specific objectives in this study were to:

(i) Determine the loading and stresses on the top rollers in the sugar mill as performance indicators.

(ii) Characterize the structural properties of the failed top roller components.

(iii) Determine the structural transient stress distribution at the different sections of the top roller.

1.4 Research Hypotheses

The research hypotheses guiding this study were:

(i) The shear stress of the top shaft used in Uganda-based sugar mills lies within the safe value of maximum shear stress for the shaft material.

(ii) The failed top roller components do not conform to known macrostructure, microstructure, chemical composition and hardness for typical shafts used in sugar mills.

(iii) Some sections of the Top roller are more stressed than others during the sugarcane crushing process.

1.5 Motivation in the Study

In the 2016 verification mission report, Kakira Sugar Works, the leading sugar mill in Uganda was reported to be operating at 50% capacity due to the closure of one production line for maintenance reasons (Ministry of Trade, industry and Cooperatives [MTIC], 2016). The sugar mill shutdowns bring about loss of production time before the mill is restored into operation. Most of the sugar mill breakdowns are associated with the top roller which drives the other rollers in a mill set. This research employs the Finite Element Method in analysing the performance of the top rollers in four mill sets for a three-roller crushing configuration under dynamic loading.

1.6 Justification of the study

Top roller related breakdowns subject sugar millers to costs in replacing the failed top rollers and also the associated sugar production losses. Secondly, mill stoppage causes sugarcane loaded on trucks in wait for processing to lose weight as the whole plant must come to a standstill paying less to the sugarcane farmers when weighed again before milling. Therefore, there is need to ensure unstopped mill operation to minimize these losses and heavy investments in unprecedented insurance covers. Furthermore, the government of Uganda

projects an increase in sugar demand which requires regular sugar mill uptime to ensure continuous sugar production to enhance competitiveness, public-private partnership and social transformation in the country (MTTI, 2010).

1.7 Contribution of the study

This study provides knowledge on the service performance of the top roller shaft of a sugar mill under dynamic loading. This information will be useful in improving the maintenance of the top roller shaft so as to increase the shaft service life resulting in increased shaft availability in production and reduced instances of downtime. The overall outcome is the improved productivity of the sugar processing industries, reduced operating costs in maintenance of the sugar mill, and increased sugar production in the country.

1.8 Conceptual Framework

In the analysis of the top rollers in a sugar mill, the conceptual framework presented in figure 1.1 describes the attribution of the service life of the top roller (dependent variable) to the shaft loading, stress concentration areas and structural properties (dependent variable). It also indicates the shaft maintainability (intervening variable); and temperature and corrosion as moderating variables that laid a basis for the study.

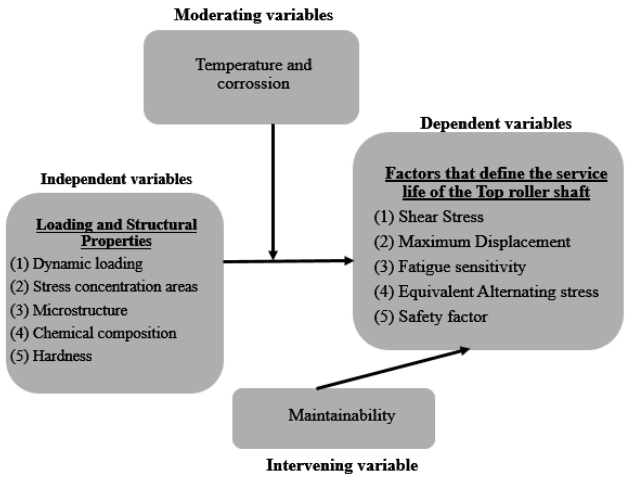

Figure 1.1: Research Conceptual framework

1.9 **Scope**

This study involved an investigation of the performance of the top roller shaft of a sugar mill shaft assembly using three specific objectives. The study on top rollers was done in four sugar mills in 3 sugar plants in the area of Lugazi, Kinyara and Kaliro with the same milling sequence in 6 top Ugandan based sugar mills. Visits to these sugar mills were in a space of three months following acceptance that is October to December 2020. Details of loading and mill speeds were read from the mill control panels in the control rooms, samples of the failed roller components were obtained, tested and analysed for microstructure from the Makerere University Material laboratory, chemical composition was tested from the UNBS materials laboratories and hardness from the Uganda Industrial Research Institute materials laboratory. Using the monotonic and cyclic loading of the top roller shaft from published research, the structural-transient examination of the stress distribution on the 4 top roller shafts was determined using ANSYS workbench with consideration of the mill speeds and the loading situation of top roller shaft used in the six (6) sugar mills. The sugar mills involved in this study could not be disclosed due to secrecy of information.

1.9.1 Limitation

This study regarding the mechanical performance of the top roller is based on limited information regarding the frequency of shaft failure and publications on shaft failures.

CHAPTER TWO

LITERATURE REVIEW

2.0 Introduction

This chapter highlights the relevant literature to close the knowledge gap relating to macrostructure, microstructure, hardness influence on shaft performance in sugar mills, stress theories and force analysis methods on the shaft are also reviewed and lastly the use of finite element method in shaft performance analysis.

2.1 The Sugarcane milling system

The harvested sugarcanes are transported to the sugar factories in a billet form (Anderson and Loughran, 1998). The raw sugarcanes are prepared for processing via high-speed hammer mills which reduce the canes to fibres (Anderson and Loughran, 1998). The sugarcane fibres (bagasse) are fed into a series of milling units which may either be four or six in number to separate juice from the bagasse (Hugot, 2014). Juice and hot water imbibition are used alongside crushing sugarcane fibres to extract about 98% of the juice (Anderson and Loughran, 1998; Hugot, 2014). Each mill set consists of three rollers arranged in a triangular form which are the top roller, feed roller and discharge rollers and other mills consist of an underfeed to improve the feeding of bagasse between the top roller and the feed roller (Khot and Mandale, 2015). The crushing rollers made of grooved shells, bare shaft with a square end on the drive end (Anderson and Loughran, 1998). The roller top roller shells are fitted in a housing held in position by roller journal bearings which move with in the housing gap which is under the pressure by the hydraulic rams (Hugot, 2014). The hydraulic rams are mounted on the journal

bearing of the top roller with one at the drive end and the other at the pintle end (Hugot, 2014). The milling process in a mill set is shown in the figure 2.2.

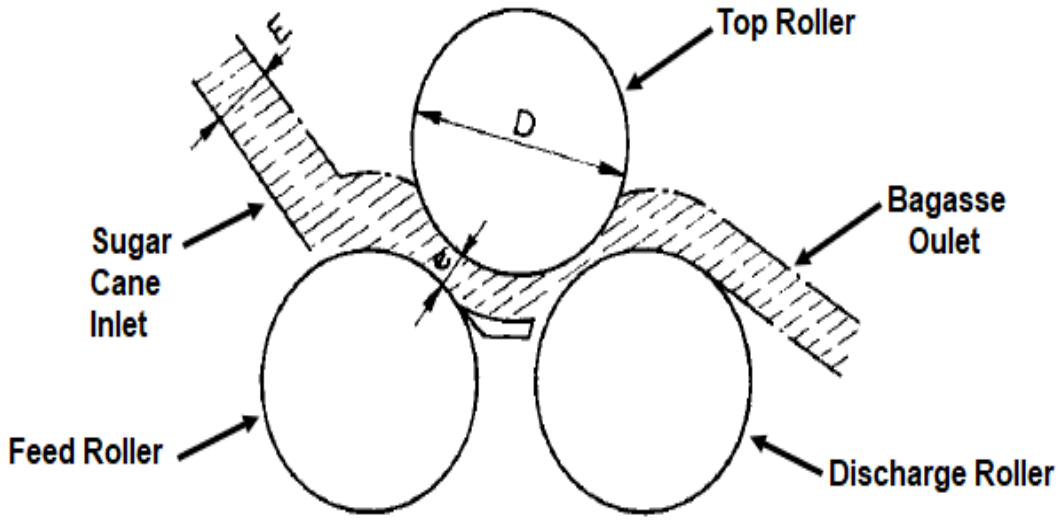

Figure 2.1: Action of Bagasse crushing in a mill set (Anderson and Loughran, 1998)

2.2 Features and Standards of Top Rollers used in Sugar Mills

2.2.1 Features of Top Rollers

The top roller used in sugar mills consists of a forged steel shaft on which a cast-iron shell is fitted with features including the roller journals on which the bearings are fitted on both ends of the shell seats, pintle end having a key way for sprocket/ gear fitting, square end on which pinions and couplings are fitted, flange fixing holes for the fitting of the flanges on either side of the shell, mild steel keeper and guard rings to safeguard shell movements during the sugar crushing operation (Bureau of Indian Standards, 1990).

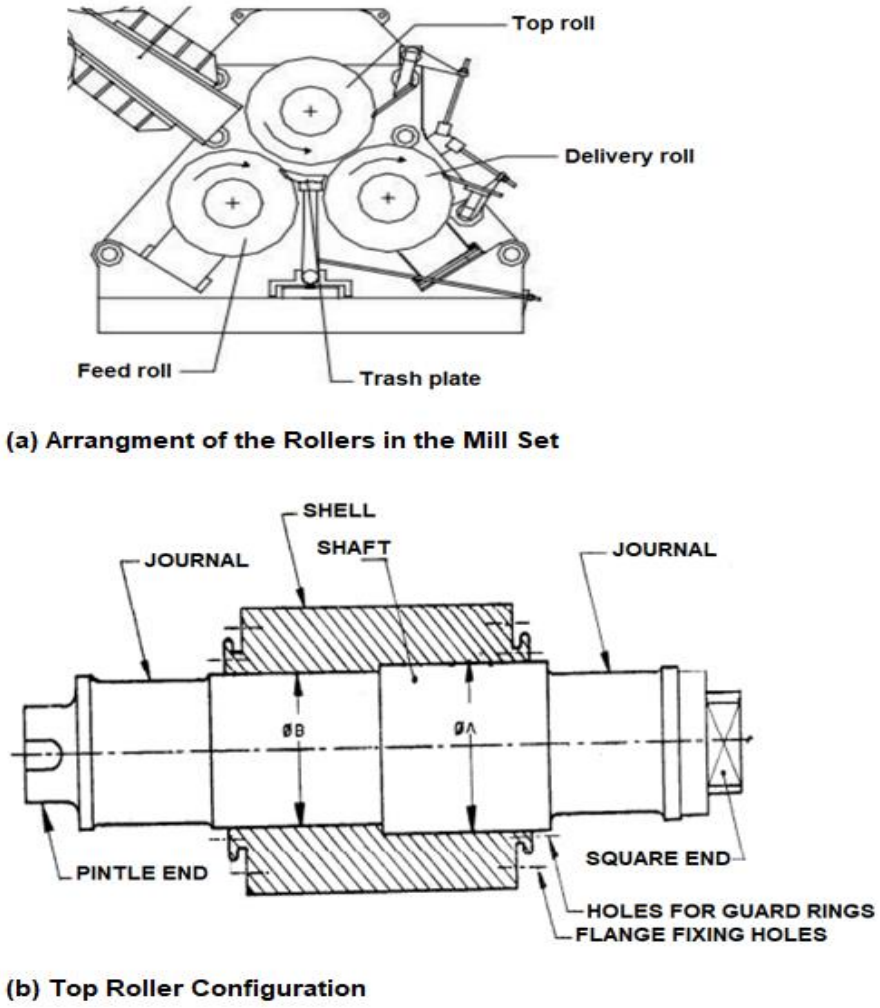

Figure 2.2: Top roller (Indian Bureau of Standards, 1990; Khot and Mandale, 2015).

2.3 Stresses and Loading on the Top Roller

2.3.1 Stress concentration in the shaft

a) At the keyways

Prajapatia et al. (2015) reported an optimal fillet radius to reduce the stress concentration on the shaft determined from the relationship between the stress concentration factor and the radius of rotation on the keyway of C40 carbon steel shaft subjected to bending, torsion and the combined bending and torsion for shaft sizes ranging from 10mm to 500mm; Implying

keyway designs have to be optimized to minimise the effect of stress concentration which accelerates fatigue failures. Xiaobin & Zelong (2013) used numerical simulation to analyse the relationship between geometric discontinuities and stress concentration factor and reported that the stress concentration factor is not related to the shaft diameter but rather to the fillet radius to width ratio of the keyway. Equations 2.1, 2.2 and 2.3 gives the stress concentration factors provided the fillet radius to width ratio for bending, torsion and axial loading respectively for $0.02 \leq \frac{r}{B} \leq 0.0832$ (Xiaobin & Zelong, 2013).

$$K_{TB} = 4.30 - 50.80\left(\frac{r}{B}\right) + 317.35\left(\frac{r}{B}\right)^2 \ldots\ldots\ldots\ldots\ldots\ldots\ldots\ldots (2.1)$$

$$K_S = 3.91 - 40.67\left(\frac{r}{B}\right) + 253.66\left(\frac{r}{B}\right)^2 \ldots\ldots\ldots\ldots\ldots\ldots\ldots\ldots\ldots\ldots (2.2)$$

$$K_{TA} = 5.43 - 62.83\left(\frac{r}{B}\right) + 390.97\left(\frac{r}{B}\right)^2 \ldots\ldots\ldots\ldots\ldots\ldots\ldots\ldots\ldots (2.3)$$

Where: K_{TB}, K_S and K_{TA} - Stress concentration factors in Bending, Torsion and axial loading respectively.

r - Fillet Radius

B - Width

$\frac{r}{B}$ - Fillet radius to width ratio

b) At the fillet shoulders and square ends

Karthi and Emmanual (2018) used the finite element method in the design and analysis of the roller shafts for sugar mill neglecting the effect of dynamic forces and reported that most failures occur on the inner fillet side of the square end and that the stress on the shoulder fillet

is more than that on the taper fillet. Tipton et al. (1996) investigated the effect of tension and bending on the stress concentrated points of the shaft and developed equations relating shaft geometry and stress concentration factor and a more accurate chart of geometry with more values compared to Peterson's chart with forty per cent of the error. Equations 2.4 and 2.5 are used to compare bending and tension with the FEA results in the range of $1.01 \leq D/d \leq 6.0$.

Stress concentration on the shaft under bending loading is given as:

$$(K_t)_{bend} = 0.632 + 0.377\left(\frac{D}{d}\right)^{-4.4} + \left(\frac{r}{d}\right)^{-0.5}\sqrt{\frac{-0.14-0.363\left(\frac{D}{d}\right)^{2}+0.503\left(\frac{D}{d}\right)^{4}}{1-2.39\left(\frac{D}{d}\right)^{2}+3.368\left(\frac{D}{d}\right)^{4}}} \quad \ldots\ldots\ldots\ldots\ldots\ldots (2.4)$$

Where: *r is the fillet radius at the changeover section,*

D and d are the big and small diameter for a stepped shaft.

2.3.2 Loading on the top roller shaft in sugar milling

According to Hugot (2014), the three crushing rollers were fixed relative to each other only adjusted using the steel plate or wedges and the pressure exerted by the bagasse on the rollers directly proportional to the layer of bagasse; the housing gave way on passage of a too hard or too big particle. Developments in the mill sets include incorporating springs in small mill which was later replaced by hydraulic pressure accumulators with a constant pressure irrespective of the roller lift related to the bagasse compression (Hugot, 2014). The relationship between pressure and the compression of bagasse are shown in the table 2.1.

Table 2.1: *Pressure and corresponding compression values of bagasse*

Pressure (kg/cm^2)	Compression
0.077	100
0.429	68.2
1.132	57.7
1.483	50.7
1.837	44.8
2.186	40.8
2.538	39.3
2.889	36.2
3.241	33.6

(Source: Hugot, 2014)

A relationship between the hydraulic pressure exerted on the top roller and the pressure exerted on the layer of bagasse is given in equation 2-7 and table 2.1 *(Hugot, 2014)*. Hugot (2014) in his review of the total pressure on the top roller reported that about twenty per cent of the total hydraulic pressure is consumed by the trash plate and 80 per cent at the entry and delivery openings.

$$p = \frac{P}{0.1LD} \quad (2.5)$$

Where: p is the pressure exerted on the layer of bagasse

P is the hydraulic pressure exerted on the top roller

L is the crushing length

D is the diameter of the crushing length

Khot and Mandale (2015) reported that the three crushing rollers in a mill are placed in a triangular form such that the feed and discharge rollers are placed at a respective angle of 35^{o} and 37^{o} from the vertical and the top roller apex angle is 72^{o} between the lines joining the top roller centre line to the discharge and delivery roller centre lines. Muhammed and Mohammed (2013) in their investigation of the effect of the excessive cement kiln weight on the resistance of the rollers' base based on limited information reported that reduction in the hole diameter caused a reduction in the principal stress and damage of one roller to offset the load concentration on the other roller causing brick lining collapse and kiln stoppage.

2.4 Macrostructure-shaft failure characterization

2.4.1 Overload failures

Neville (2015) reported that brittle overload failures occur when the applied load exceeds the yield or tensile strength of the material which failure may show no visible distortions on the fracture surface evident in grey cast iron, hardened steel or instantaneous loaded ductile material (Neville, 2015). Brittle failure proceeds in form of cracks beginning at the maximum stress point and grows across by material grain cleavage indicated by chevron marks pointing towards the failure origin (Neville, 2015). Figure 2.3 shows shaft failure under tension, torsion and compression.

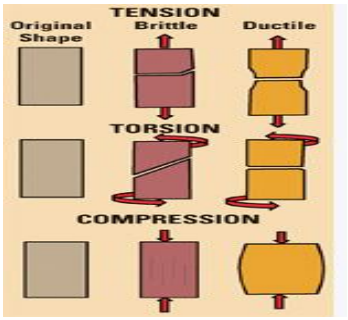

Figure 2.3: Shaft failures under tension, torsion and compression forces (Neville, 2015)

2.4.2 Fatigue failures

Neville (2015) reported that the crack initiates at the origin which slowly develops across the fatigue zone resulting in rotating-bending failure either with multiple fracture origins having a bigger Instantaneous Zone or a single fracture origin with a smaller instantaneous zone. Variation in the shaft loading causes the fast fracture zone to develop progression marks with the fatigue failed surface relatively smooth near the origin and ends in a rough final fracture (Neville, 2015); Implying the features on the failed surfaces of the shaft characterizes fatigue failure. The crack growth rate across the Instantaneous zone increases tremendously at about 8000 feet per second (Neville, 2015). *Figure 2.4 shows the shear-bending failures with a single or multiple fracture origins.*

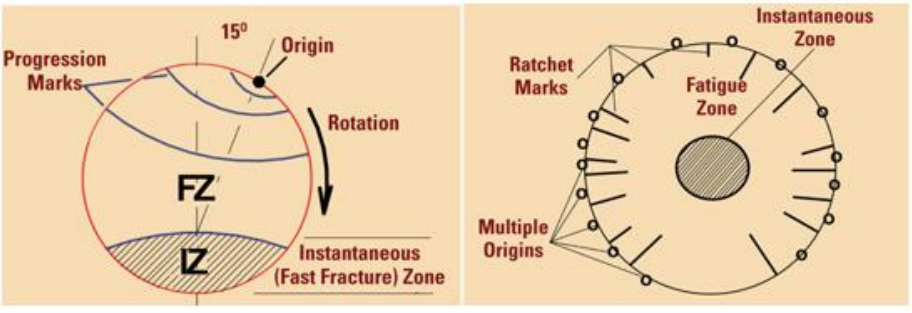

Figure 2.4: Shear-bending failure with a single or multiple fracture origin (Neville, 2015)

Dalvi et al. (2017) in their investigation of the failure on a carbon steel roller shaft of a continuous pad steam machine reportedly observed crack initiation points on the failed shaft and in the fractography examination, the material conformed to standard hardness, chemical composition, tensile and microstructure properties and stress concentration at the shaft step zones using finite element method.

Ebara (2010) conducted corrosion fatigue tests on TMCP made NSSC250 plate specimens in 3%NaCl aqueous solution at frequencies 20 and 0.167Hz and R-value 0.05 and reported that the corrosion fatigue strength reduction of base metal sampled at 20Hz happened at less than $2x10^5$ cycles whereas at the same frequency there was a reduction at 10^7cycles for the base metal; Implying corrosion affects the fatigue strength of the material in service. Corrosion pits develop at the surface near the corrosion-fatigue initiation sites observed for base metals and welded joints which does not cause failure but accelerates the shaft failure at the corrosion sites of the shaft surface (Ebara, 2010).

2.5 Material Standards for Top Roller Components

2.5.1 Bare Shaft

The material of the top roller shaft is forged steel 45C8 conforming to IS: 1570-1979/ **BS EN ISO 683-1:2018** with minimum hardness 175 HB and the chemical composition specification shown in table 2.2 (Bureau of Indian Standard, 2001, p. 1).

Table 2.2*: Standard Chemical composition ranges for forged steel 45C8*

C	**Si**	**Mn**	**S**	**P**
0.40%-0.50%	0.15%-0.35%	0.60%-0.90%	0.04% max	0.04% max

2.5.2 Roller shell

The roller shell is made up of cast iron conforming to **IS: 11202-1985** with hardness ranging from 180-210 BHN, microstructure with A-type distribution of graphite flakes conforming to **IS: 7754-1975** and the chemical composition specification shown in table 2.3 (Bureau of Indian Standards, 1990, p. 2).

***Table 2.3**: Standard Chemical composition ranges for sugar mill roller shells*

C	Si	Mn	S	P
3.20%-3.60%	1.2%-2.2%	2.2%-3.2%	0.15% max	0.5% max

2.5.3 Coupling

Hage *et al.,* 2017 reported that square couplings are made up of low carbon steel grade A4 which conforms to **ISO 14737:2015** and hardness ranging from 152-207 HB which conform to **BS 3100: 1976** having the chemical composition shown in table 2.4 (Singapore Institute of Standards and Industrial Research, 1976; Qingdao Casting Quality Industrial Co., Ltd, 2009).

***Table 2.4:** Standard Chemical composition for low carbon steel A4 box coupling*

C	Si	Mn	S	P
0.18%-0.25%	0.6% max	1.2%-1.6%	0.05% max	0.05% max

Hage et al., 2017 reported new development of the rope coupling to replace the square couplings because of their inability to handle axial thrust on the tailing bar which could be solved by making the female part of the coupling bigger implying a high cost of the material. However, the steel wire ropes on the rope couplings have reportedly been subject to fatigue

failures which called for replacing the wire ropes with polyester slings and link plates with spherical plain bearings (Hage et al., 2017).

2.6 Microstructure versus mechanical properties of the shaft

Sieniawski et al. (2013) investigated the microstructural effect on the mechanical performance of two-phase of Ti-6Al-2Mo-2Cr (α-phase) and Ti-6Al-5Mo-5V.1Cr-1Fe (β-phase) being vacuum melted and rolled and reported that the thickness and the length of the α-phase reduced with increasing cooling rate and increasing β stabilizing elements characteristically slowing down the crack propagation. Mishnaevsky et al. (2004) in their probabilistic and numerical analysis of clustered and uniformly distributed particle reinforced composites on the damage evolution found out that the failure strain of the composite with clustered composite was lower than for uniformly distributed particle ordered composites which also attributed to 2.3% increase in the stiffness and flow stress in clustered composites more than in uniform particle arrangement. Al-Hassan et al. (1998) investigated the microstructural effect on the corrosion of steel in a carbon dioxide aqueous solution using electrolysis and found out that the corrosion rate increased with the carbon content depicted by a bigger pearlite phase in normalized specimen than in annealed specimens. Micrographs of the normalized and annealed specimens are shown in the Figure 2.5.

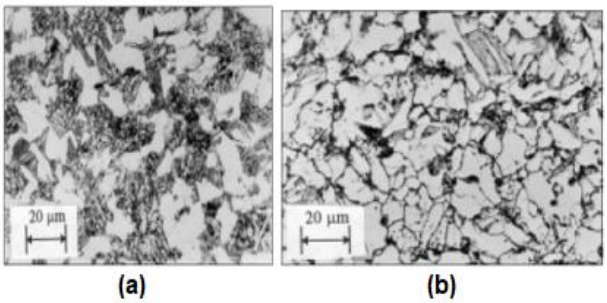

Figure 2.5: Microstructure of (a) normalized and (b) annealed steel (Al-Hassan et al., 1998)

Taylor and Knot (1981) investigated the effect of microstructure on the fatigue crack propagation behaviour of short cracks and found out that high strength materials with fine microstructure developed minute crack sizes of less than 100μm. Chiang et al. (2011) investigated the characterization of microstructure on retained Austenite stability and work hardening of TRIP (Transformation Induced Plasticity) steels with lamellar and equiaxial microstructure and found out that the equiaxial microstructure showed a better strength and higher hardening rate at a tensile strain of 0.05 which is sustained up to the maximum tensile strength of the material.

2.7 Effect of Chemical composition on the mechanical performance of steel shafts

Hashimoto et al. (2004) investigated the effect of addition of Nb and Mo on the mechanical properties of a steel specimen 2mm thick by 50mm long by 25mm wide; and of composition 0.2%C, 1.5%Si and 1.5%Mn at testing the speed of 27mm/min, and reported an increase in the yield strength with corresponding reduction in the tensile strength at a coiling temperature of 450^0c. Yonezawa et al. (2013) investigated the effect of Ni, Mo, Cr, Mn, Si, N and C alloying elements on the Stacking Fault Energy (SFE) for Fe-Cr-Ni Austenitic stainless steel under SHTWC, SHTFC and AGG heat treatment condition and reported that Ni, Mo content increased with the SFE, Cr and Mn slightly increased the value of SFE; Silicon content increase strongly decreased the SFE values and slightly decreased with an increase in carbon content. High values of stalking fault energy foster ratcheting damage and low SFE accelerate fatigue damage for FCC metals under fully repeated loading (Sakaki et al., 2014).

Virupaksha *et al*. (2017) in their investigation of the chemical composition effect on the impact strength of the certain steel material grades using SEM for chemical composition and Charpy impact tester for impact tests on 5 by 10 by 55mm specimen at temperatures 20^0c, 0^0c, -20^0c and -40^0c reported that an increase in the carbon and manganese content decreased the impact energy and had no effect on the grain size; addition of V, Nb and Ti in steel increased the impact energy.

2.8 Hardness-fatigue strength relationship in steel shafts

Hassan, (2017) used the data values of fatigue strength (S_f) and corresponding Brinell hardness (HB) and ultimate tensile strength (σ_u) of steel materials from other researcher's investigation and generated the relationship S_f=1.3HB + 0.02 σ_u which is a line of best fit with a correlation coefficient R=92% for Brinell hardness number ranging from 163 to 536, fatigue strength and tensile ultimate strength related weakly. Zubko and Pešek (2015) Conducted experimentation tests for API 5L steel X60 and X70 under static and fatigue loading conditions and reported that the reached minimum and maximum hardness values were consistent for each material under the two loading conditions; Implying that hardness of a material is related to its fatigue strength.

Casagrande *et al.*, (2011) in their experimental investigation of the relationship between fatigue limit and Vickers hardness in 100Cr6, low carbon, medium and high carbon steel machined to 10mm by 10mm by 50mm annealed for 60 minutes at a temperature of 900^0c reported that there is a linear relationship between the estimated fatigue limit and experimental fatigue limit

and established a direct relationship between the fatigue limit and Vickers hardness for metallic inclusion free steels which was inconsistent for steels with metallic inclusion.

2.9 Corrosion Effect of Sugar on the Steel Top Rollers

Muñoz Cubillos *et al.,* (2016) investigated the corrosion effect on a rotating and bending SAE 1045 steel using a Hung TA machine in an air and sugar juice environment at 300^0c and 600^0c and reported that the steel had better fatigue strength in air compared to that in sugar cane juice at 300^0c than at 600^0c. The research proposed investigation of the thermal chemical treatment and coating as ways of improving fatigue strength (Muñoz Cubillos *et al.,* 2016).

2.10 Temperature-fatigue growth properties of steel

Puskar and Varkoly (1986) subjected low carbon unalloyed steel CSN412013 and CSN415313 steel to temperatures from 200^0c to 500^0c in Argon and at 200^0c using water coolant at a frequency 22kHz and reported an increase in the fatigue growth rate with temperature increase at a constant rate but CSN412013 steel showed no effect for the temperatures range from 250^0c to 300^0c and a negative relationship between temperature and the fatigue growth rate.

2.11 Definition of Reliability

Reliability is the probability that a product will continue to perform as expected under the stated condition without fail for a specified period (Bloch, 1998). Reliability as a measure of failure-free operation over a given time interval and Maintenance professionals conduct reliability-cantered maintenance to reduce the frequency of failures over time and to suppliers; reliability is measured by completion of a failure-free warranty period under specified

operating conditions. Mathematically, reliability can be measured based on Mean Time Between Failure (MTBF) or Mean Time to Failure (MTTF) as shown in figure 2.6 (Bloch, 1998, p. 612). Equation 2.6 is a *r*eliability equation relating time and Mean Time Between Failures or Mean Tine To Fail.

$$R(t) = e^{\frac{-t}{MTTF}} = e^{\frac{-t}{MTBF}} = e^{-\lambda t} \quad \ldots\ldots\ldots\ldots\ldots\ldots\ldots\ldots\ldots\ldots\ldots\ldots (2.6)$$

Where: λ - The failure rate

$R(t)$ - Reliability of the Equipment and t is the time at which the measurement is taken.

t - Time

MTBF - Mean Time Between Failures

MTTF - Mean Time To Fail

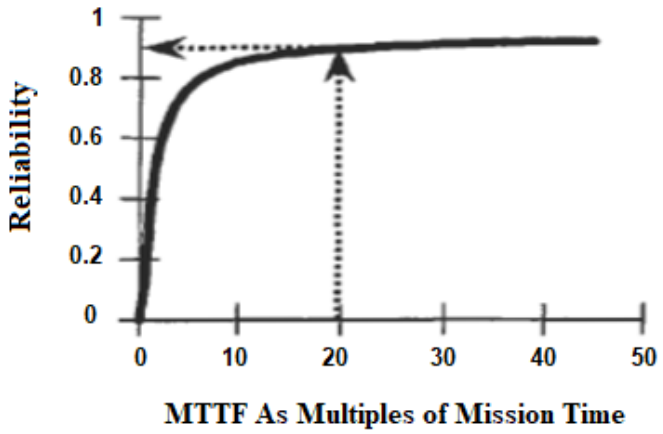

Figure 2.6: Reliability vs MTTF (*Bloch, 1998)*

Not all failures can be eliminated at the design level hence through reliability engineering, the likely causes of failure can be identified and measures identified to mitigate the consequences of the failure (Publishing, 2020). Reliability may be expensive capital wise but improve availability, lower downtime and associated maintenance costs and is the pivot for increase production rate and profitability in the company (Bloch, 1998). Utkin (2011) based on limited information reported that there is a relationship between loading on the shaft and its strength in the probabilistic computation of reliability.

2.12 Structural Analysis by Finite Element Method

Finite Element Method (FEM) is a mathematical technique constituting arranging and solving integral and differential equations whose behaviour cannot be predicted using closed-form equations (elements) whose solutions can be closely known or approximated (Mary & John, 2017). System geometry is defined by nodes with a set of the degree of freedom varying based on the system inputs which are linked by elements defining the mathematical interactions of the degree of freedom (Mary & John, 2017). Individual elements forming a model are combined into a set of equations representative of the system under analysis; these equations constitute the vital information about the system behaviour associated with computer programs that build, solves and visualizes the solution of a large set of equations (Mary & John, 2017). Finite Element Analysis involves ten steps which include defining the solid model geometry, select the element types, defining the material properties, Mesh, defining boundary conditions, defining loads, Set the solution options, Solve, plot, view and export the results, compare and verify the results (Mary & John, 2017).

Mary & John (2017) conveyed that ANSYS containing forty elements of various types was first developed by NASA as a finite element program to predict transient stress and displacements in the reactor's systems due to thermal and pressure loads. ANSYS allows the input of new generated material properties apart from inbuilt material properties in the software material library. ANSYS has been improved over time and better versions released over time which improves the usability and results of the software (Mary & John, 2017).

Mohammadi (2008) reported that the Finite Element Method can also be used in the study of fracture mechanics of rotatory models relating to the crack growth, critical crack growth and direction for a given material under study. Experimental study of crack growth in the shaft has limitation in accurately determining the crack extension path since a notch has to be created in the material to study the fracture mechanics of the crack (Mohammadi, 2008). ANSYS software can assist accordingly in determining the mode of shaft failure under given loads, crack growth propagation, and critical crack size at which the shaft is bound to fail (Mohammadi, 2008).

Ismail (2018) in the study of the correlation between the Experimental Model Analysis and the Finite Element Method (FEM) on parameters such as natural frequency, modal shapes and damping ratios reported discrepancies in the results averaging to 4%; errors are supposedly due to the model simplification and inaccuracies in parameter assumptions which could be solved by updating the model (Ismail, 2018). Lourdes and Hassan (2018) reviewed Experimental Model Analysis (EMA) and normal mode FEA of Engineering structural dynamics and reported that FEA gives a component investigation of a product whereas, in

EMA, dynamic attributes of the product relating to the modal shape, natural frequencies and damping ratios can be obtained.

Meshram and Wanjari (2015) in their review of the causes of failure of the rolling key for static and impact loading reported that Finite Element Analysis could be employed for stress analysis for the given shaft material and geometry to investigate the root cause of the rolling key failure. Khot & Mandale (2015) in their static structural analysis of three rollers crushing sugar mill using finite element method reported forged steel as the best material considering the deformation and the cost of the material for the discharge, top and feed rollers. The ultimate shear stress was found to be less than the material's yield strength hence there is room for weight optimization of the material (Khot & Mandale, 2015). The study focused on the static analysis of the shaft material and this study focuses on the dynamic analysis of the roller material. Kamal et al. (2013) reported that for all multiaxial in phase and out of phase loading, the endurance function model resulted in accurate fatigue life prediction for a stable material fatigue life for EN8 and C40 steel and suggested further studies for the nonlinear fatigue behaviour of the materials.

CHAPTER THREE

MATERIALS AND METHODS

3.0 Introduction

This chapter presents the methods employed to determine the macrostructure, microstructure, chemical composition and hardness properties of the failed top roller components, shear stress criterion to determine regions of maximum shear stress on the top roller and transient structural examination of the stress distribution on the top roller using finite element method.

3.1 Research Design

A quasi-experimental research design was used involving characterization of mechanical performance of pre-existing top roller shafts in the sugar mills, pre-existing operating speeds and hydraulic loading subject to the top rollers.

3.2 Instruments and Software Used

Top roller speeds were read from the speed control boards, hydraulic loadings read from the pressure gauges, top roller geometry determined from the drawings and direct measurements, hardness determined by the Mutitoyo hardness testing machine (HRC machine), chemical composition by thermo-scientific spark arc spectrometer, microstructure determined by Kruss optronic metagraphical microscope, the phone camera used for taking photos of failed surfaces and ANSYS 15.0 tool used as the finite element modeller; Solidworks 15.0 for generating the top roller model.

3.3 Sample Selection

The research was conducted in 4 mill sets 3 sugar millers representing 6 Uganda based sugar mills with the same configuration from which sample components were identified and obtained. Given a population size of 11 sugar millers and a sample size of 6 indicates 80% confidence levels, margin error € 20%, and the Z value corresponding to the confidence level is 1.28 (Ministry of Trade, Industry and Cooperatives, 2016; Survey Monkey, 2020).

3.4 Shaft specifications

Shaft geometry and sizes were obtained from technical shaft drawings and direct measurements to obtain diameters, fillet radii and width sizes of the shafts. The top roller shaft solid model was developed using solid works.

3.5 Loading and Stress on the shaft

The hydraulic loading on the bearing points, the shaft RPMs and the power transmitted to the top roller shaft and the average distances between the loaded points on the shaft for force analysis were used to compute maximum shear stress on the different top roller regions.

3.5.1 Forces Subjected on the Top Shaft

The following force elements are subjected to the top roller:

(a) Force on the top roller pinion required to drive the feed roller and discharge roller pinions.

(b) Weight of the pinion.

(c) Pressure force exerted by the hydraulic ram on the bearing shoulders to crush the bagasse between the rollers.

(d) The reaction due to the bagasse compression between the rollers (feed and discharge rollers) and the top roller, bagasse compression between the top roller and the trash plate.

(e) Weight of the top roller shaft and shell and the reactions at the bearing shoulders.

3.5.1.1 Forces on the crushing length

Force, F, exerted by hydraulic loading on top roller was calculated using equation 3.1 as:

$$F = \frac{2 \times \pi \times d_T^2 \times P \times 9.81}{4} \ldots\ldots\ldots\ldots\ldots\ldots\ldots\ldots\ldots (3.1)$$

Where: F - Force due to pressure

P - Hydraulic pressure on Mill (kg/cm^2)

d_T - Diameter of the Ram (cm)

The ratio of reaction of bagasse on top roller of the feed entry, F_E to the reaction of Bagasse on the top roller at the discharge opening, F_S is 5. Equation 3.2 gives the relationship between bagasse reactions on the top roller at the feed entry to that at the discharge opening (Hugot, 2014).

$$F_E = \frac{F_S}{5} \ldots\ldots\ldots\ldots\ldots\ldots\ldots\ldots\ldots\ldots (3.2)$$

Where: F_E - Reaction of bagasse on top roller at the feed entry in kN

F_S - Reaction of Bagasse on the top roller at the discharge opening in kN

Out of total pressure force exerted by the hydraulic ram on the top roller 80% is absorbed by the crushing of bagasse at the feed and delivery opening (Hugot,2014). Equation 3.3 gives the relationship between the bagasse crushing force at the feed and delivery opening with the pressure force at the hydraulic ram on top roller.

$$F_E + F_S = 0.8F \ldots\ldots\ldots\ldots\ldots\ldots\ldots\ldots\ldots\ldots\ldots\ldots (3.3)$$

Equation 3.4 gives the relationship between crushing force at the delivery opening and the ram force on the top rollers.

$$F_S = \frac{2}{3}F \ldots\ldots\ldots\ldots\ldots\ldots\ldots\ldots\ldots\ldots\ldots\ldots\ldots (3.4)$$

From the free body diagram in Figure 3.1, the horizontal and vertical components of the crushing forces due to hydraulic pressure were be determined using equations 3.5 and 3.6 respectively.

$$\rightarrow + \sum H_C = F_E \sin 35^\circ - F_S \sin 37^\circ \ldots\ldots\ldots\ldots\ldots\ldots\ldots\ldots\ldots\ldots (3.5)$$

$$\uparrow + \sum V_C = -F + F_E \cos 35^\circ + F_S \cos 37^\circ \ldots\ldots\ldots\ldots\ldots\ldots (3.6)$$

Where: $\sum H_C$ − Sum of the horizontal crushing forces due to hydraulic pressure.

$\sum V_C$ − Sum of the horizontal crushing forces due to hydraulic pressure.

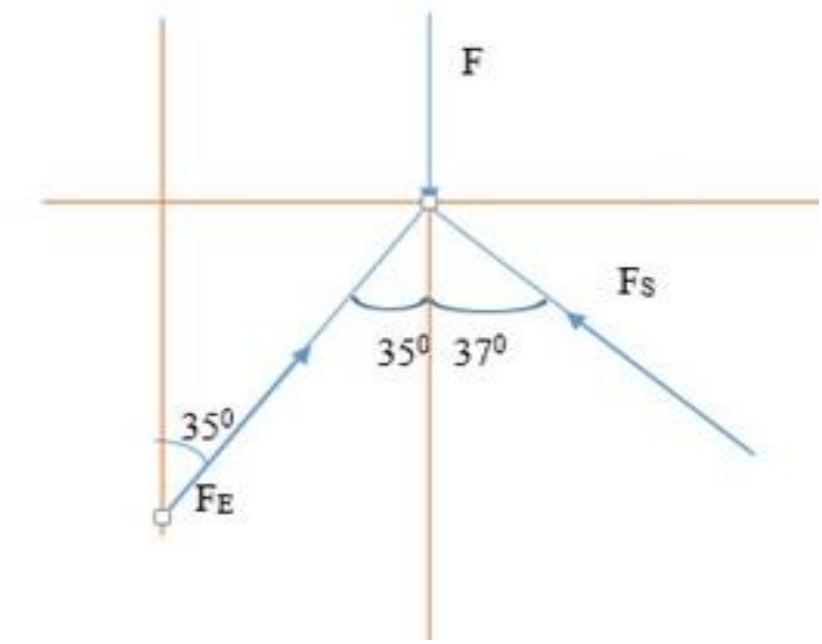

Figure 3.1: Crushing forces on top roller shell for mill 1 through 4

Assumption: Equal loading on the entire crushing length of the top roller, therefore the force due to bagasse compression is a uniform distributed load (Hugot, 2014; Khot $ Mandale, 2015).

3.5.1.2 Forces at the pinion

The top roller pinion transmits about 50% of power to drive the top roller and the other 50% of power drives the feed and discharge roller pinions in the three-roller pinion configuration.

Assumptions: No fiction losses at the pinion gear contact surfaces since mating surfaces are adequately lubricated and the gear meshing happens at the pitch centre diameter

Equation 3.7 gives the power transmitted to the mill set from the variable frequency motors through the gearing system to the crushing rollers and equation 3.8 gives the angular velocity given the number of revolutions per minute (Khot & Mandale, 2015).

$$P = Tw \ldots\ldots\ldots\ldots\ldots\ldots\ldots\ldots\ldots\ldots\ldots\ldots\ldots (3.7)$$

$$w = \frac{2\pi N}{60} \ldots\ldots\ldots\ldots\ldots\ldots\ldots\ldots\ldots\ldots\ldots\ldots\ldots . (3.8)$$

Where: P – Power transmitted,

T – Torque

w - Angular velocity

Equation 3.9 gives the Torque on Top roller pinion given the number of revolutions per minute, N and the power transmitted to the roller shaft, P is given by equation 3.9.

$$T_P = \frac{15P}{\pi N} \ldots\ldots\ldots\ldots\ldots\ldots\ldots\ldots\ldots\ldots\ldots\ldots\ldots . . (3.9)$$

Where T_P - Torque transmitted to the top roller pinion

Equation 3.10 and 3.11 gives the module and the pitch centre diameter of the top roller pinion. Equation 3.12 gives the tangential force on the pinion and Equation 3.13 gives the radial force on the pinion given the pressure angle of the gear and the tangential force between meshing gears.

The Pitch Centre Diameter of the pinion;

$$m = \frac{d_e}{Z+2} \ldots\ldots\ldots\ldots\ldots\ldots\ldots\ldots\ldots\ldots (3.10)$$

$$P.C.D = mZ \ldots\ldots\ldots\ldots\ldots\ldots\ldots\ldots\ldots\ldots\ldots (3.11)$$

Tangential force on the pinion,

$$F_t = \frac{\text{Torque}, T_P}{(\frac{P.C.D}{2})} \ldots\ldots\ldots\ldots\ldots\ldots\ldots\ldots\ldots\ldots\ldots\ldots (3.12)$$

Where: P.C.D - Pitch Centre Diameter

Z - Number of teeth, Z= 17

De - Outer pinion diameter, De =900mm

M - Module of the pinion gear

$$F_r = F_t \tan\varphi \ldots\ldots\ldots\ldots\ldots\ldots\ldots\ldots\ldots\ldots\ldots\ldots (3.13)$$

Where: F_r - radial component of force at the meshing gears

F_t - tangential force at the meshing gears

φ - Pressure angle of the meshing gear

Using the free body diagram in figure 3.2, the resultant horizontal and vertical forces at the Pinion can be determined using equations 3.14 and 3.15 respectively.

$$\sum H_p = F_t(\sin 35^\circ + \sin 37^\circ) + F_r(\sin 35^\circ - \sin 37^\circ) \ldots\ldots\ldots\ldots\ldots\ldots\ldots (3.14)$$

$$\sum V_p = F_t(\cos 35^\circ - \cos 37^\circ) + F_r(\cos 35^\circ + \cos 37^\circ) - W_p \ldots\ldots\ldots\ldots (3.15)$$

$$W_p = m_p g \ldots\ldots\ldots\ldots\ldots\ldots\ldots\ldots\ldots\ldots\ldots\ldots\ldots\ldots\ldots\ldots (3.16)$$

$$W_t = m_t g \ldots\ldots\ldots\ldots\ldots\ldots\ldots\ldots\ldots\ldots\ldots\ldots\ldots\ldots\ldots\ldots\ldots (3.17)$$

Where: $\sum H_p$ −Summation of horizontal forces at the pinion

$\sum V_p$ − Summation of vertical forces at the pinion

$W_p \; and \; W_t$ – Weights of the pinion gear and the top roller

$m_p \; and \; m_t$ – Masses of the pinion gear and top roller, $g = 9.81 ms^{-2}$

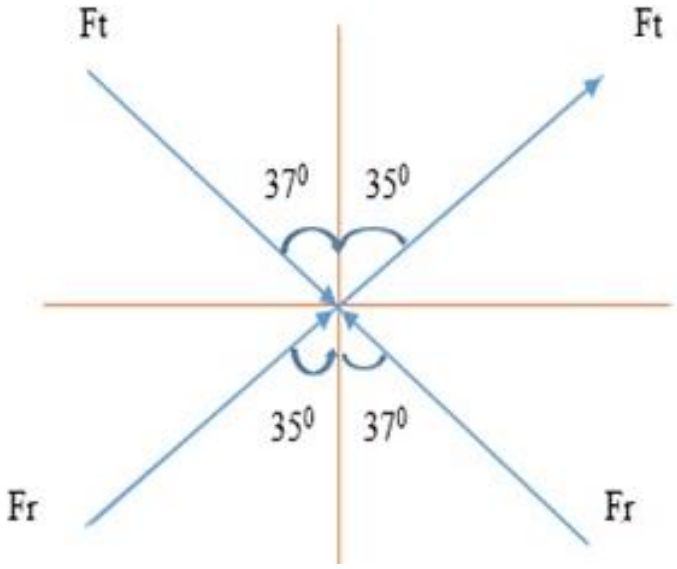

Figure 3.2: Free body diagram for forces on top roller pinion gear mill 1 through 4

3.5.1.3 Reactions at the Bearing

The vertical and the horizontal components of the reactions at the top roller bearings can be determined taking moments using static force equilibrium conditions and taking moments about the bearing points on the pintle and drive side using top roller force diagrams in Appendix. 1 (d) (i), (ii), (iii), (iv) and 1 (e) for the 4 Top Rollers.

3.5.2 Stress determination

Vertical and horizontal shear force and bending moment diagrams were used to determine points of maximum bending moments on the shaft and bending moment at the stress concentration points. The following equations were employed in the computations (Xiaobin & Zelong, 2013; AFFDL, 2019).

Torsion stress concentration factor at the keyway was calculated using equation 3.18.

$$K_t = 3.91 - 40.67\left(\frac{r}{b}\right) + 253.66\left(\frac{r}{b}\right)^2 \ldots\ldots\ldots\ldots\ldots\ldots\ldots\ldots\ldots\ldots (3.18)$$

Where: K_t - Torsion stress concentration factor

r - Fillet Radius

b - Width

$\frac{r}{b}$ - Fillet radius to width ratio

Bending stress concentration factor at the keyway was calculated using equation 3.19.

$$K_b = 4.30 - 50.80\left(\frac{r}{b}\right) + 317.35\left(\frac{r}{b}\right)^2 \ldots\ldots\ldots\ldots\ldots\ldots\ldots\ldots\ldots (3.19)$$

Where: K_b - Bending stress concentration factor

r - Fillet Radius

b - Width

$\frac{r}{b}$ - Fillet radius to width ratio

Torsion stress was computed using equation 3.20.

$$Torsional\ stress, \tau_{max} = K_t \frac{16T}{\pi d^3} \ldots\ldots\ldots\ldots\ldots\ldots\ldots\ldots\ldots\ldots (3.20)$$

Where: τ_{Max} - Torsional stress

K_t - *Torsion* stress concentration factor

T - Torque

d - Diameter

The bending stress was computed using equation 3.21:

$$Bending\ stress, \delta_{max} = K_b \frac{32M}{\pi d^3} \ldots\ldots\ldots\ldots\ldots\ldots\ldots\ldots\ldots\ldots (3.21)$$

Where: σ_{Max} - Bending stress

K_b - Bending stress concentration factor

M - Bending Moment

d - Diameter

Shear force and bending moment diagrams for the vertical and horizontal loading on top rollers for mill 1 through 4 are generated and used to determine the point of maximum bending moment on the top roller and compute the maximum shear stress. The maximum shear stress was then compared to the safe working value of stress of the material.

Equation 3.22 gives the Maximum resultant moment on top roller, given the maximum vertical and horizontal components of moment

$$M_e = \sqrt{M_v^2 + M_H^2} \ldots\ldots\ldots\ldots\ldots\ldots\ldots\ldots\ldots\ldots\ldots\ldots (3.22)$$

Where: M_e - Maximum resultant moment

M_v - Maximum vertical component of moment

M_H - Maximum horizontal component of moment

Equation 3.23 gives the maximum shear stress on the shaft, given the maximum equivalent bending moment and the torque on the top roller.

$$\tau_{max} = \frac{16}{\pi d^3}\sqrt{M_e^2 + T^2} \ldots\ldots\ldots\ldots\ldots\ldots\ldots\ldots\ldots\ldots (3.23)$$

Where: τ_{max} - Maximum shear stress

T - Torque

Equation 3.24 gives the maximum shear stress at the stress concentration points on the shaft given the torque and the bending and torsion stress concentration factors.

$$\tau_{max} = \frac{16}{\pi(d)^3}\sqrt{[K_b \times M_e]^2 + [K_t \times T]^2} \ldots\ldots\ldots\ldots\ldots\ldots\ldots\ldots\ldots\ldots\ldots\ldots (3.24)$$

Where: K_b - Bending stress concentration factor

K_t - Torsion stress concentration factor

D - Shaft diameter at the point of the stress concentration

3.2.3 Force and Stress Analysis of the Top Roller Performance in the different mills

Graphs in Excel used for force analysis, Reliability analysis and ANOVA in XLSTAT were used to determine the loading and failure sequence of the top rollers in mills 1 to 4 and the highly stressed points on particular shaft sections.

3.3 Structural Properties of Top Roller Failed Components

Structural properties of the failed top roller components were tested for macrostructure, microstructure, hardness test and chemical composition to check for conformance with the internationally recognized standards.

3.3.1 Preparation of the Specimens

Specimens were cut from the broken top roller component material and ground to the required size for tests. The failed part of the top roller and box coupling was cut off using oxy-acetylene cutting and immediately preserved under the oil for 8 days before the tests to allow it cool and inhibit any alteration in the material structural properties. Figures 3.3, 3.4, 3.5 and 3.6 are the samples of specimens that were cut for tests.

Figure 3.3: Specimen 1 cut from a failed top roller shaft KE-3 in 4th mill

Figure 3.4: Specimen 2 cut from broken top roller SB-1 in 3rd mill

Figure 3.5: Specimen 3 cut from the broken square end for top roller shaft KE-8 in 4th Mill

Figure 3.6: Specimen 4 cut from a worn box coupling for the top roller mill 4

3.3.2 Coding of specimen

For non-disclosure of the sugar mills, the letter has been assigned for the two sugar millers and the specimens numbered as 1 and 2. Details of the specimen coding given in the Table 3.1 are as follows:

(i) AM1 represent the macrostructure for specimen 1 from Sugar miller A,

(ii) AMi1 represents the microstructure for speciment1 from Sugar miller A,

(iii) AC1 represents the chemical composition for specimen 1 from Sugar miller A,

(iv) AH1 represents the Hardness of specimen 1 from Sugar miller A,

(v) AM2 represent the macrostructure for specimen 2 from Sugar miller A,

(vi) AMi2 represents the microstructure for specimen 2 from Sugar miller A,

(vii) AC2 represents the chemical composition for specimen 2 from Sugar miller A,

(viii) AH2 represents the Hardness of specimen 2 from Sugar miller A,

(ix) AM3 represent the macrostructure for specimen 3 from Sugar miller A,

(x) AMi3 represents the microstructure for speciment3 from Sugar miller A,

(xi) AC3 represents the chemical composition for specimen 3 from Sugar miller A,

(xii) AH3 represents the Hardness of specimen 3 from Sugar miller A,

(xiii) BM4 macrostructure for specimen 4 from Sugar miller B,

(xiv) BMi4 represents the microstructure for speciment4 from Sugar miller B,

(xv) BC4 represents the chemical composition for specimen 4 from Sugar miller B,

(xvi) BH4 represents the Hardness of specimen 4 from Sugar miller B.

Table 3.1: *Coding of failed specimens under investigation*

Component	Sugar Millers	Macrostructure	Microstructure	Chemical Composition	Hardness Tests
1	A	AM1	AMi1	AC1	AH1
2	A	AM2	AMi2	AC2	AH2
3	A	AM3	AMi3	AC3	AH3
4	B	BM4	BMi4	BC4	BH4

3.3.3 Macrostructural Test

Close (about 15cm) and far Photos (about 35cm) of the failed top roller components were taken indicating the failed parts or faces. Visual inspection of the fractured surface of the shaft was used to define the failure mode of the top roller component and measurement of the estimated diameter of the failed zone of the box coupling and compare to the diagonal length of the square end of the shaft.

3.3.4 Microstructure Test

Kruss Optical Microscope OLYMPUS – 412 made in German in Figure 3.7, polishing disks and 3% Nital solution were considered for the test. The prepared piece was polished by

grinding disk and 3%Nital solution applied on the surface of the prepared piece of length 20 mm. Micrographs are used to analyse the specimen's microstructure.

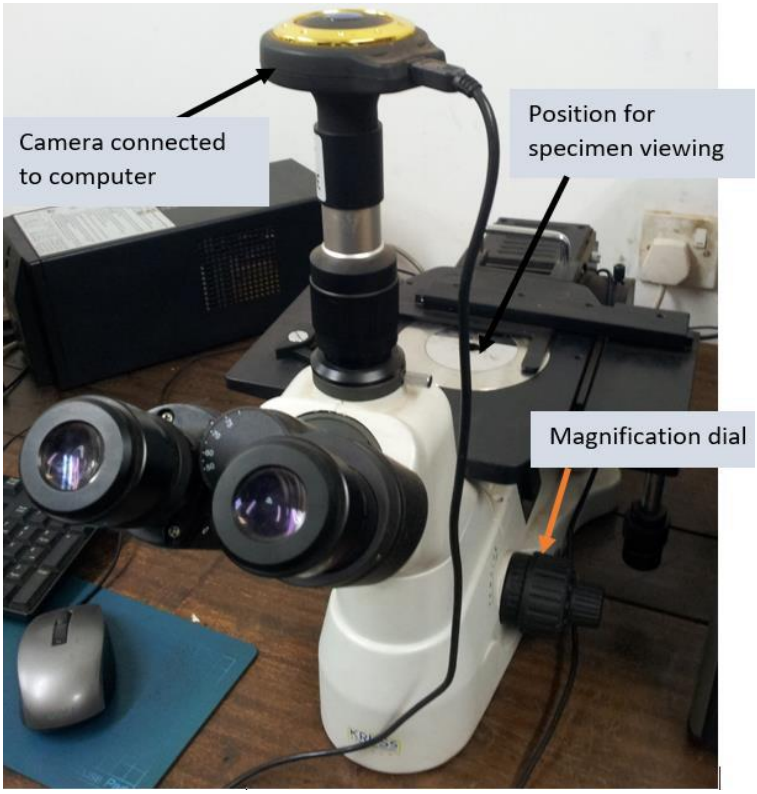

Figure 3.7: Kruss Optronic Metagraphical Microscope

3.3.5 Chemical Composition Test

A Spark Emission Spectrometer SPECTROLAB in figure 3.8 for AMi1 and Thermo Scientific ARL OES Spectrometer for BMi2, Test pieces of 20mm were cut from the main shaft, polished and placed at the test position of SPECTROLAB/ Thermo Scientific ARL OES Spectrometer made in UK and a spark is directed towards the surface of the test piece. A printout from the computer attached to the microscope was printed out for chemical composition analysis.

Figure 3.8: Computerized Spark Arc Spectrometer

3.3.6 Hardness Test

Test pieces were cut from the parent metal and machined to the required diameter of length 20mm and mounted on the Rockwell hard testing machine (WIZHARD) to determine the HRC number of the test piece. HRC number was used for the analysis of the performance of the shaft under fatigue loading. Figure 3.9 is the HRC machine used during the experiment.

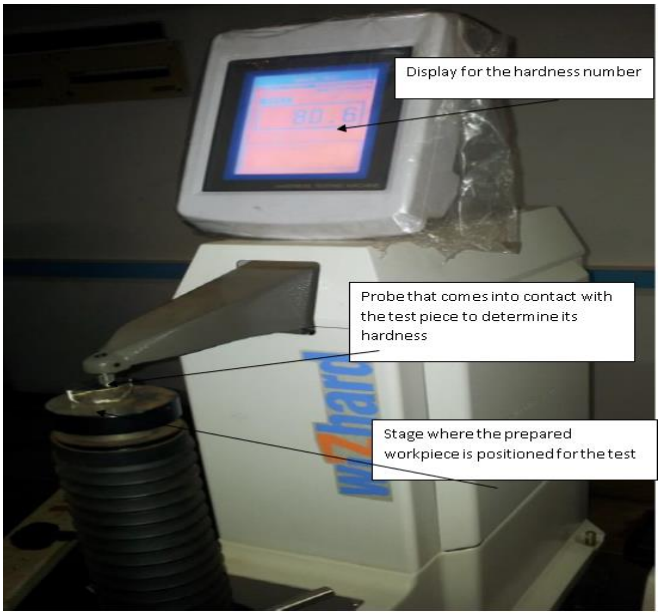

Figure 3.9: Mutitoyo Digital Hardness Testing Machine

3.4 Determination of Top Roller Stress Distribution by Finite Element Method

Geometrical Models of the top rollers were created in solid works and imported to Ansys workbench software as IGES files for structural transient analysis under the given defined boundary conditions for loading, material and geometry. ANSYS workbench software was used to determine the transient structural stress distribution on the top roller for the four mill sets and the number of cycles the shaft undergoes before final failure, the factor of safety and fatigue sensitivity of the material. Fatigue and monotonic values of forged steel and ductile cast iron for the same material of a crankshaft were fed into the ANSYS software and used in the analysis.

Williams et al. (2007) performed fatigue tests at room temperature on forged steel and ductile cast iron material of the crankshaft which was monitored together with humidity. Monotonic and fatigue tests were performed according to ASTM standard E8 (7) and ASTM standard E606 (Williams et al., 2007). Constant amplitude uniaxial fatigue tests with amplitudes ranging from 0.16% to 2% for forged steel and 0.135% to 2% for ductile cast iron at frequencies ranging from 0.1Hz to 1Hz with an exception of some long-life tests converted to load control after the load stabilized in stain control and frequency increased to 25Hz. The following values were fed into the ANSYS software for dynamic analysis of the roller shaft (Williams et al., 2007). The top roller made up of a forged steel and cast-iron shell with the same materials analysed for the crankshaft. Monotonic and cyclic properties of forged steel and ductile cast ion were considered for transient structural analysis in ANSYS software (Williams et al., 2007). Table 3.2 shows the monotonic and cyclic properties of forged steel and ductile cast iron.

Table 3.2: *Cyclic and Monotonic properties of forged steel and ductile cast iron*

Cyclic properties	**Forged steel**	**Cast Iron**
Fatigue strength coefficient, δ_f', MPa	1124	927
Fatigue ductility coefficient ε_r'	0.671	0.202
Fatigue strength exponent, b	-0.079	-0.087
Cyclic yield strength, YS', MPa	505	519
Fatigue ductility exponent, c	-0.597	-0.696
Cyclic strain hardening exponent, n'	0.128	0.114
Cyclic strength coefficient, K', MPa	1159	1061
Fatigue strength at $N_f = 10^6$, MPa	359	263
Monotonic properties	**Forged steel**	**Cast Iron**
Average hardness, HRB	101	97
Average hardness, HRC	23	18
Yield strength (0.2% offset), YS, MPa	625	412
Modulus of elasticity, E, GPa	221	178
Percentage elongation % EL	54%	10%
Ultimate strength, Su, MPa	827	658
Strength coefficient, k, MPa	1316	1199
Percentage reduction in area %, RA	58%	6%
True fracture strength, δ_f, MPa	980	562
Strain hardening exponent, n	0.152	0.183
True fracture ductility, ε_f	87%	6%
Poisson ratio	0.3	0.275
Physical Properties		
Material Density (Kgm^{-3})	7850	7200
Thermal Properties		
Coefficient of thermal expansion (10^{-6}m/m ^oC)	11.3	10.3-11

(Source: Williams et al., 2007; Canadian Conservation Institute, 2017; Engineering Toolbox, 2003)

Fatigue equations relating X variable the number of stress cycles (N) to failure up to 10^6 cycles and Y variable for moment amplitude (N-m) for forged steel and cast iron are given by equations 3.25 and 3.26, respectively (Williams et al., 2007). For corresponding values of the

number of cycles (N) between 10 and 1,000,000, the corresponding values of moment amplitude can be generated for forged steel and cast iron.

$$Y = 2555.8X^{-0.1331} \ldots\ldots\ldots\ldots\ldots\ldots\ldots\ldots (3.25)$$

$$Y = 2144.6X^{-0.1389} \ldots\ldots\ldots\ldots\ldots\ldots\ldots\ldots (3.26)$$

Where: Y is the moment amplitude

X is the number of cycles

Given the corresponding fatigue strength at 10^6 cycles as 359 MPa and 263MPa, alternating stress values corresponding to moment amplitudes in the given range of stress cycles was determined and used in the alternating stress table in ANSYS. Table 3.3 gives the values of alternating stress values generated from moment using excel and values input in ANSYS for analysis of equivalent alternating stress against the number of cycles. The mean stress for the two materials is taken as 0.

***Table 3.3**: Moment, Alternating stress and stress cycles of forged steel and ductile cast iron*

Forged steel		
Moment (N-m)	**Cycles**	**Alternating Stress (MPa)**
1881.165	10	1661.860015
1715.378	20	1515.400221
1518.427	50	1341.409974
1384.608	100	1223.191456
1262.583	200	1115.39154
929.3082	2000	820.9701115
750.1133	10000	662.665619
684.0058	20000	604.2648697
552.1116	100000	487.7468112
503.454	200000	444.7616639
406.3749	1000000	358.9999919
Ductile Cast iron		
Moment (N-m)	**Cycles**	**Alternating Stress (MPa)**
1557.565	10	1304.585064
1414.599	20	1184.838986
1245.545	50	1043.242974
1131.218	100	947.4851284
1027.385	200	860.5167646
746.1622	2000	624.9702374
596.6866	10000	499.7725537
541.9176	20000	453.8991147
433.3575	100000	362.9713963
393.5802	200000	329.6547483
314.7359	1000000	263.6163861

3.9 Summary of the Methods

The details of the specific objectives, methods/ tools, data sources and expected results are summarized in the Table 3.4.

***Table 3.4**: Methodology table*

No	Specific Objective	Method/ Tool	Data Sources
1	To determine the loading and stresses on the top roller in a sugar mill.	Average loading determined from the hydraulic loading (kg/cm^2) on the shaft and average rpm on the shaft from the RPMs monitored from the mill set control panels, force analysis on shaft free body diagram to determine forces on the shaft by theoretical approach	Records of hydraulic pressure read from the pressure gauge for the mill sets, rpm read from the mill control panels, dimensions taken from the roller shaft by direct measurements and shaft drawings
2	To characterize structural properties of the failed top roller components and comparison with international standards.	Experimental tests for chemical composition, microstructure and hardness for the material of the top roller failed components.	Visual inspection, Printout test report
3	To determine the structural transient stress distribution at the different sections of the top roller	Top roller models were generated from solid works and converted to IGES file read by ANSYS software	Forces subject to the shaft from objective 1, monotonic and fatigue properties of forged steel and cast iron from research journals, structural transient analysis by ANSYS workbench.

3.10 Limitations

The Covid-19 pandemic limited access to some of the sugar milling plant identified in this study as research permission was denied by some of the sugar millers as a restriction imposed by the covid-19; only 3 out of the 6 sugar mills granted permission.

CHAPTER FOUR

RESULTS AND DISCUSSIONS

4.0 Introduction

This chapter presents the results obtained from the application of the analytical stress theory of forces subjected to the top roller, experiments conducted on the failed top roller components' materials and structural transient examination of the top roller using finite element analysis. The mechanical performance of the top roller was analysed in this study. The force and stress on the top roller were determined, structural properties of the failed top roller shaft components were characterized using visual inspection, microstructure analysis, chemical composition and hardness tests. And then the structural transient examination of the top roller was done using ANSYS finite element analytical tool.

4.1 Force and Stress on the Top Rollers

The top rollers in the 4-millset sequence are directly attached to and driven by variable frequency motors through a gear reduction system and box couplings of the following specifications: output power of 300 kW, maximum speed of 1200 rpm, and gear ratio of 1:200. The motor Speeds for the four mills during the milling were monitored from the mill control panel and recorded to compute the average speeds for the top rollers in the different mills. Four sets of values of speeds in rpm were noted and recorded given in the Table 4.1.

Table 4.1: *Average top roller speed for Top roller mills 1 through 4*

Mill No.	Speeds (rpm)				Average speed (rpm)	Top Roller Average Speed (rpm)
	Value 1	Value 2	Value 3	Value 4		
Mill 1	717	718	749	751	733.75	3.7
Mill 2	665	664	676	663	667	3.3
Mill 3	676	659	698	700	683.25	3.4
Mill 4	568	624	649	712	638.25	3.2

4.1.1 Top Roller Specifications

The top roller specifications were taken by actual measurement using a string and a tape measure and depth of holes measured using the vernier calliper on reserved top roller similar in specification to the rollers in operation from mill 1 through 4; the top roller specifications are given in Table 4.2 and the hydraulic loading values on the Top Rollers in the 4 mills are given in the Table 4.3.

Table 4.2: *Top Roller Specifications*

SN	Top Roller Specification	Measured Value
1.	Shaft diameter at the roller	920 mm
2.	Shaft diameter at the bearing	386.7 mm
3.	Shaft diameter at the pinion	407.4 mm
4.	Crushing length of shell	1540 mm
5.	Mass of the top roller, m_t	9.3 tonnes (solid works)
6.	Centre of mass of Roller	862.06 mm from the pintle end (generated from solid works)
7.	Mass of the pinion, m_p	1.22 tonnes (solid works)

Table 4.3: *Hydraulic loading values on the top rollers in the 4 mills*

Mill No.	Hydraulic Loadings (kg/cm^2)			Average loading (kg/cm^2)
	Value 1	Value 2	Value 3	
Mill 1	155	160	165	160
Mill 2	205	230	200	211.7
Mill 3	190	210	170	190
Mill 4	210	235	205	216.7

4.1.2 Forces and Stresses on the Top Rollers

4.1.2.1 Forces on the crushing length

The sugarcane Bagasse was crushed with the help of a hydraulic piston with about 20% of the pressure loss to the trash plate, 80% for crushing the bagasse at the discharge opening and delivery opening (Hugot, 2014). Force, F, exerted by hydraulic loading on top roller was calculated using Equation 3.1 and the values of the forces exerted on each of the four top rollers are given in appendix 1(a).

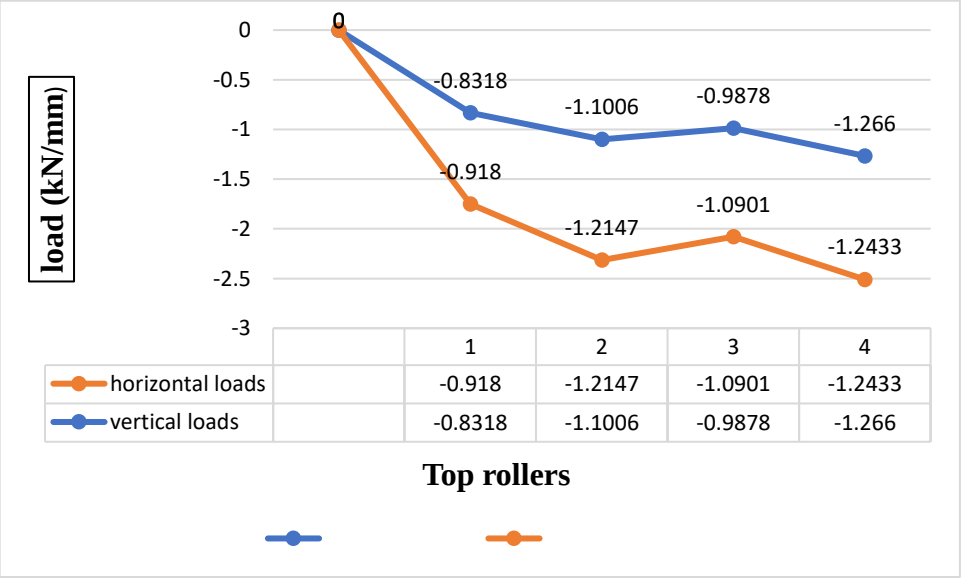

Figure 4.1: Forces on the crushing length of the top rollers

From Figure 4.1, the value of horizontal and vertical crushing force on the crushing length of the top roller 4 is the greatest indicating that the shell grooves are susceptible to breaking and so welding of the grooves will be more often compared to other top rollers in other mill sets; followed by top rollers mill set 2 then 3 and lastly 1.

4.1.2.3 Forces at the pinion

The forces at the pinion are obtained using Equation 3.12, 3.13, 3.14, 3.15, 3.16 and 3.17 and the forces on the pinions for rollers 1, 2, 3, and 4.

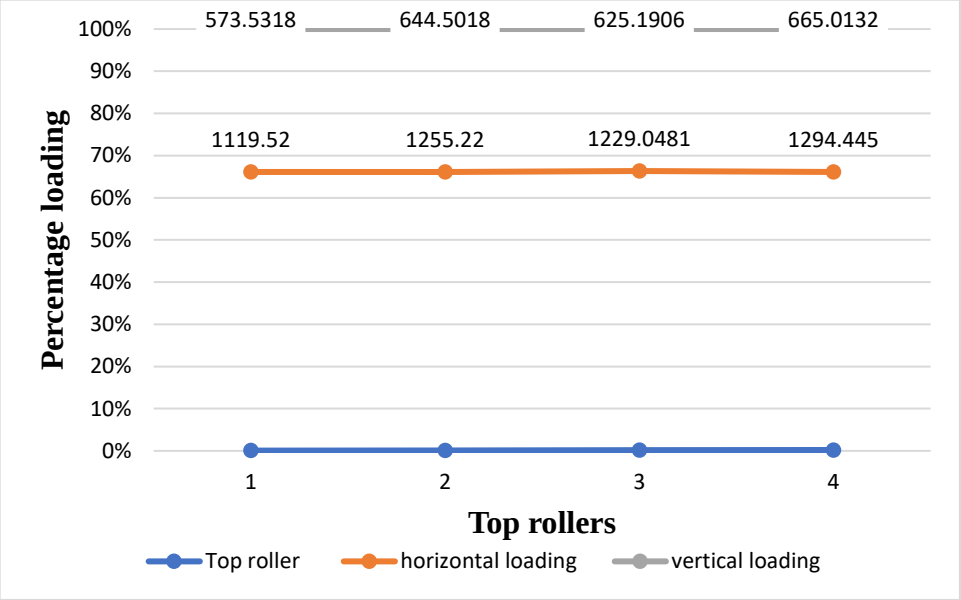

Figure 4.2: Forces on the pinion

From Figure 4.2, the percentage change in the horizontal loading for top roller 1 through 4 is between 60% and 70%, and percentage change in the vertical loading at the pinions for top rollers is 100% and above; indicative of a significant change in the vertical loading than in horizontal loading overtime. Time based failures are more supported by the vertical loadings than horizontal loadings.

4.1.2.4 Reactions at the Bearing

The vertical and the horizontal components of the reactions at the top roller bearings were determined using top roller force diagrams for the 4 Top Rollers.

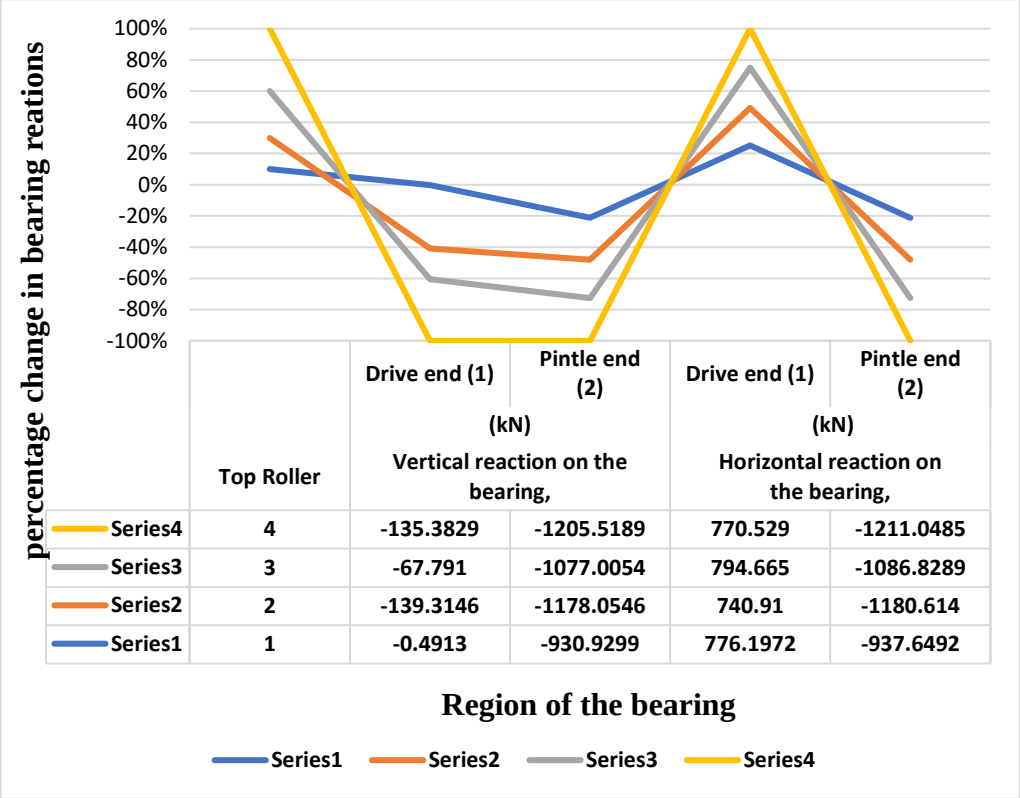

	Top Roller	Vertical reaction on the bearing, (kN) Drive end (1)	Vertical reaction on the bearing, (kN) Pintle end (2)	Horizontal reaction on the bearing, (kN) Drive end (1)	Horizontal reaction on the bearing, (kN) Pintle end (2)
Series4	4	-135.3829	-1205.5189	770.529	-1211.0485
Series3	3	-67.791	-1077.0054	794.665	-1086.8289
Series2	2	-139.3146	-1178.0546	740.91	-1180.614
Series1	1	-0.4913	-930.9299	776.1972	-937.6492

Figure 4.3: Reactions at the bearings

From Figure 4.3, the percentage change in the vertical bearing reactions increases from top roller mill 1 through to mill 4 in the downward direction and the horizontal change in the bearing reactions overtime increases to the left overtime.

4.1.2.5 Forces on the top roller

The summary of vertical and horizontal loading on the Top Rollers 1 through 4 at the pinion, bearing, weight of the Top Roller and Shell, and at the crushing length are shown in the appendix 1(f).

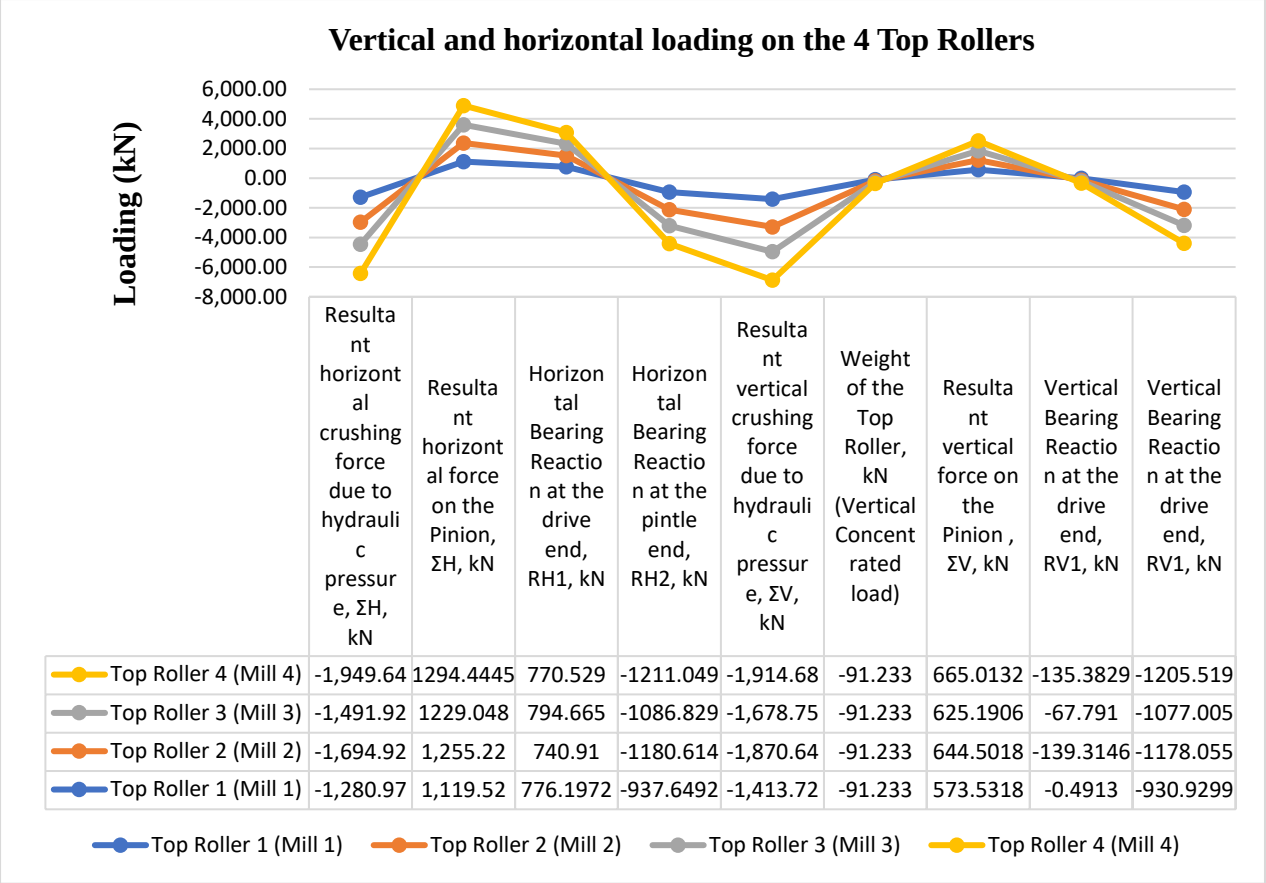

	Resultant horizontal crushing force due to hydraulic pressure, ΣH, kN	Resultant horizontal force on the Pinion, ΣH, kN	Horizontal Bearing Reaction at the drive end, RH1, kN	Horizontal Bearing Reaction at the pintle end, RH2, kN	Resultant vertical crushing force due to hydraulic pressure, ΣV, kN	Weight of the Top Roller, kN (Vertical Concentrated load)	Resultant vertical force on the Pinion , ΣV, kN	Vertical Bearing Reaction at the drive end, RV1, kN	Vertical Bearing Reaction at the drive end, RV1, kN
Top Roller 4 (Mill 4)	-1,949.64	1294.4445	770.529	-1211.049	-1,914.68	-91.233	665.0132	-135.3829	-1205.519
Top Roller 3 (Mill 3)	-1,491.92	1229.048	794.665	-1086.829	-1,678.75	-91.233	625.1906	-67.791	-1077.005
Top Roller 2 (Mill 2)	-1,694.92	1,255.22	740.91	-1180.614	-1,870.64	-91.233	644.5018	-139.3146	-1178.055
Top Roller 1 (Mill 1)	-1,280.97	1,119.52	776.1972	-937.6492	-1,413.72	-91.233	573.5318	-0.4913	-930.9299

Figure 4.4: Horizontal and vertical loading on the Top Roller 1 through 4

The horizontal crushing forces due to hydraulic loading on all Top Rollers are higher than other forces subject to the top roller, followed by vertical crushing forces due to hydraulic loading followed by horizontal forces on the pinions, followed by horizontal bearing reaction at the pintle end, followed by vertical bearing reaction at the drive end, followed by horizontal bearing reaction at the drive end, followed by vertical force at the pinion, followed by vertical bearing reaction at the drive end, and lastly the weight of the top roller; the highest value of loading is 1,949.64kN and 1,914.68kN at Top Roller No.4 which is a horizontal and the vertical crushing force due to the hydraulic loading and the minimum value of loading is 91.233kN which is the weight of the Top Roller 1 through 4. Figure 4.4 shows the Horizontal and vertical loading composition on the Top Rollers 1 through 4.

4.1.3.7 Shear stress at maximum bending moment and stress concentration points

Maximum bending moment for vertical and horizontal loading on the top rollers 1 through 4 was determined from the shear force and bending moment diagrams shown in appendix 1(g) (i), (ii), (iii), (iv), (v), (vi), (vii), and (viii) using Equation 3.22 ; the Top Roller shaft has the maximum bending moment point and three stress concentration points at the drive end shoulder A, at the pintle end named shoulder B, and the keyway. Maximum shear stress is determined using Equation 3.22 and considering stress concentration, maximum shear stress can be determined using equation 3.24. Stress concentration factors at the keyway can be determined using Equations 3.18 and 3.19, and stress concentration factors at the shoulders were determined using Equation 2.4 and stress concentration charts in appendix 5. The values of shear stress at maximum bending moment and stress concentration points are shown in appendix 1(h) (i) and (ii).

Where:

K_t - torsion stress concentration

K_b - bending stress concentration

K_{kt} - torsion stress concentration factors at the keyway

K_{kb} - bending stress concentration factors at the keyway,

K_{bA} - bending stress concentration factors at A

K_{bB} - bending stress concentration factors at B,

K_{tA} - torsion stress concentration factors at A

K_{tB} - torsion stress concentration factors at A and B.

K - Keyway

B - Shoulder B

A - Shoulder A

4.1.3.8 Analysis of stresses on the top roller shafts

Analysis done using XLSTAT at 95% confidence interval, observation (n) =16, DF= 12 and R^2= 0.022 and variable Y is the mean shear stress. The top roller shaft is made up of forged steel 45C8 and cast-iron shell having average yield strengths of 560MPa and 515MPa respectively. Safety of safety for rotating shaft, n =3 (Engineering Toolbox, 2010). The average safe working shear stress values for the shaft and the shell are 186.7MPa and 171.7 MPa. If $\tau_{max} \leq 186.7$Mpa for the shell and 171 for the shaft, then the region is safe otherwise unsafe. Table 4.4 shows the safe and unsafe stresses on the top roller sections in mills 1 through 4 and table 4.5 contains values of minimum and maximum stress on the 4 Top Rollers.

Table 4.4: Safe and Unsafe Top Roller sections from mill 1 through 4

	$\tau_{max}(MPa)$				
Top roller Mill No.	**1**	**2**	**3**	**4**	**Deductions**
Maximum bending moment point	77.8	95.5	88.85	98	safe
Shoulder A	97.1	108.9	106.2	112.3	safe
Shoulder B	200	237	245	244	unsafe
Keyway	191.5	204	191.5	207.75	unsafe
Number of unsafe points	2	2	2	2	

Table 4.5: Minimum and maximum values of stress on Top Rollers 1 to 4

Minimum and Maximum values of stresses on the top rollers					
Variable	**Observations**	**Obs. with missing data**	**Obs. without missing data**	**Minimum**	**Maximum**
Top roller Mill No.1	4	0	4	77.800	200.000
Top roller Mill No.2	4	0	4	95.500	237.000
Top roller Mill No.3	4	0	4	88.850	245.000
Top roller Mill No.4	4	0	4	98.000	244.000
Summary statistics of loading on different shaft sections:					
Variable	**Observations**	**Obs. with missing data**	**Obs. without missing data**	**Minimum**	**Maximum**
Maximum bending moment point	4	0	4	77.800	98.000
Shoulder A	4	0	4	97.100	112.300
Shoulder B	4	0	4	200.000	245.000
Keyway	4	0	4	191.500	207.750

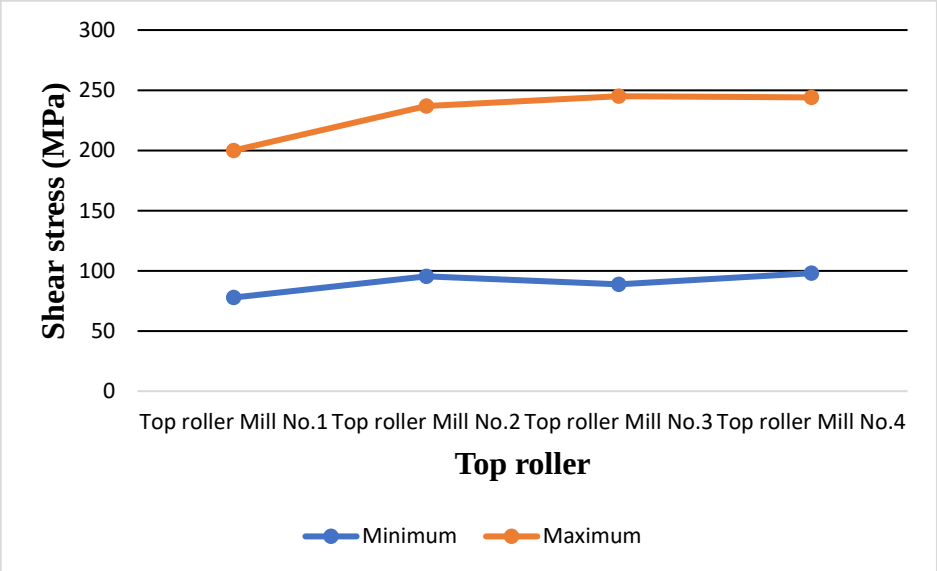

Figure 4.5: Minimum and maximum shear stress on different Top roller Mills

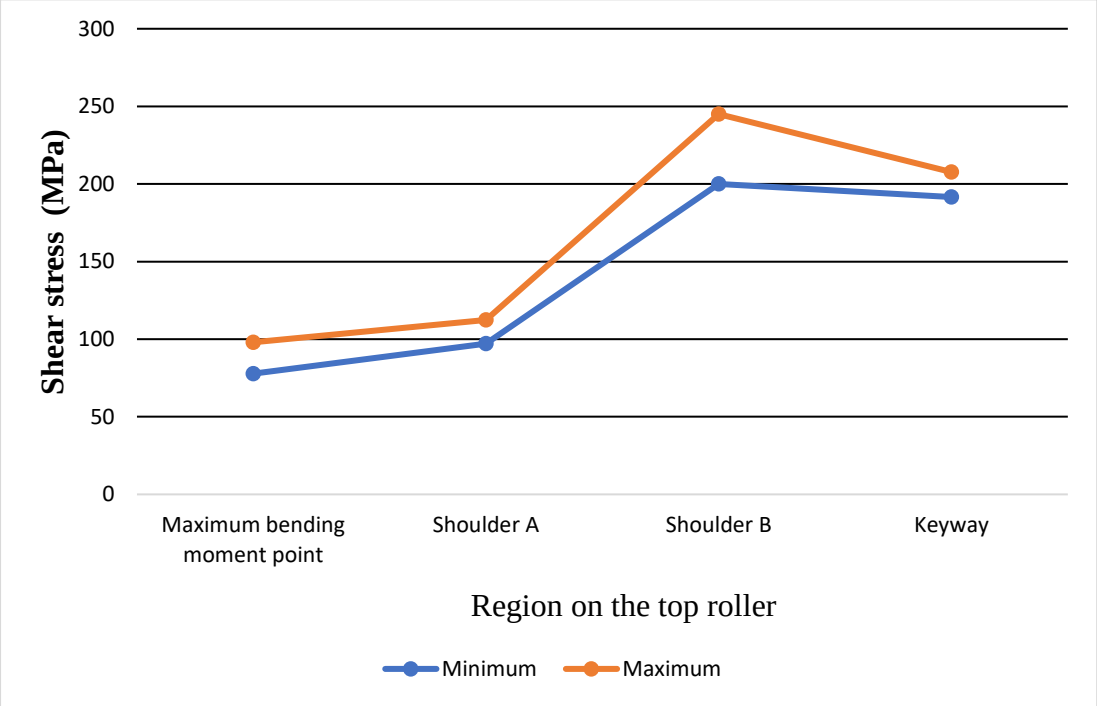

Figure 4.6: Stress distribution on different top roller sections

4.1.3 Discussion of results

The top rollers 1 through 4 are most likely to fail at shoulders A and B and the keyway region with unsafe values of shear stress; The maximum value of shear stress is 245 MPa which is at shoulder B of Top roller 3 then 244 MPa for top roller 4 still at shoulder B. The order of magnitude of the unsafe shear stress on top rollers is from top roller mill No.3 as the highly stressed followed by Mill No.4 then Mill No.2 and lastly Mill No.1 as shown in the Table 4.4 & 4.5 and Figure 4.5. All top roller 1 through 4 experience the highest value of stress at shoulder B, followed by key way, shoulder A and finally the maximum bending point at the drive end as shown in the Figure 4.6. Top rollers in mill 3 and 4 are highly susceptible to failure at shoulder B as they experience the greatest stress at shoulder B than top roller 1 and 2 which is characteristic of failure of the Top roller KE-3 and SB1.

4.2 Characterization of the structural properties of the failed components

4.2.1 Visual inspection of the top roller failed component

4.2.1.1 Macrostructural characterization of top roller KE-3

The features at the parted surfaces including the crack initiation sites, crack progression marks, fracture zone which is a smooth zone in texture and feel, the instantaneous zone which is a rough final fracture are characterized by a rotation- bending fatigue failure and the bigger instantaneous zone reveals that there was a quick change in the loading caused the final failure (Neville, 2015). The details of the fractured surfaces are shown in the Figure 4.7 below.

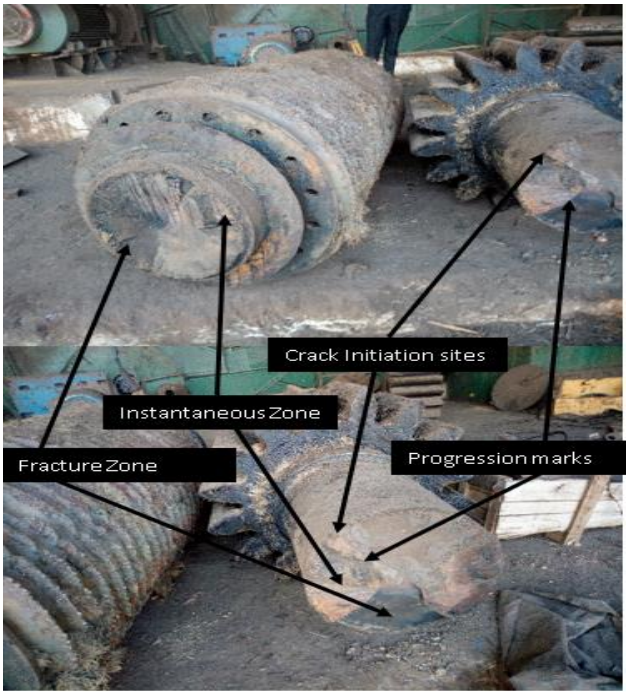

Figure 4.7: Fracture features of the top roller KE-3 relating to specimen AM1

4.2.1.2 Macrostructural characterization of top roller SB1

The fractured surface has the same features as that of KE-3 that is the crack progression marks, initiation sites, fracture zone and instantaneous zone characteristic of rotation-bending fatigue

failure and the bigger instantaneous zone reveals a quick change in loading caused the final failure (Neville, 2015). The details of the fratured surface of the top roller are shown in the Figure 4.8.

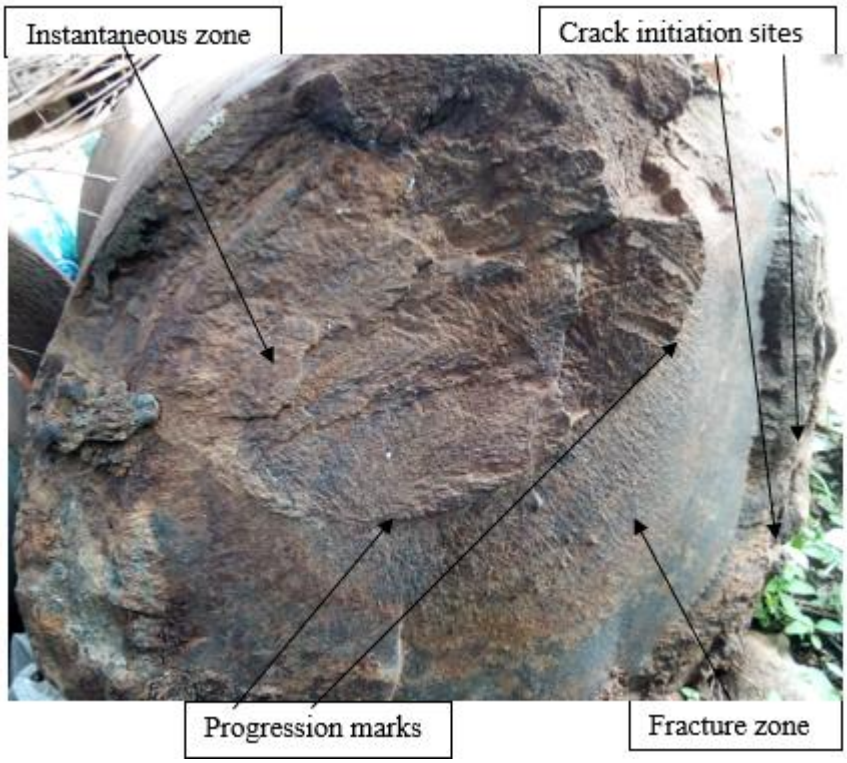

Figure 4.8: Fracture features of the top roller SB1 relating to specimen AM2

4.2.1.3 Macrostructural characterization of top roller KE-8

The fractured surface of the parted square end of the shaft has crack initiation sites, crack progression marks, a smooth feel at the Fracture Zone and a rough Instantaneous zone which characterizes rotational-bending fatigue failure (Neville, 2015). The detailed features of the fractured surface are shown in the Figure 4.9.

Figure 4.9: Fracture feature for Top roller KE-8 relating to unprepared specimen AM3

4.2.1.3 Macrostructural characterization of a box coupling for mill 4

From the photo in figure 4.10, the inner square peripheral of the coupling square hole in which the square end of the top roller shaft is fitted deformed into a circular section. The diameter of the circular section measured 398mm which is approximate 396mm being the diagonal measurement of the square shaft end of side 280mm by 280mm evidence of the square end wobbling inside the box coupling resulting in wearing away material.

Figure 4.10: Fracture features of a box coupling relating to specimen BM4

4.2.1.4 Discussion of macrostructural characterization of the specimens

The fracture characterization reveals that top rollers are highly stressed at the square ends and the shoulder between the journal bearings and the crushing shell on the drive end causing the bare shaft and the square coupling to break (Karthi and Emmanual, 2018). From objective 1, shoulder B subjected to the highest value of stress which could have originated the failure related to the top rollers KE3 and SBI in the same region and the high stress values at the keyway could have contributed to the failure of the square coupling. The summary of the macroscopic failure associated to the four specimens are presented in the table 4.6 below.

Table 4.6: *Regions of Macrostructural failures*

Specimen	Failed component (broken Section of Shaft)
AM1	Bare shaft (Shoulder between journal bearing and the crushing shell)
AM2	Bare shaft (Shoulder between journal bearing and the crushing shell)
AM3	Square end (shoulder between the pinion and square end)
BM4	Square coupling (at the square end)

4.2.2 Microstructural characterization of the failed component

The micrographs of the prepared specimens of the failed components AMi1, AMi2, AMi3 and BMi4 were taken by the Kruss Optronic Metagraphical Microscope and analysed accordingly to characterize the component failure.

4.2.2.1 Microstructure for Specimen AMi1

The pearlite and the ferrite phases are segregated in the microstructure indicating that the top roller shaft was normalized (Al-Hassan et al., 1998). The pearlite phase is bigger than ferrite giving the material better hardness properties to resist crack formation although crack failure could still be accelerated by corrosion agents due to high carbon content in the material (Taylor and Knot, 1981; Muñoz Cubillos *et al.,* 2016). The pearlite phase contains a larger brown zone indicating a high Manganese content in the steel which increases toughness but many of the alloy modifications deplete the normal high reserve of toughness causing early failure of the component in service (David Havel, 2017). Figure 4.11 shows the micrographs of specimen AMi1.

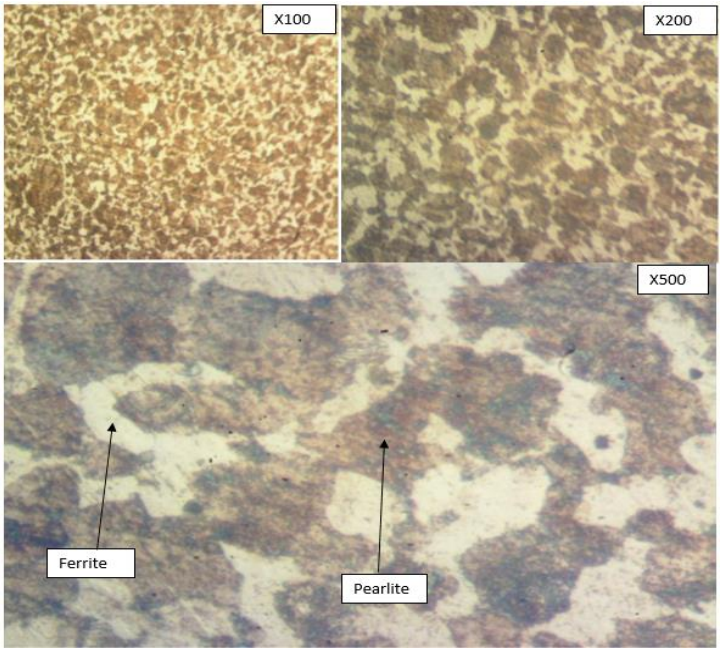

Figure 4.11: Micrographs for AMi1(X100, X200, X500)

4.2.2.2 Microstructure for specimen AMi2 by Kruss Optronic Metagraphical Microscope

The pearlite phase is segregated from the ferrite phase indicating that the shaft was normalized (Al-Hassan et al., 1998). The pearlite phase is bigger than the ferrite phase giving the shaft a better hardness property (Taylor and Knot, 1981; Muñoz Cubillos *et al.*, 2016). The microstructure is characterized by a larger brown zone in the pearlite phase than the black zone indicating the presence of Manganese. The pearlite phase contains a larger brown zone indicating a high Manganese content in the steel which increases toughness but many of the alloy modifications deplete the normal high reserve of toughness causing early failure of the component in service (David Havel, 2017). Figure 4.12 shows the micrographs of specimen AMi2.

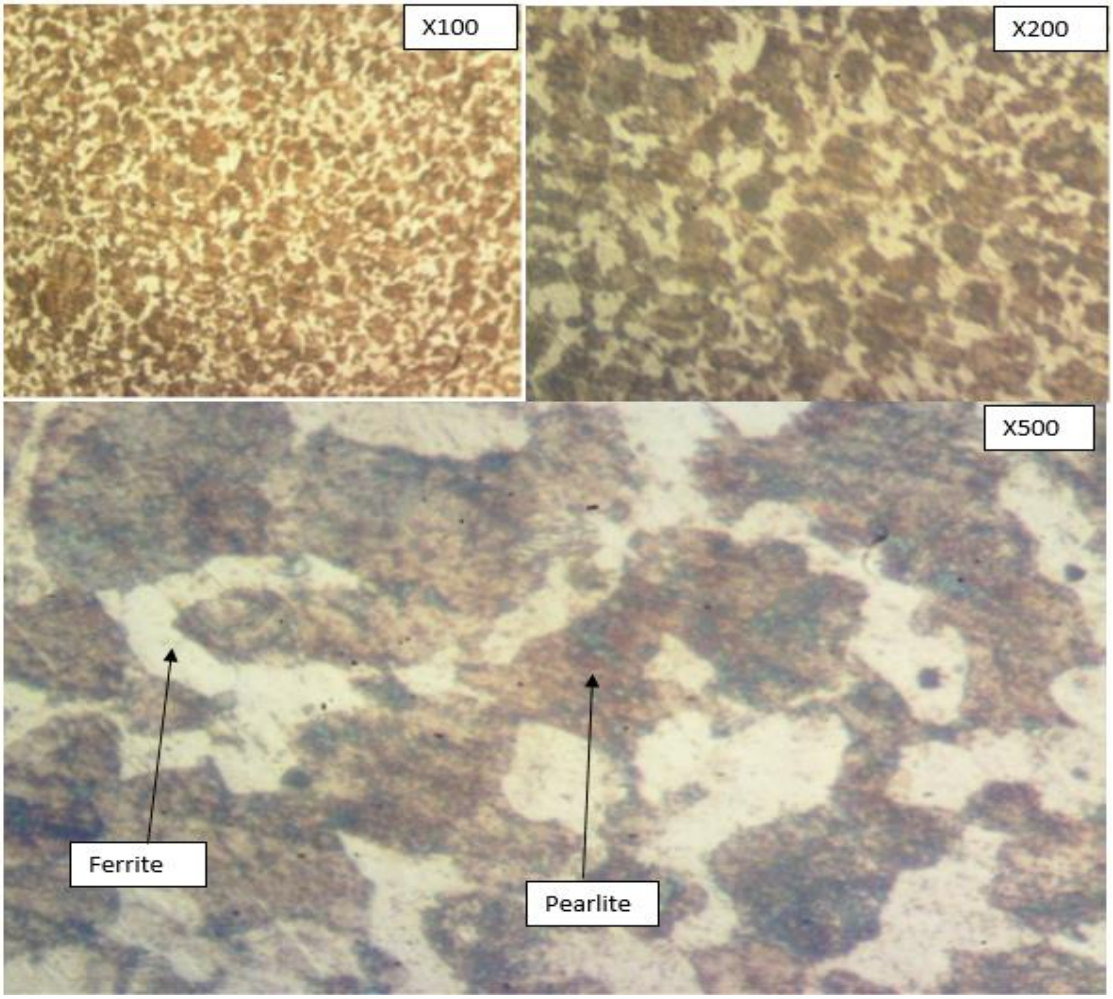

Figure 4.12: Micrographs for AMi2(X100, X200, X500)

4.2.2.3 Microstructure for specimen AMi3

The pearlite phase is segregated from the ferrite phase hence the shaft was normalized which improves the hardness properties of the material (Al-Hassan et al., 1998). The pearlite phase is bigger than the ferrite phase which reflects a high value of hardness and contains black and brown zones with the black zone slightly dominating the brown zone (Taylor and Knot, 1981; Muñoz Cubillos *et al.*, 2016; David Havel, 2017). Figure 4.13 shows the micrographs of the specimen AMi3 taken by the Kruss Optronic Metagraphical Microscope.

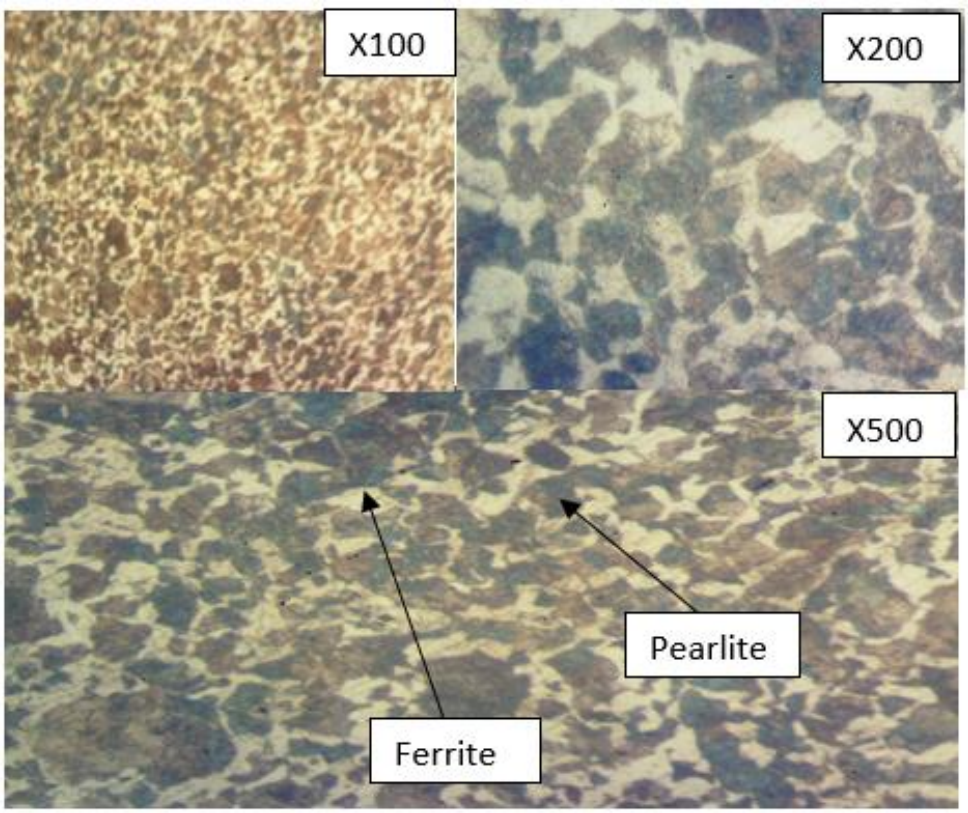

Figure 4.13: Micrographs for AMi3 (X100, X200, X500)

4.2.2.4 Microstructure for specimen BMi4

The pearlite phase is segregated from the ferrite phase therefore the steel is normalized to improve the material hardness value (Al-Hassan et al., 1998). The ferrite phase is bigger than the pearlite

phase therefore the material is averagely harder (Taylor and Knot, 1981; Muñoz Cubillos *et al.*, 2016). Figure 4.14 shows the micrographs of the specimen BMi4 taken by the by Kruss Optronic Metagraphical Microscope.

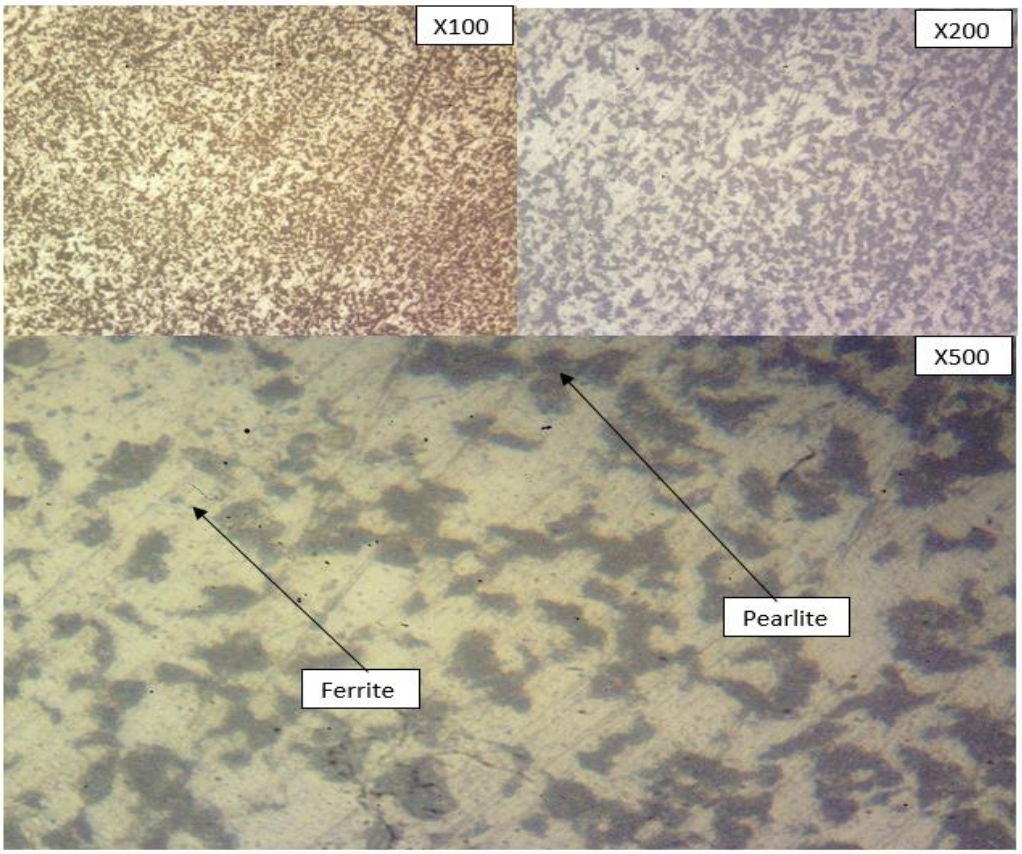

Figure 4.14: Micrographs for BMi4 (X100, X200, X500)

4.2.2.4 Discussion of the microstructural examination of the specimens

AMi1, AMi2, AMi3 and BMi4 samples are normalized steels that reduce internal stresses and increases the toughness of the material (Al-Hassan et al., 1998). The first three specimen micrographs have brown and black patches in the pearlite phase indicating the presence of manganese and carbon (David Havel, 2017). BMi4 has dominantly black patches in the pearlite phase. Table 4.7 shows a summary of the microstructural characterization of the failed components.

Table 4.7: *Summary of the Microstructural characterization of failed components*

Specimen	Microstructural characterization
AMi1	*Pearlite phase segregated from ferrite with brown patches in the pearlite zone*
AMi2	*Pearlite phase segregated from ferrite with brown patches in the pearlite zone*
AMi3	*Pearlite phase segregated from ferrite with brown patches in the pearlite zone*
BMi4	*Pearlite phase segregated from ferrite with black patches in the pearlite zone*

4.2.3 Chemical composition characterization of the failed components

4.2.3.1 Chemical composition characterization for specimen AC1

The average value of carbon indicates low carbon steel since it is below 0.3% and not in the required range of (0.4%-0.5%), the values of silicon is 3.3% above the required range of (0.15%-0.35%) and manganese 17.58% far above the required range of 0.6% to 0.9%. Therefore, the shaft is manganese steel and does not conform to IS: 1570-1979/ BS EN ISO 683-1:2018 for forged steel 45C8. Table 4.8 shows the average chemical composition of specimen AC1.

Table 4.8: Average values of the chemical composition of specimen AC1

Test Runs	C (%)	Si (%)	Mn (%)	S (%)	P (%)
1	0.222	3.35	17.66	0.0005	0.0005
2	0.223	3.32	17.58	0.0005	0.0005
3	0.224	3.25	17.50	0.0005	0.0005
4	0.224	3.28	17.48	0.0005	0.0005
Average	**0.223**	**3.3**	**17.555**	**0.0005**	**0.0005**

4.2.3.2 Chemical composition characterization for specimen AC2

The average value of carbon indicates low carbon steel since it is below 0.3% and not in the required range of (0.4%-0.5%), the values of silicon is 3.7525% above the required range of (0.15%-0.35%) and manganese 18.5775% far above the required range of 0.6% to 0.9%. Therefore, the shaft is manganese steel and does not conform to IS: 1570-1979/ BS EN ISO 683-1:2018 for forged steel 45C8. Table 4.9 shows the average chemical composition of specimen AC2.

Table 4.9: *Average values of the chemical composition for specimen AC2*

Test Runs	C (%)	Si (%)	Mn (%)	S (%)	P (%)
1	0.0289	3.89	18.78	0.0005	0.0005
2	0.0282	3.84	18.64	0.0005	0.0005
3	0.226	3.45	18.22	0.0005	0.0005
4	0.0378	3.83	18.67	0.0005	0.0005
Average	**0.16045**	**3.7525**	**18.5775**	**0.0005**	**0.0005**

4.2.3.3 Chemical composition characterization for specimen AC3

The average value of carbon indicates low carbon steel since it is below 0.2255% and not in the required range of (0.4%-0.5%), the values of silicon is 3.35% above the required range of (0.15%-0.35%) and manganese 17.58% far above the required range of 0.6% to 0.9%. Therefore, the shaft is manganese steel and does not conform to IS: 1570-1979/ BS EN ISO 683-1:2018 for forged steel 45C8. Table 4.10 shows the average chemical composition of specimen AC3

Table 4.10: *Average values of the chemical composition for specimen AC3*

Test Runs	C (%)	Si (%)	Mn (%)	S (%)	P (%)
1	0.223	3.37	17.40	0.0005	0.0005
2	0.224	3.35	17.39	0.0005	0.0005
3	0.229	3.31	17.40	0.0005	0.0005
4	0.226	3.37	17.35	0.0005	0.0005
Average	**0.2255**	**3.35**	**17.385**	**0.0005**	**0.0005**

4.2.3.4 Chemical composition characterization for specimen BC4

The average percentage of carbon content is 0.3058% which is medium carbon steel slightly above the recommended range of 0.18% -0.25%, Mn content is slightly below the standard range of 1.2% to 1.6%. Therefore, the coupling material BH4 does not conform to **BS 3100: 1976**. Table 4.11 shows the average chemical composition of specimen BC4.

Table 4.11: Average values of the chemical composition for specimen BC4

Test Runs	C (%)	Si (%)	Mn (%)	S (%)	P (%)
1	0.3427	0.4310	1.0055	0.0358	0.0046
2	0.3165	0.4240	0.9708	0.0093	0.0020
3	0.2927	0.4122	0.8995	0.0065	0.0017
4	0.3061	0.4197	0.8890	0.0048	0.0027
5	0.3076	0.4226	0.9240	0.0117	0.0029
6	0.3239	0.4214	0.8771	0.0083	0.0015
7	0.2956	0.4226	0.8827	0.0031	0.0009
8	0.2829	0.4144	0.8477	0.0034	0.0009
9	0.2868	0.3896	0.8209	0.0050	0.0011
10	0.3032	0.3896	0.8209	0.0050	0.0011
Average	**0.3058%**	**0.4189%**	**0.8963%**	**0.0092%**	**0.0021%**

4.2.3.5 Discussion of results of Chemical composition

All the four specimens are low carbon steels but the three specimens ACI, AC2 and AC3 have anomaly high values of silicon lying between 2% and 4% and high values of manganese lying between 16% and 20% characterized by brown patches in the pearlite phase which does not conform to the recommended standard of IS: 1570-1979 for forged steel 45C8 (Bureau of Indian Standard, 2001, p. 1). The anomaly high value of silicon and manganese in these low carbon steels increases hardness but reduces the stacking fault energy of the material which makes cracks easily develop on the material surface (Yonezawa *et al*., 2013). This could be the reason for the fatigue fracture of the top roller shaft before it served the expected time. BC4 on the other hand is medium carbon steel that has all values of carbon, silicon, Manganese, Sulphur and phosphorous between 0% and 1% and does not conform to BS 3100: 1976 for steel A4 (Singapore Institute of Standards and Industrial Research, 1976). Table 4.12 shows the summary of the average chemical composition of the specimens and figure 4.15 presents the relative chemical compositions of elements for the specimens.

Table 4.12*: Summary of average specimen chemical composition*

Specimen	C (%)	Si (%)	Mn (%)	S (%)	P (%)
AC1	0.223	3.3	17.555	0.0005	0.0005
AC2	0.16045	3.7525	18.5775	0.0005	0.0005
AC3	0.2255	3.35	17.385	0.0005	0.0005
BC4	0.3058%	0.4189%	0.8963%	0.0092%	0.0021%

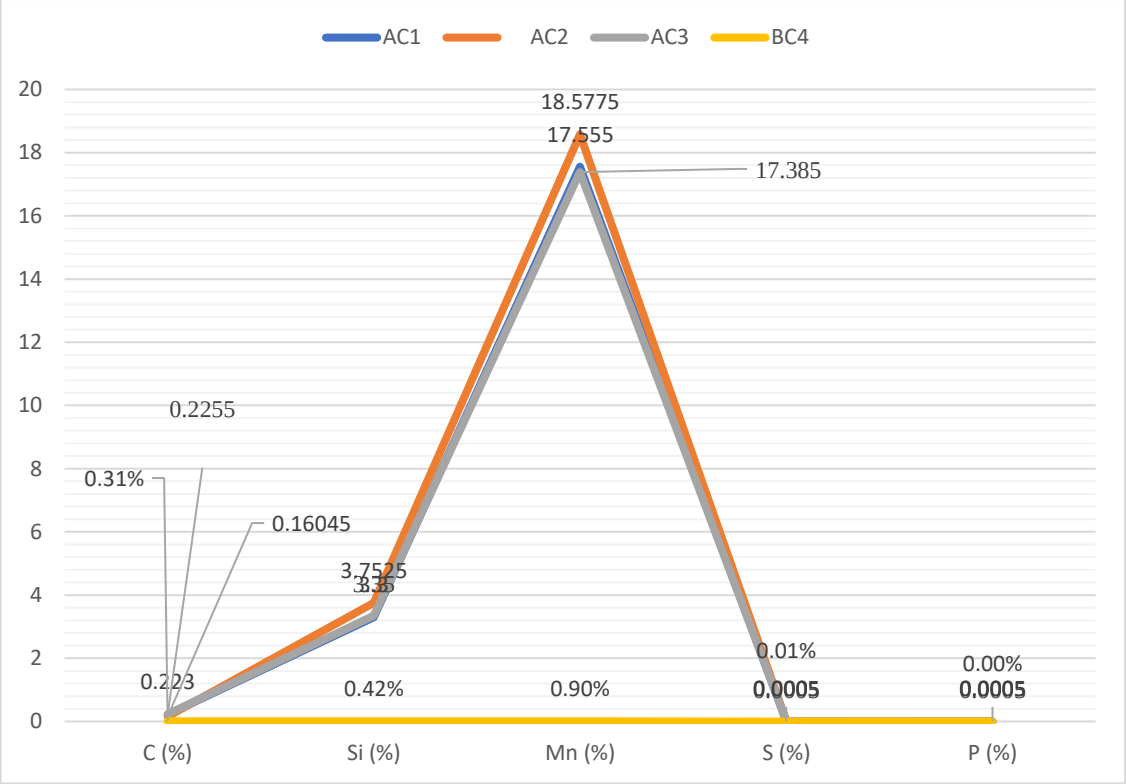

Figure 4.15: Relative Average chemical compositions of the specimens

4.2.4 Hardness characterization of the failed components

4.2.4.1 Hardness characterization of AH1

Hardness was determined by the HRC Mutitoyo Digital Hardness Testing Machine was the average values of hardness for the components were compared to that of the standard material. The value of 30.97 HRC was equivalent to 277HB from online conversion tables (UK steel stockholders and suppliers, 2021). The hardness is above the minimum hardness of 175HB hence the hardness conforms to *IS: 1570-1979/ BS EN ISO 683-1:2018* for forged steel 45C8 (Bureau of Indian Standard, 2001, p. 1). The hardness of the material has a relationship with the fatigue strength of the material since it falls in the range 163 to 536 HB but the relationship is inconsistent for steels with metallic inclusions (Hassan, 2017; Casagrande *et al.*, 2011). Table 4.13 shows the average HRC value for AH1.

Table 4.13: *Average values of hardness for AH1*

Indentations	1	2	3	4	5	6	Average HRC
AH1	30.5	32.7	31.1	32.1	29.1	30.2	30.95

4.2.4.2 Hardness characterization of AH2

The value of 31.2 HRC was equivalent to 290HB from online conversion tables (UK steel stockholders and suppliers, 2021). The hardness is above the minimum hardness of 175HB hence the hardness conforms to IS: 1570-1979/ **BS EN ISO 683-1:2018** for forged steel 45C8 (Bureau of Indian Standard, 2001, p. 1). The hardness of the material has a relationship with the fatigue strength of the material since it falls in the range 163 to 536 HB but the relationship is inconsistent for steels with metallic inclusions (Hassan, 2017; Casagrande et al., 2011). Table 4.14 shows the Average HRC value of hardness for AH2.

Table 4.14*: Average values of hardness for AH2*

Indentations	1	2	3	4	5	6	Average HRC
AH2	31.8	31.6	30.5	31.1	32.0	30.2	**31.2**

4.2.4.3 Hardness characterization of AH3

The value of 31.38 HRC was equivalent to 290HB from online conversion tables (UK steel stockholders and suppliers, 2021). The hardness is above the minimum hardness of 175HB hence the hardness conforms to IS: 1570-1979/ **BS EN ISO 683-1:2018** for forged steel 45C8 (Bureau of Indian Standard, 2001, p. 1). The hardness of the material has a relationship with the fatigue strength of the material since it falls in the range 163 to 536 HB but the relationship is inconsistent for steels with metallic inclusions (Hassan, 2017; Casagrande et al., 2011). Table 4.15 shows the Average values of HRC for AH3

Table 4.15: *Average values of hardness for AH3*

Indentations	1	2	3	4	5	6	Average HRC
AH3	31.2	30.7	31.3	30.7	31.9	32.5	**31.38**

4.2.4.4 Hardness characterization of BH4

The average value of 21 HRC was equivalent to 229HB which is above the range of 152-207HB which meets the requirement of **BS 3100: 1976** (UK steel stockholders and suppliers, 2021; Singapore Institute of Standards and Industrial Research, 1976; Qingdao Casting Quality Industrial Co., Ltd, 2009). The value of hardness for the shaft is more than that of the coupling hence the square end can wear away material from the square hole of the box coupling. Table 4.16 shows the average HRC for BH4.

Table 4.16: *Average values of hardness for BH4*

Indentations	1	2	3	4	5	6	Average HRC
BH4	20.9	21	21.1	20.8	21.2	21	**21**

4.2.4.5 Discussion of results for specimen hardness

The average hardness for the failed bare shaft components AH1, AH2 and AH3 lie between an average hardness of 30 HRC and 32.5 HRC which is greater than the average hardness of the coupling material BH4 by about 32.65%. Therefore, the box coupling is expected to fail before the bare shaft. Table 4.17 is the summary of the 4-specimen hardness and figure 4.16 is the graphical representation for hardness of the 4 failed components.

Table 4.17: *Summary of specimen hardness*

Specimen	Average hardness (HRC)
AH1	30.97
AH2	31.2
AH3	31.38
BH4	21

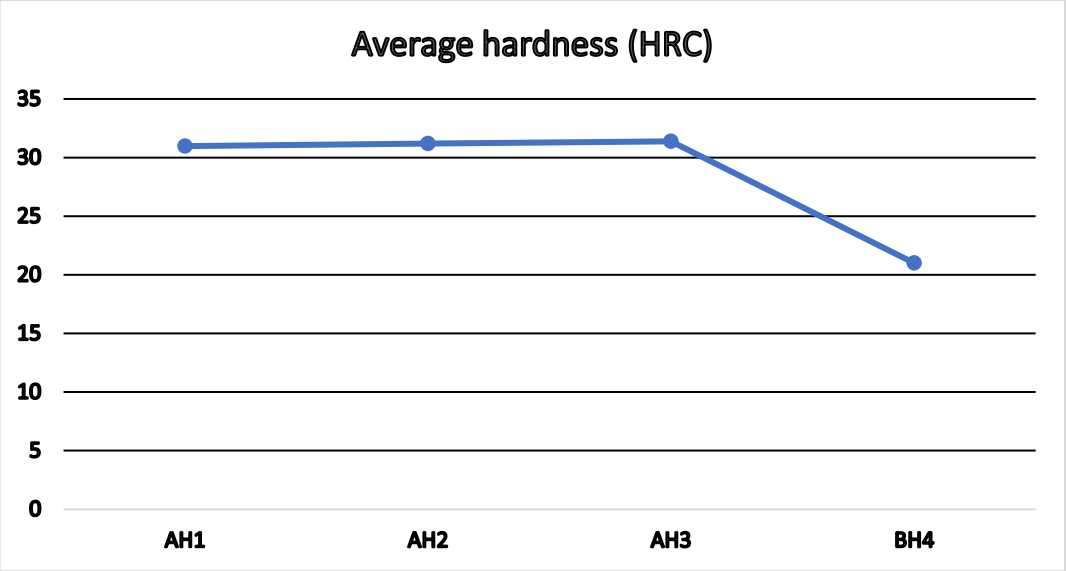

Figure 4.16: Average hardness for the 4 failed shaft material specimens

4.3 Structural transient examination of stress distribution on the Top rollers

4.3.1 Top roller geometry

The top roller geometry was generated by solid works and converted to IGES file format for analysis in the ANSYS software. The solid shaft model generated in the ANSYS work environment is shown in the figure 4.17. Ductile cast iron crushing roller shell was assigned part 1 and the forged steel bare shaft was assigned part 2.

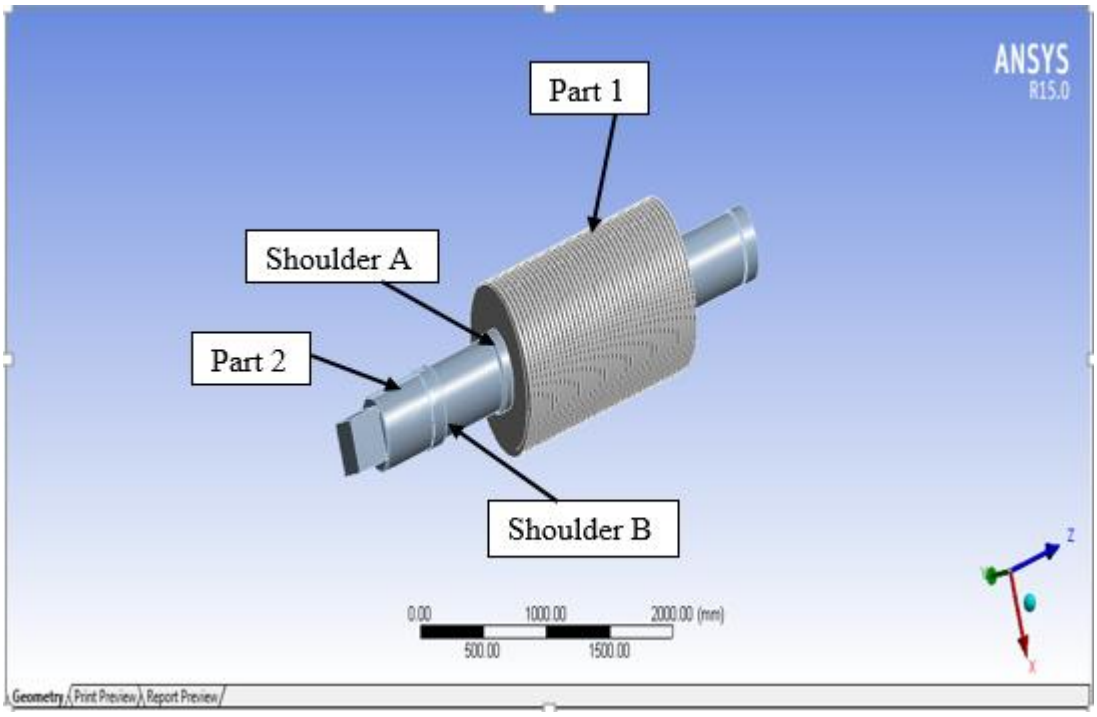

Figure 4.17: Top roller Solid Model

4.3.2 Mesh generation

Mesh generated on part 1 consists of 35417 nodes and 18604 elements with unspecified mesh metric and part 2 consists of 17434nodes and 10620 elements for all the four top rollers.

4.3.3 Analytical set-up

The mechanical APDL solver was employed for the fully defined structural transient analysis of the top roller under dynamic loading using defined rotational speed and forces subject to the top rollers from objective 1 at an environmental temperature of 22^{o}C and the top roller under standard earth gravitational effect and having fixed supports at the bearing positions of the top roller. The loading on the top roller is a constant amplitude load fully reversed for a load ratio between 1.2 and -1.2 as shown in the figure 4.18 below.

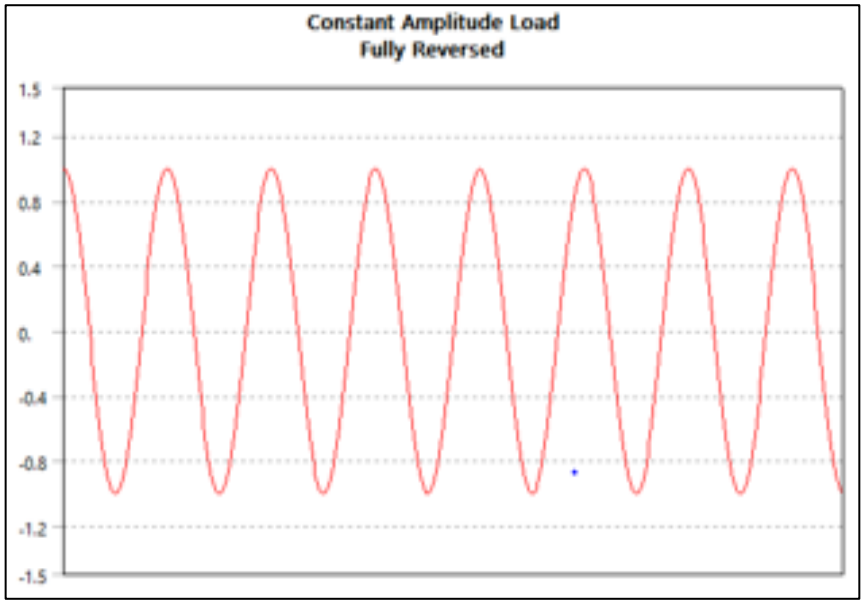

Figure 4.18: Fully reversed constant Amplitude load for top rollers mill 1 through 4

4.3.4 Results of the transient structural analysis of top rollers Mill 1 to Mill 4

The generated top roller was subjected to forces and speeds from objective 1, the monotonic and cyclic properties of forged steel and cast iron were input in the software. The top roller geometry was analysed for maximum and minimum equivalent alternating stress, total deformation, safety factor and life.

4.3.4.1 Results of equivalent alternating stress analysis on top roller mill 1

The value of maximum equivalent alternating stress is 181.92MPa which is subjected on part 2 at the shoulder region next to the keyway and the value of minimum equivalent alternating stress is 2.4085e-003 MPa subjected on part 1 at the pintle end. Figure 4.19 shows the equivalent alternating stress distribution on the top roller mill 1.

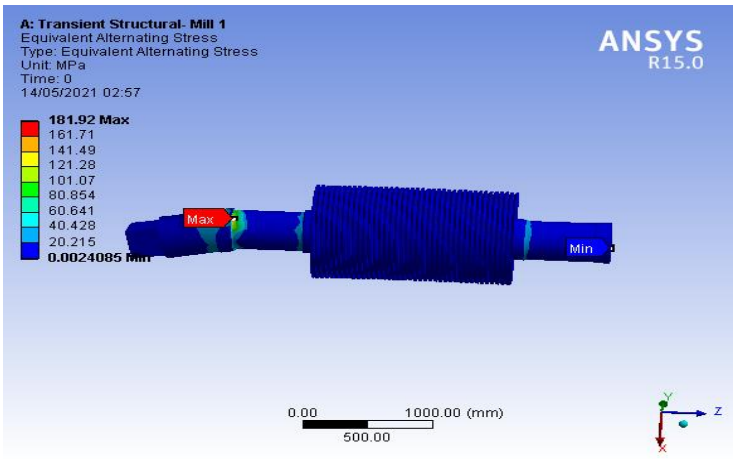

Figure 4.19: Equivalent Alternating stress for mill 1

4.3.4.2 Results of safety factor and life for top roller mill 1

The minimum value of factor of safety is 1.9734 on part 2 of the top roller at the shoulder next to the keyway and the design life is 1.e+009 cycles and the minimum service life of the top roller is 1.e+006 cycles which occur on part 1 at the crushing rollers for a loading variation from 50% to 150%. Figure 4.20 shows the minimum and maximum values of safety factor and life on the top roller mill 1.

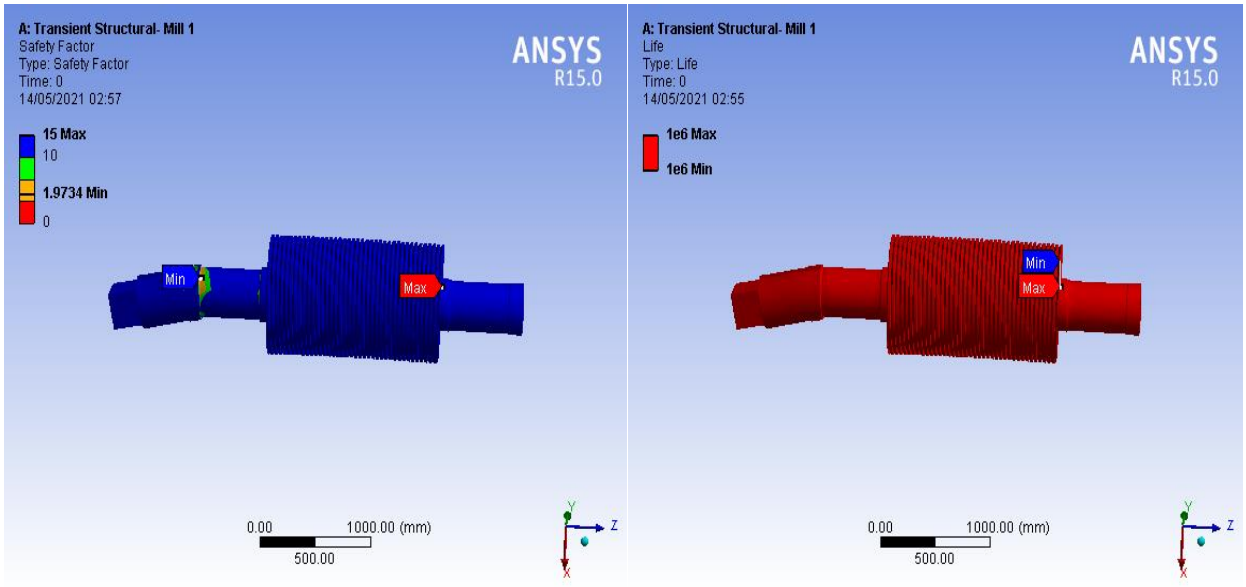

Figure 4.20: Safety factor and life for top roller mill 1

4.3.4.3 Results of total deformation analysis on top roller mill 1

The maximum value of deformation of the top roller mill 1 is 0.24462mm at the square end of part 2 and the minimum deformation value is 0mm at the pintle end of part 2. Figure 4.21 shows the regions and values of minimum and maximum total deformation on top roller mill 1.

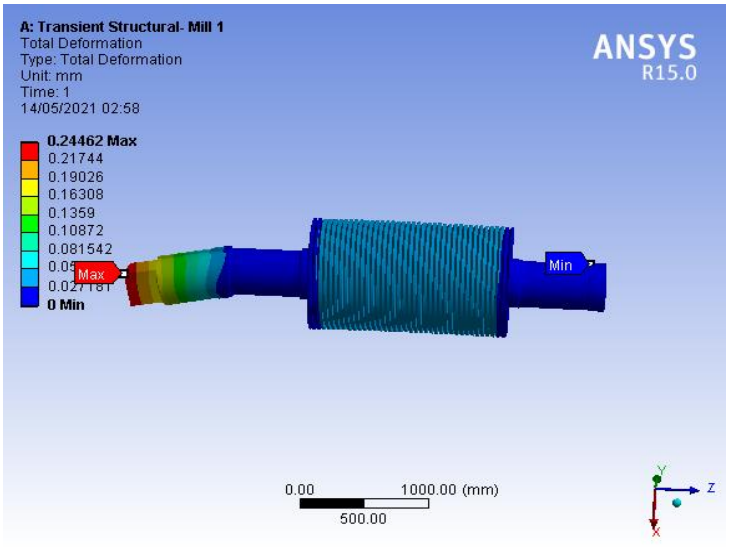

Figure 4.21: Total deformation of top roller mill 1

4.3.4.4 Results of the equivalent alternating stress analysis of top roller mill 2

The maximum value of equivalent alternating stress on the top roller mill 2 is 204.08MPa at the shoulder next to the keyway on part 2 and the minimum value is 2.2819e-003 MPa on part 2 at the pintle end. Figure 4.22 shows equivalent stress distribution on the top roller mill2.

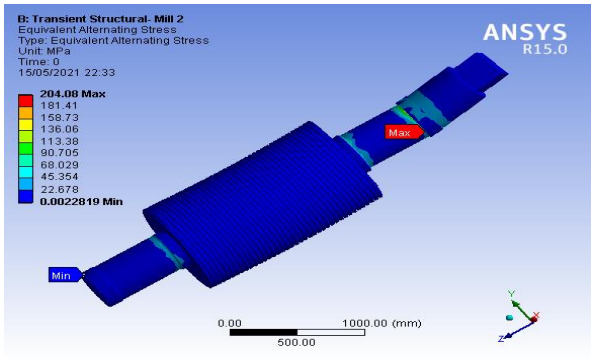

Figure 4.22: Equivalent Alternating Stress for top roller mill 2

4.3.4.5 Results of safety factor and life analysis of top roller mill 2

The minimum value of the factor of safety is 1.7591 on part 2 at the shoulder next to the keyway and the minimum life of the top roller is 1.e+006 cycles on part 1 at the crushing rollers for a loading variation from 50% to 150%. Figure 4.23 shows minimum and maximum values of safety factor and life at different regions of the top roller mill 2.

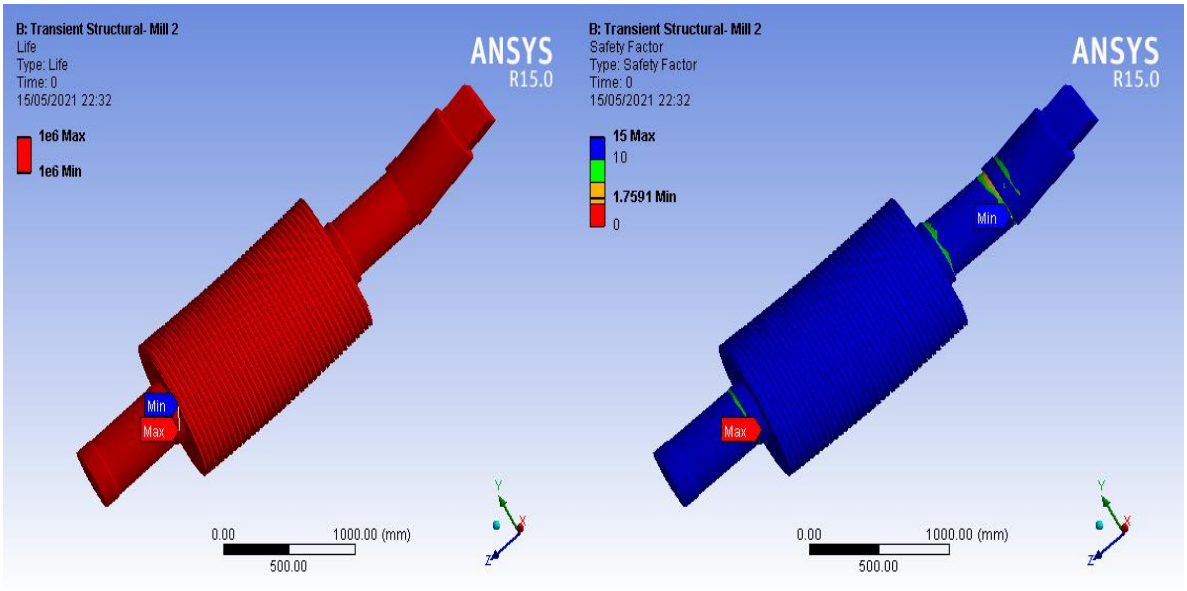

Figure 4.23: Safety factor and life for mill 2

4.3.4.6 Results of total deformation analysis of top roller mill 2

The maximum value of deformation on the top roller mill 2 is 0.27441mm at the square end of part 2 and the minimum deformation is 0mm at the pintle of part 2. Figure 4.24 shows regions and values of maximum and minimum total deformation on top roller mill 2.

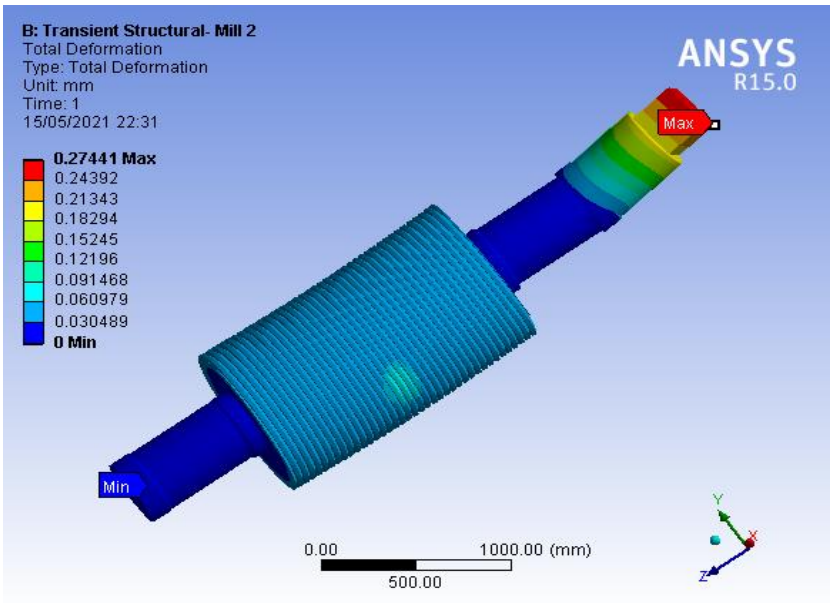

Figure 4.24: Deformation for top roller mill 2

4.3.4.7 Results of the equivalent alternating stress analysis of top roller mill 3

The maximum value of alternating stress on the top roller mill 3 is 199.27 MPa subjected to part 2 at the shoulder next to the keyway and the minimum value is 2.4924e-003 MPa subjected to part 2 at the pintle end. Figure 4.25 shows equivalent alternating stress distribution on the different regions of the top roller.

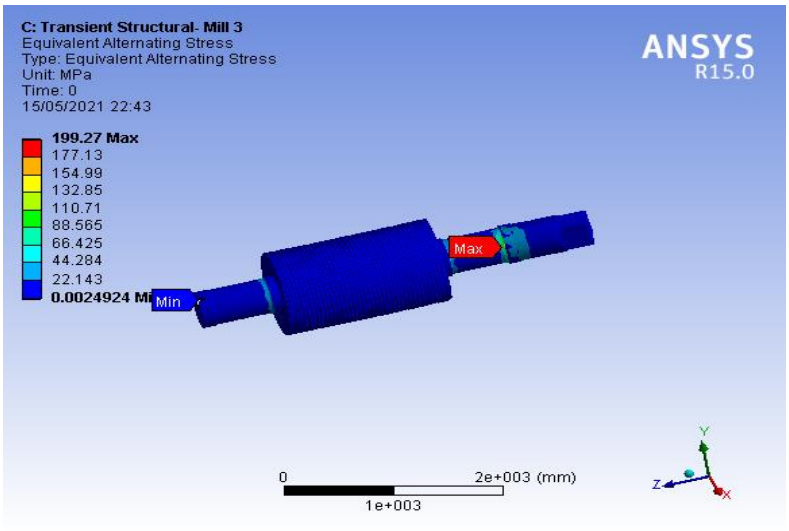

Figure 4.25: Equivalent Alternating Stress for top roller mill 3

4.3.4.8 Results of safety factor and life analysis of top roller mill 3

The minimum value of the safety factor is 0.43258 at the shoulder next to the keyway for part 2 and the design life of the top roller is 1.e+009 cycles and the minimum value of life is 25981 cycles at the shoulder next to the keyway of part 2 for a load variation from 50% to 150%. Figure 4.26 shows the minimum and maximum safety factor and life of the top roller mill 3.

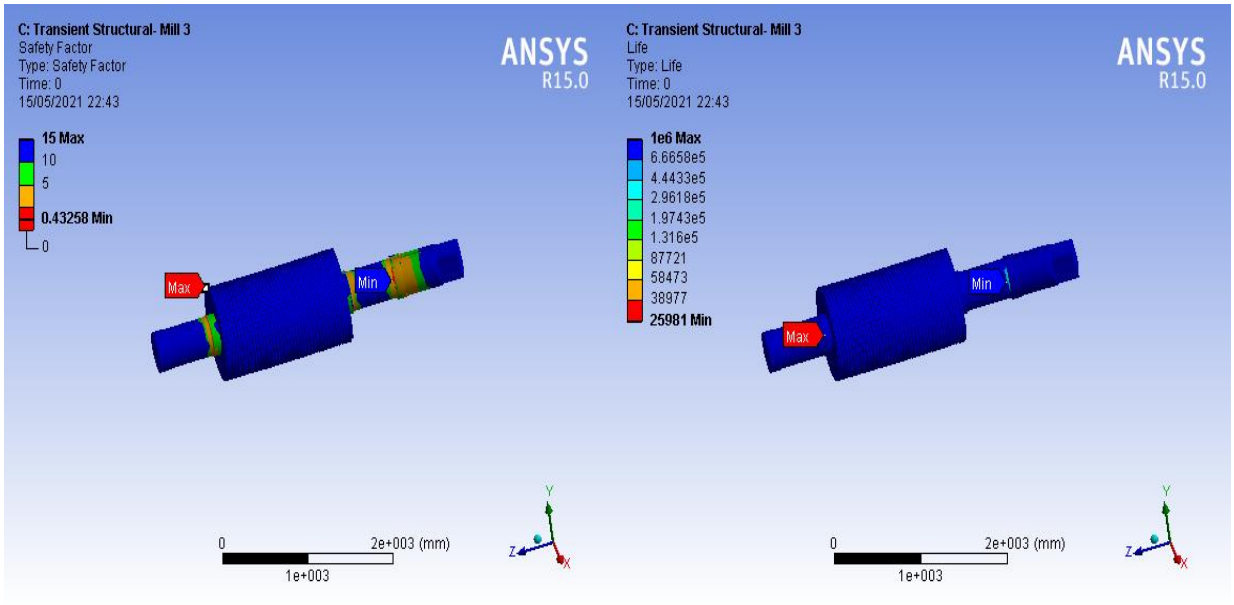

Figure 4.26: Safety factor and life for top roller mill 3

4.3.4.9 Results of total deformation analysis of top roller mill 3

The maximum value of deformation on the top roller mill 3 is 0.29632mm at the square end of part 2 and the minimum value is 0mm at the pintle end of part 2. Figure 4.27 shows the total deformation in mm at the different sections of the top roller mill 3.

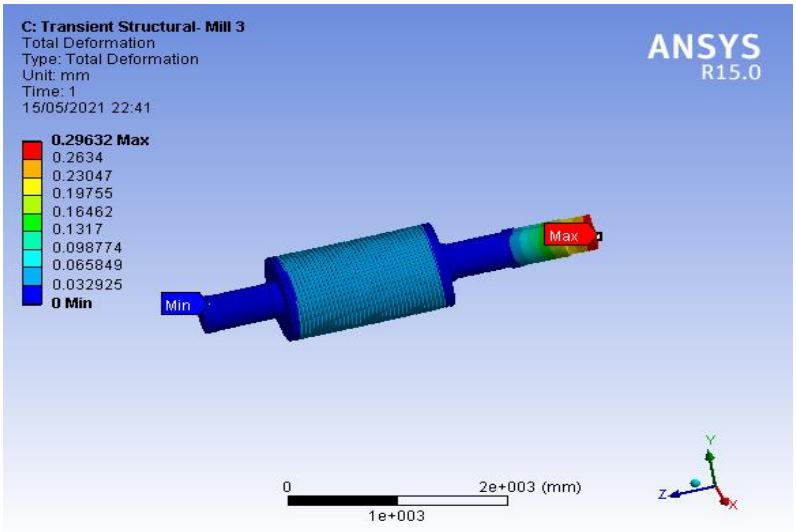

Figure 4.27: Total deformation for top roller mill 3

4.3.4.10 Results of the equivalent alternating stress analysis of top roller mill 4

The maximum value of equivalent alternating stress on the top roller mill 4 is 210.49MPa subject to part 2 at the shoulder next to the keyway and the minimum value is 2.2703e-003 MPa subject to part 2 at the pintle end. Figure 4.28 shows the distribution of the alternating stress at the different sections of the top roller mill 4.

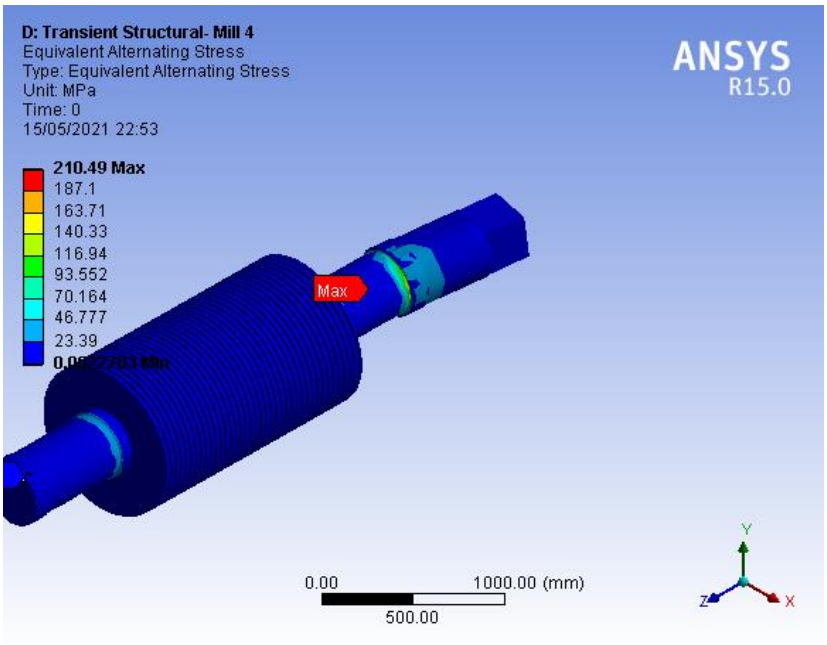

Figure 4.28: Equivalent Alternating Stress for top roller mill 4

4.3.4.11 Results of the safety factor and life analysis of top roller mill 4

The minimum value for the factor of safety is 1.7056 at part 2 and the design life of the top roller is 1.e+009 cycles and the minimum value of life is 1.e+006 cycles at part 1 for a load variation from 50% to 150%. Figure 4.29 shows the minimum and maximum safety factor and life on the top roller mill 4;

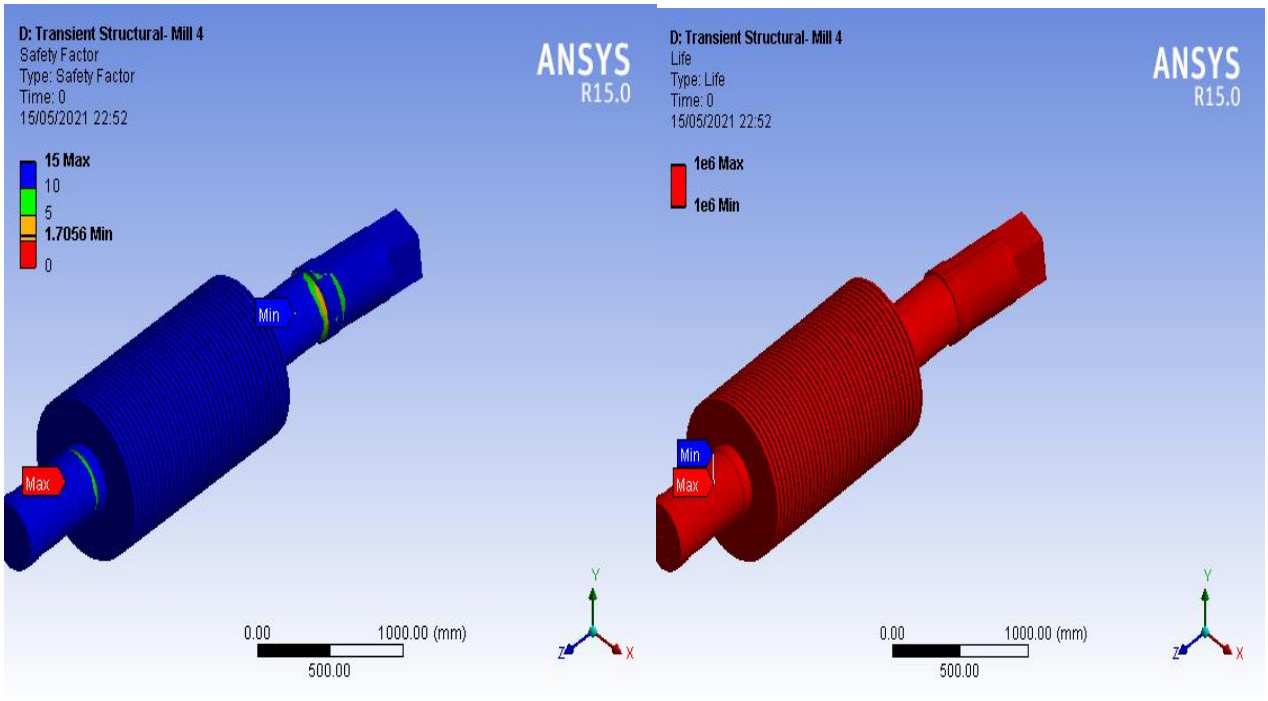

Figure 4.29: Safety factor and life for top roller mill 4

4.3.4.12 Results of the total deformation analysis of the top roller mill 4

The maximum value of deformation on the top roller mill 4 is 0.28302mm on part 2 at the square end and the minimum deformation value is 0mm at the pintle of part 2. Figure 4.30 shows the total deformation at the different sections of the top roller mill 4.

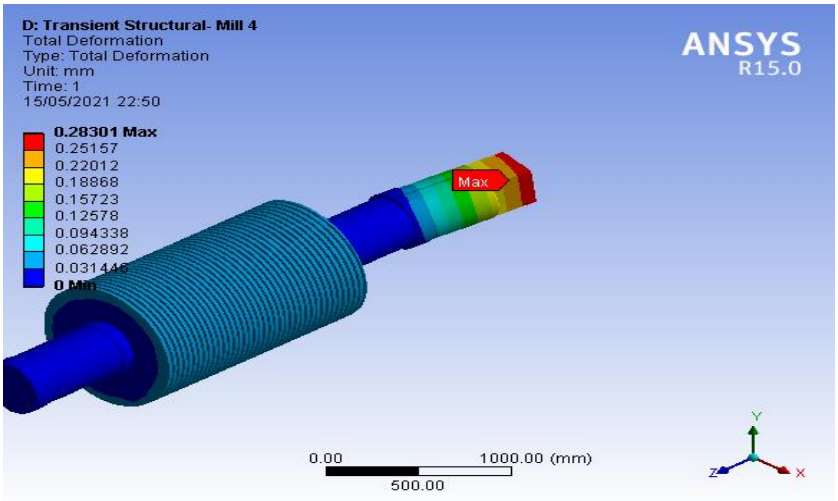

Figure 4.30: Total deformation for top roller mill 4

4.3.5 Fatigue sensitivity for the four top rollers

The available number of life cycles for top roller mill 1,2 and 4 is constant at 1e+6 for load variation from 50% to 150% but the number of cycles reduces exponentially from 4.3434e+5 cycles to 6654.4 cycles for top roller mill 3 under the same load variation as shown in figure 4.31.

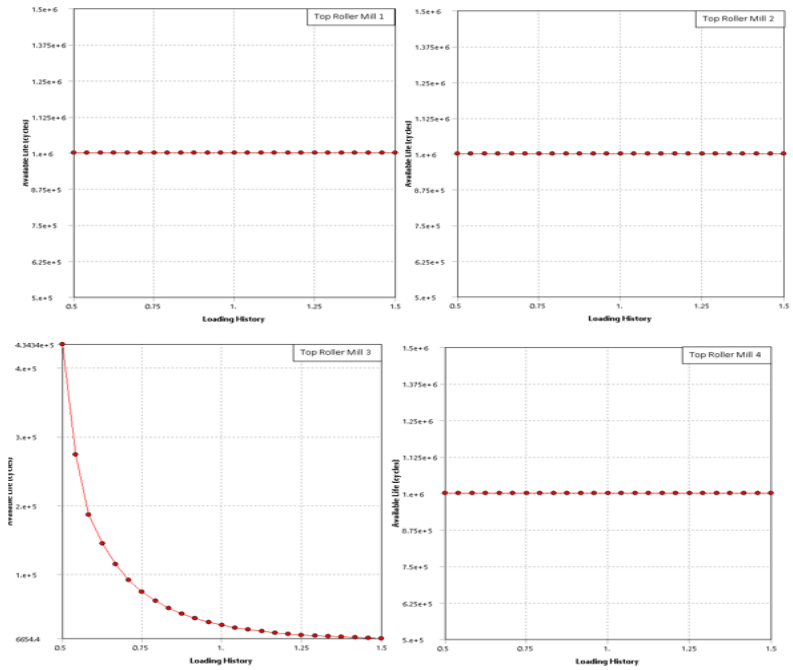

Figure 4.31: Available life cycles against load variation for top roller mill 1 through 4

4.3.9 Reliability analysis of the mill

Top roller Mill 3 has the highest value of deformation and top roller Mill 1 has the lowest point of deformation and the reliability performance for the 4 mill sugar crushing plant at 1.e+006 cycles is 46.93% considering a Mean Time To Failure of 756,495.25cycles per top roller. Top roller Mill 1 has the highest value of safety and top roller Mill 3 has the lowest safety value and lowest value of life, top roller Mill 4 is subject to the highest value of equivalent alternating stress and top roller Mill 1 has the lowest value of equivalent alternating stress. Table 4.18 shows the summary of the structural transient values of safety, deformation, life and alternating stress.

***Table 4.18**: Summary of the structural transient analysis*

	Deformation(mm)		Safety	Life (cycles)		Equivalent Alternating stress(MPa)	
Top Roller	**Min**	**Max**	**Min**	**Min**	**Max**	**Min**	**Max**
Mill 1	0	0.24462	1.9734	1.e+006	1.e+009	2.4085e-003	181.92
Mill 2	0	0.27441	1.7591	1.e+006	1.e+009	2.2819e-003	204.08
Mill 3	0	0.29632	0.43258	25981	1.e+009	2.4924e-003	199.27
Mill 4	0	0.28302	1.7056	1.e+006	1.e+009	2.2703e-003	210.49

4.3.10 Discussion of results

Top roller Mill 1 has the minimum value of alternating shear stress and top roller 3 has the minimum value of safety factor as shown in figure 4.32. The order of magnitude of maximum equivalent alternating stress increases from top roller mill 4 followed by mill 2, then mill 3 and lastly mill 1, maximum deformation increases from top roller 3 to 4 to 2 to 1 and is maximum at the square end which is consistent with the failure of KE-8 shown in figures 4.24, 4.27 and 4.30. Top roller Mill 3 has the lowest value of minimum safety followed by mill 4, then mill 2 and top roller in mill 1 has the highest safety factor hence the least susceptible to failure. The minimum value of life cycles is 1e+006 at part1 for top roller mill 1, 2 and 4 but for mill 3 the minimum life cycles are 25981 for part 2 at the shoulder next to the keyway indicating that the bare shaft for the mill 3 is expected to fail before the crushing shell contrary to the normal condition where the crushing shell is expected to fail before the bare shaft as on top rollers for mills 1, 2 and 4. The reliability of the entire sugar plant is 46.93% hence the entire plant is expected to come to a standstill due to failure of the top rollers most likely in either mill 3 or 4 before their service life.

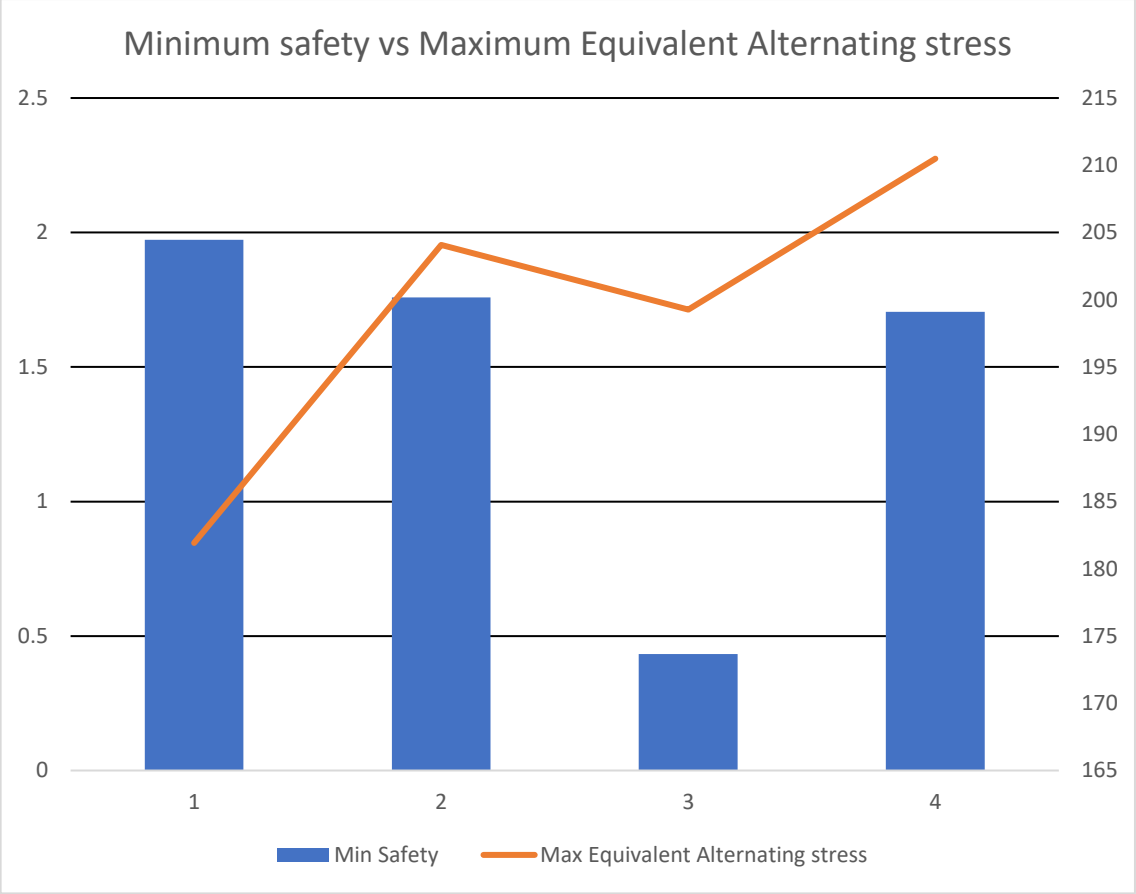

Figure 4.32: Minimum safety vs maximum Equivalent alternating stress

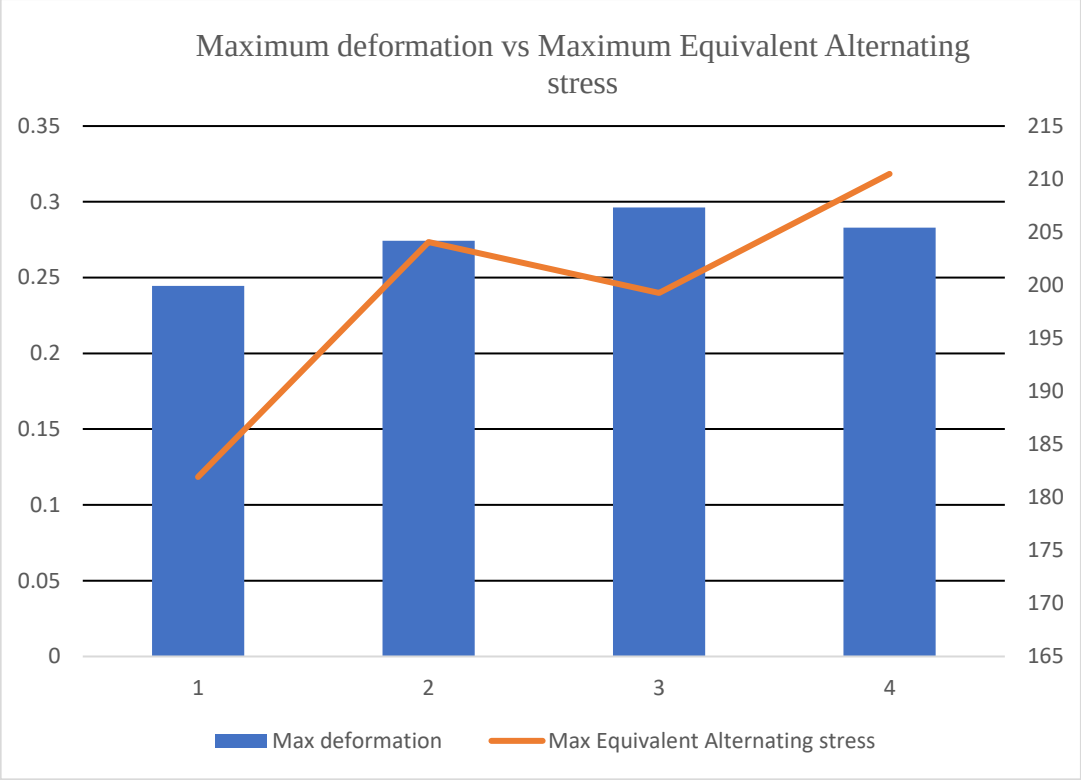

Figure 4.33: Maximum deformation vs maximum Equivalent alternating stress

Figure 4.34: Maximum deformation vs minimum safety

CHAPTER FIVE

CONCLUSION AND RECOMMENDATION

5.0 Introduction

From the results of the investigation on the mechanical performance of top roller in sugar mills, the following conclusions and recommendations were made based on the analytical shear stress method of bending moments and shear forces, physical and chemical tests conducted and transient structural examination of the top roller.

5.1 Remarks

The study is now complete and all objectives addressed and achieved. Conclusions have been drawn and recommendations given.

5.2 Conclusion

The change in vertical crushing loads overtime is higher than the change in the horizontal loads on the top rollers hence they highly contribute to fatigue failure. Shoulder A and B on the drive end of the shaft and the keyway are found to be highly stressed sections of the shaft characterized by most of the top roller shaft failures with values of maximum shear stress highest in top roller mill 3 and 4 and lowest in top roller mill 1. However, the tested failed top rollers were found not to conform to the known standards when it comes to chemical compositions which may alter the shaft physical properties like crack resistance, toughness and fatigue strength causing the shaft to fail in service save the values of hardness for the failed components were found to be in the acceptable range. The mechanical performance of the top rollers in mill 1 through mill 4 under dynamic loading has been analysed using ANSYS finite element modeller and noted that the overall reliability of the 4 mill sugar crushing plant is 46.93% indicating that the plant is expected to stop due to failure in one of

the mills before service life; the value of equivalent alternating stress is maximum at shoulder A and maximum shear stress is at shoulder B under static loading consistent with Khot and Mandale (2015). The maximum deformation on the top roller in all mills from 1 through 4 at the square end which is less than 0.3mm sets in misalignment of the square end inside the coupling causing failure of either the square end or the box coupling or both. Top rollers in Mill 3 and 4 are highly prone to fail reflected by lower safety factors of 0.43258 and 1.70056 respectively which is consistent with the reported failures of KE-3, KE-8 and SB1 and square coupling whilst in service. The maximum equivalent alternating stress values are found to be highest in top roller mill 4, followed by 2, then 3 and lastly 1. Therefore, the need to introduce dampers to absorb vibrations from the shaft that could accelerate fatigue failure due to high-stress amplitudes. The shear stress is still less than the yield strength of the shaft material leaving room for weight optimization of the bare shaft. The flexible coupling that allows the maximum misalignment of about 0.3mm at the top roller square end should be employed to avoid square end related failures. The bare shaft for Top roller mill 3 fails faster than the shell. There is need to Research on the fatigue performance of other high strength materials as compared to forged steel and the effect of chemical composition on the fatigue performance of the high strength material.

5.3 Recommendation

Sugar millers should invest in materials laboratories to test samples delivered with the purchased shafts whether their structural properties agree with the forwarded material test certificate by the shaft manufacturers and they conform to the known standards. The Sugar millers should invest in research and development to come up with new high fatigue strength materials that can perform to expected service life at the critically loaded sections of the shaft and improvement on the flexible coupling that is appropriate to handle misalignment to avoid square end failures that can bring about mill stoppages and maintenance related overheads as the case of top roller KE-8 and to revise meshing around sharp points in ANSYS.

REFERENCES

Air Force Flight Dynamics Laboratory. (2019). *Shaft analysis*. Engineering Library. https://engineeringlibrary.org/reference/shaft-analysis-air-force-stress-manual

Al-Hassan, S., Mishra, B., Olson, D. L., & Salama, M. M. (1998). *Effect of microstructure on corrosion of steels in aqueous solutions containing carbon dioxide*. Corrosion, 54(6), 480-491. https://doi.org/10.5006/1.3284876

Anderson, S. I., & Loughran, J. G. (1998). *Finite element and durability modelling of roller shells and shafts.* Semantic Scholar | AI-Powered Research Tool. https://www.semanticscholar.org/paper/Finite-element-and-durability-modelling-of-roller-Anderson-Loughran/d413365e89b747762db75b0076dc09be81b38fe9

Arzola, N., Goytisolo, R., Perez, R., & Fernandez, A. (2005). *Prediction of the Sugar Mill Shaft Failure Using a Fracture Mechanics Method. Design Engineering*, Parts A and B, 1-7. https://doi.org/10.1115/imece2005-80418

Babakr, A., Bradley, R., & Al-Ahmari, A. (2009). *Failure Analysis of Mill Shaft Roll*. Journal of Failure Analysis and Prevention, 9(2), 107-113. https://doi.org/10.1007/s11668-009-9215-4

Bloch, H. P. (1998). *Improving Machinery Reliability*. Gulf Professional Publishing.

Casanova, F. (2010). *Failure analysis and redesign of a wagon wheel shaft for sugar cane transport*. www.scielo.org.co/. http://www.scielo.org.co/pdf/dyna/v78n166/a06v78n166.pdf

Bureau of Indian Standard. (2001). *Carbon Steel Forgings for General Engineering Purposes* (IS 2004 1991). Reprography Unit, BIS, New Delhi. https://law.resource.org/pub/in/bis/S10/is.1570.2.1979.pdf

Bureau of Indian Standards. (1990). IS 11201 (1985): *Cane Crushing Rollers for Sugar Industry* (AFDC 8: 2311). Arcee Press, New Delhi, India. https://law.resource.org/pub/in/bis/S06/is.11201.1985.pdf

Canadian Conservation Institute. (2017). *How to determine metal density* – Canadian conservation institute (CCI) notes 9/10. Government of Canada. https://www.canada.ca/en/conservation-institute/services/conservation-preservation-publications/canadian-conservation-institute-notes/metal-density.html

Chiang, J., Lawrence, B., Boyd, J., & Pilkey, A. (2011). *Effect of microstructure on retained austenite stability and work hardening of TRIP steels*. Materials Science and Engineering: A, 528(13-14), 4516-4521. https://doi.org/10.1016/j.msea.2011.02.032

Cornelius, N. J., & Jean, B. B. (2018). *Effective Maintenance Strategy of Cane Crushing Mills for Improvement of Sugar Production in Kenya*. Academia.edu. https://www.academia.edu/36804786/

David Havel, P. E. (2017). *Austenitic Manganese Steel. Steel Founders' Society of America*. https://www.sfsa.org/doc/2017-4.1%20Columbia%20-%20Havel.pdf

Dalvi, S. D., Hariom, Chandrababu, D., Satav, S., & Vijoykumar. (2017). *Failure analysis of a carbon steel roller shaft of continuous pad steam machine*. Case Studies in Engineering Failure Analysis, 9, 118-128. https://doi.org/10.1016/j.csefa.2017.11.001

Deepan Marudachalam, M. G., Kanthavel, K., & Krishnaraj, R. (2011). *Optimization of shaft design under fatigue loading using the Goodman method*. Online International Journal,

Peer-Reviewed Scholarly Journals. https://www.ijser.org/paper/Optimization-of-shaft-design-under-fatigue-loading-using-Goodman-method.html

Ebara, R. (2010). *Corrosion fatigue cracks initiation behaviour of stainless steels*. Procedia Engineering, 2(1), 1297-1306. https://doi.org/10.1016/j.proeng.2010.03.141

El May, M., Palin-Luc, T., Saintier, N., & Devos, O. (2013). *Effect of corrosion on the high cycle fatigue strength of martensitic stainless steel X12CrNiMoV12-3*. International Journal of Fatigue, 47, 330-339. https://doi.org/10.1016/j.ijfatigue.2012.09.018

Engineering Toolbox. (2010). *Factors of safety. [Online] Available* at: https://www.engineeringtoolbox.com/factors-safety-fos-d_1624.html

Engineering Toolbox. (2003). *Coefficients of linear thermal expansion*. https://www.engineeringtoolbox.com/linear-expansion-coefficients-d_95.html

Evins, J. L. (2004). *Dependence of Strength on Corrosion-Fatigue Resistance of AISI 4130 Steel. SMARTech* Home. https://smartech.gatech.edu/bitstream/handle/1853/5265/evins_joseph_l_200405_mast.pdf

Giordani, E., Guimara, V. A., Pinto, T. B., & Ferreira, I. (2004). *Effect of precipitates on the corrosion. Fatigue crack initiation of ISO 5832-9 stainless steel biomaterial*. International Journal of Fatigue, 26(10), 1129-1136. https://doi.org/10.1016/j.ijfatigue.2004.03.002

Hage, V. P., Gandigude, A. U., & Iratkar, G. (2017). *Literature Review on Sugar Mill Coupling and Its Bearing Materials*. International Journal Publication | Research Paper Publication and Submission - IJARIIT. https://www.ijariit.com/manuscripts/v3i3/V3I3-1546.pdf?581fc7&581fc7 ISSN: 2454-132X

Hashimoto, S., Ikeda, S., Sugimoto, K., & Miyake, S. (2004). *Effects of NB and Mo addition to 0.2%C-1.5%Si-1.5%Mn steel on mechanical properties of hot rolled TRIP-aided steel sheets*. ISIJ International, 44(9), 1590-1598. https://doi.org/10.2355/isijinternational.44.1590

Hugot, E. (2014). *Handbook of cane sugar engineering* (1st Ed.). Elsevier.

Ismail, M. F. (2018). (PDF) *A study of the correlation between finite element analysis and experimental modal analysis in structural dynamic analysis*. Research Gate. https://www.researchgate.net/publication/325257046 A study of the correlation between finite element analysis and experimental modal analysis in structural dynamic analysis

Kamal, M., Rahman, M. M., & Sani, M. S. (2013). *Fatigue life prediction using simplified endurance function model.* Advances in Mechanical Engineering, 5, 581754. https://doi.org/10.1155/2013/581754

Karthi, R. R., & Emmanual L. (2018). *Design and analysis of roller shafts for sugar cane mills by using the FEA technique with different parameters*. ResearchGate. https://www.researchgate.net/publication/324129340_Design_and_Analysis_of_Roller_Shafts_for_Sugar_Cane_Mills_by_Using_FEA_Technique_with_Different_Parameters

Khangar, V. S., & Jaju, S. B. (2012). *A Review of Various Methodologies Used for Shaft Failure Analysis*. www.semanticscholar.org. https://pdfs.semanticscholar.org/ecc8/bc88a57254b97c06325d8f17cd96eadecc04.pdf

Khot, J. S., & Mandale, M. B. (2015). *Static structural analysis of crushing rollers of three roller sugar mill.* International Journal of Engineering Research and, V4 (05). https://doi.org/10.17577/ijertv4is051293

Lourdes, E. R., & Hassan, M. H. (2018). *Review on experimental modal analysis and normal mode finite element analysis of engineering structural dynamics*. Research Gate. https://www.researchgate.net/publication/328759445_Review_on_experimental_modal_analysis_and_normal_mode_finite_element_analysis_of_engineering_structural_dynamics

Mary, T. K., & John, T. M. (2017). *Introduction to ANSYS and finite element modelling*. ScienceDirect.com | Science, health and medical journals, full-text articles and books. https://www.sciencedirect.com/science/article/pii/B9780128129814000010

Marín, J. J. (2005). *Fracture Mechanics Approach of Repaired Top Roll Shafts in Sugar Cane Mills*. Journal of the Mechanical Behaviour of Materials, 16(6). https://doi.org/10.1515/jmbm.2005.16.6.419

Meshram, V. V., & Wanjari, P. M. (2015). *Design and analysis of rolling key—a review*. www.ijmerr.com. https://www.ijmerr.com/v4n1/ijmerr_v4n1_40.pdf

Ministry of Tourism, Trade and Industry. *(2010). National Sugar Policy*. https://www.mtic.go.ug/wp-content/uploads/2019/08/National-Sugar-Policy.pdf

Ministry of Trade Industry and Cooperatives. (2016). *Uganda has Surplus Sugar.* Ministry of Trade Industry and Cooperatives – Republic of Uganda. https://www.mtic.go.ug/uganda-has-surplus-sugar/

Ministry of Trade, Industry and Cooperatives. (2016). *Report of the verification mission on Uganda sugar sector*. Mtic. https://mtic.go.ug/2016/index.php?/doc_download/307-uganda-sugar-verification-report/

Mohammadi, S. (2008). *Extended finite element method: For fracture analysis of structures*. John Wiley & Sons.

Muñoz Cubillos, J., Rodríguez, S., & Coronado, J. (2016). *On the fatigue behaviour of quenched and tempered at 300 and 600 °C SAE 1045 steel in an environment of sugar cane juice*. Fatigue & Fracture of Engineering Materials & Structures, 39(10), 1299-1308. https://doi.org/10.1111/ffe.12454

Mishnaevsky, L., Derrien, K., & Baptiste, D. (2004). *Effect of microstructure of particle reinforced composites on the damage evolution:* Probabilistic and numerical analysis. Composites Science and Technology, 64(12), 1805-1818. https://doi.org/10.1016/j.compscitech.2004.01.013

Muhammed, A. S., & Mohammed, M. A. (2013). *The effects of excessive weight of cement kiln on the resistance of rollers base.* ResearchGate. https://www.researchgate.net/publication/316440772_The_Effects_of_Excessive_Weight_of_cement_Kiln_on_the_Resistance_of_Rollers_Base

Mulengani, A. K. (2019). *The Uganda Sugar Sector Crisis.* New Vision. https://www.newvision.co.ug/news/1503629/uganda-sugar-sector-crisis

Neville, S. (2012). *Failure Analysis of Machine* Shafts. Efficient Plant. https://www.efficientplantmag.com/2012/07/failure-analysis-of-machine-shafts/

Padhal, D. K., & Meshram, D. B. (2013). *Analysis and Failure Improvement of Shaft of Gear Motor in CRM Shop*. www.semanticscholar.org. https://pdfs.semanticscholar.org/956c/81a72d9ec31cecb37493abd5c995d44fa123.pdf

Puškár, A., & Várkoly, L. (1986). *Influence of temperature on fatigue crack growth behaviour of steels at the ultrasonic frequency.* Fatigue & Fracture of Engineering Materials and Structures, 9(2), 143-150. https://doi.org/10.1111/j.1460-2695.1986.tb00442.x

Pérez-Mora, R., Palin-Luc, T., Bathias, C., & C. Paris, P. (2015). *Very high cycle fatigue of high strength steel under seawater corrosion: A strong corrosion and mechanical damage*

coupling. International Journal of Fatigue, 74, 156-165. https://doi.org/10.1016/j.ijfatigue.2015.01.004

Reid, M. J. (2009). *Analysis of the causes of recent roll shaft failures in natal sugar mills*. Semantic Scholar | AI-Powered Research Tool. https://www.semanticscholar.org/paper/Analysis-of-the-causes-of-recent-roll-shaft-in mills /0910e03e2b99d80329c38f529f7684e22e164898

Sakaki, S., Yoshida, M., & Horibe, S. (2014). *Effect of stacking fault energy on pulsating fatigue behaviour for FCC metals under the fully repeated loading*. Materials Science and Engineering: A, 607, 1-5. https://doi.org/10.1016/j.msea.2014.03.142

Sieniawski, J., Ziaja, W., Kubiak, K., & Motyk, M. (2013). *Microstructure and mechanical properties of high strength two-phase titanium alloys.* Titanium Alloys - Advances in Properties Control. https://doi.org/10.5772/56197

Singapore Institute of Standards and Industrial Research. (1976). *BS 3100 A4 - Standard cast steel.* Scribd. https://www.scribd.com/doc/137282268/BS-3100-A4-Standard-Cast-Steel

Suhas, J. S., Sushant, J. S., & Sharma, S. B. (2016). *Influence of Cracks on Shaft: A Review*. www.irjet.net. https://www.irjet.net/archives/V3/i8/IRJET-V3I8270.pdf

Survey Monkey. (2020). *Sample Size Calculator: Understanding Sample Sizes.* https://www.surveymonkey.com/mp/sample-size-calculator/

Taylor, D., & Knott, J. F. (1981). *Fatigue crack propagation behaviour of short cracks; the effect of microstructure.* Fatigue & Fracture of Engineering Materials and Structures, 4(2), 147-155. https://doi.org/10.1111/j.1460-2695.1981.tb01116.x

Xiaobin, P. E., & Zelong, L. (2013). *Asee peer - Stress concentration factors due to typical geometric discontinuities for shaft design by numerical simulation.* Asee peer Document

Repository. https://peer.asee.org/stress-concentration-factors-due-to-typical-geometric-discontinuities-for-shaft-design-by-numerical-simulation

Prajapatia, H. R., Patel, B. P., & Patel, N. V. (2015). *Investigation of stress concentration factor for Keyway on the shaft under different loading conditions*: A case study. Research Gate. https://www.researchgate.net/publication/325870524 Investigation of Stress Concentration Factor for Keyway on Shaft under Different Loading Conditions A Case Study

Qingdao Casting Quality Industrial Co., Ltd. (2009). *Casting Material: Carbon Steel BS3100 Gr. A4*. www.castingquality.com. http://www.castingquality.com/castings-picture/Casting-Material-BS3100-GR-A4.pdf

Tipton, S. M., Sorem, J. R., & Rolovic, R. D. (1996). *Updated stress concentration factors for filleted shafts in bending and tension.* Journal of Mechanical Design, 118(3), 321-327. https://doi.org/10.1115/1.2826887

UK steel stockholders and suppliers. (2021). *Steel hardness conversion table.* Steel Express - Stockholders. Suppliers of stainless steel, engineering, and tool steels. https://www.steelexpress.co.uk/steel-hardness-conversion.html

Utkin, V. S. (2011). *Calculation of shaft reliability (Strength) based on limited information*. Russian Engineering Research, 31(2), 119-122. https://doi.org/10.3103/s1068798x11020262

Williams, Jonathan & Montazersadgh, Farzin & Fatemi, Ali. (2007). *Fatigue performance comparison and life prediction of forged steel and ductile cast iron crankshafts*.

Xiaobin, L., & Zelong, L. (2013). *Stress concentration factors due to typical geometric discontinuities for shaft design by numerical simulation.* Home: American Society for

Engineering Education.
https://www.asee.org/public/conferences/20/papers/6755/download

Yonezawa, T., Suzuki, K., Ooki, S., & Hashimoto, A. (2013). *The effect of chemical composition and heat treatment conditions on stacking fault energy for Fe-CR-Ni austenitic stainless steel.* Metallurgical and Materials Transactions A, 44(13), 5884-5896. https://doi.org/10.1007/s11661-013-1943-0

Zubko, P., & Pešek, L. (2015). *Correlation between hardness and fatigue properties.* Key Engineering Materials, 662, 197-200. https://doi.org/10.4028/www.scientific.net/kem.662.197

APPENDICES

This section contains information relevant to the report but not included in the main body of the research report which includes the computations of forces and stresses on the Top Rollers, mass properties of the gear pinion and top roller, chemical composition report printouts, mill photos, acceptance letters and a chart of theoretical stress concentration factors.

Appendix 1: Detailed computation of Forces and Stresses on the Top rollers

a) Forces on the crushing length of top rollers 1 through 4

Top Roller	P $\left(\frac{\text{Kg}}{\text{cm}^2}\right)$	$\text{F} = 2\pi d_T^2 \text{P}$ (kN)	$\text{F}_s = \frac{2}{3}\text{F}$ (kN)	$\text{F}_E = \frac{\text{F}_s}{5}$ (kN)	$\frac{\sum H_c}{\text{L}}$ $(\frac{\text{kN}}{\text{mm}})$	$\frac{\sum V_c}{\text{L}}$ $\left(\frac{\text{kN}}{\text{mm}}\right)$
	$\mathbf{d_T = 40cm}$				$\mathbf{L = 1540mm}$	$\mathbf{L = 1540mm}$
1	160	3944.835	2629.89	525.978	-0.8318	-0.9180
2	211,7	5219.51	3479.67	695.93	-1.1006	-1.2147
3	190	4684.492	3122.995	624.599	-0.9878	-1.0901
4	216.7	5342.786	3561.857	712.3714	-1.266	-1.2433

b) Forces at the pinion for Top Roller Mill 1 through 4

Top Roller	**N (rpm)**	$T_P = \frac{15P}{\pi N}$ (kNmm)	$\text{F}_t = \frac{T_P}{\left(\frac{P.C.D}{2}\right)}$ (kN) $\boldsymbol{P.C.D = 805.8mm}$ $\boldsymbol{Z = 17}$ $\boldsymbol{m = 47.4mm}$	$\text{F}_r = F_t \tan\varphi$ (kN) $\varphi = 20^\circ$	$\sum H_p$ (kN)	$\sum V_p$ (kN) $\boldsymbol{W_p = 11.9682kN}$
1	3.7	387134	960.869	349.728	1119.52	573.5318
2	3.3	434060	1077.34	392.12	1255.22	644.5018
3	3.4	421292	1045.65	380.585	1229.0481	625.1906
4	3.2	447623	1111.003	404.372	1294.445	665.0132

c) Summary of loading on the Top Rollers 1 through 4

Top roller	Region	↑V (kN)	→ H (kN)	Load detail
1	At the pinion	573.5318	1119.52	concentrated
	Weight of Roller + shaft, W_t	-91.233	0	concentrated
	At the top Roller shell	-0.9180kN/mm	-0.8318kN/mm	U.D.L
2	At the pinion	644.5018	1,255.22	concentrated
	Weight of Roller + shaft	-91.233	0	concentrated
	At the top Roller shell (U.D.L)	-1.2147kN/m	-1.1006kN/mm	U.D.L
3	At the pinion	625.1906	1,229.0481	concentrated
	Weight of Roller + shaft	-91.233	0	concentrated
	At the top Roller shell (U.D.L)	-1.0901kN/mm	-0.9878kN/mm	U.D.L
4	At the pinion	665.0132	1,294.4445	concentrated
	Weight of Roller + shaft	-91.233	0	concentrated
	At the top Roller shell (U.D.L)	-1.2433kN/mm	-1.1266kN/mm	U.D.L

d) Calculations of reactions at the Bearing for top rollers 1 through 4

i) Top Roller Mill 1

Vertical loading force diagram for Top Roller mill 1

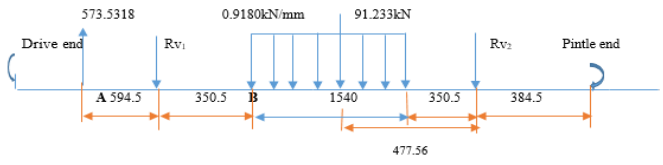

Rv_1 and Rv_2 are the reactions in the Vertical direction at bearing points

Taking amount about Rv_2

$$573.5318 \times 2835.5 = R_{V1} \times 2240.5 + 91.233 \times 477.56 + 1413.72 \times 1120.5$$

$$R_{V1} = -0.4913\ kN\ (upwards)$$

Finding R_{v2}

$$573.5318 = R_{V1} + 1413.72 + R_{V2}91.233$$

$$R_{V2} = -930.9299\ kN\ (upwards)$$

Horizontal loading force diagram on the top roller mill 1

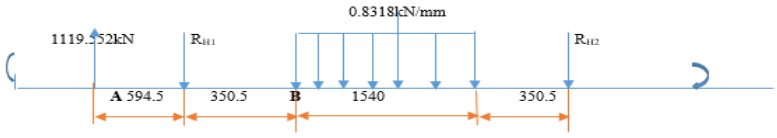

Taking moment about R_{H2} to find R_{H1}

$$1119.52 \times 2835.5 = R_{H1} \times 2240.5 + 1280.972 \times 1120.5$$

$$R_{H1} = 776.1972\ kN$$

Finding R_{H2}

$$1119.52 = R_{H1} + R_{H2} + 1280.972$$

$$R_{H2} = -937.6492\ kN\ (Right)$$

ii) Top Roller Mill No.2

Vertical loading force diagram for Top Roller mill 2

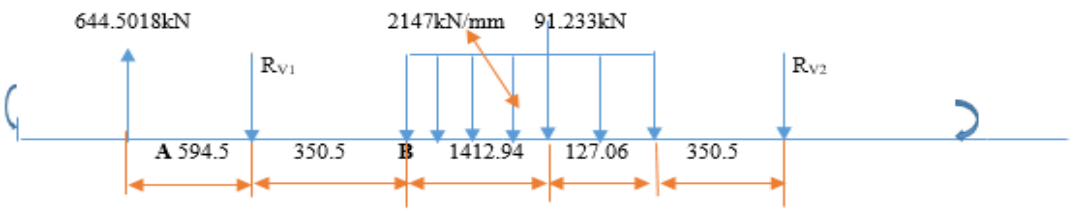

Taking moments about R_{V_2}

$$644.5018 \times 2835.5 = R_{V1} \times 2240.5 + 1870.638 \times 1120.5 + 91.233 \times 477.56$$

$$R_{V1} = -139.3146\ kN$$

$$644.5018 = -139.3146 + 91.233 + 1870.638 + R_{V2}$$

$$R_{V1} = -1178.0546\ kN$$

Horizontal loading force diagram for Top Roller mill 2

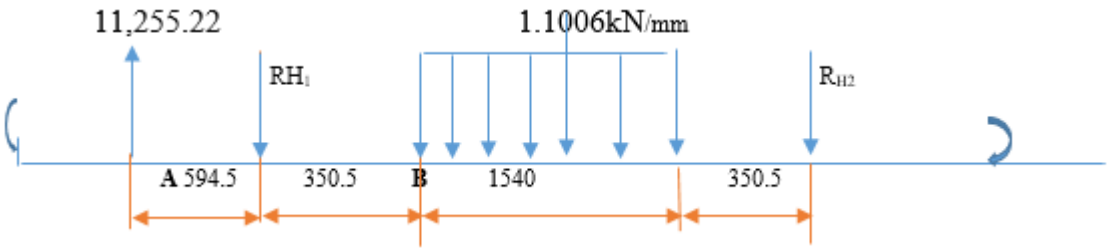

Taking moments about RH_2

$$1{,}255*(2835.5) = R_{H1}*(2240.5) + 1694.924(1120.5)$$

$$R_{H1} = 740.91kN$$

$$1{,}255.22 = 740.91 + 1694.924 + R_{H2}$$

$$R_{H2} = -1{,}180.614kN \text{ (upwards)}$$

iii) Top Roller Mill No. 3

Vertical Loading force diagram for top roller mill no. 3

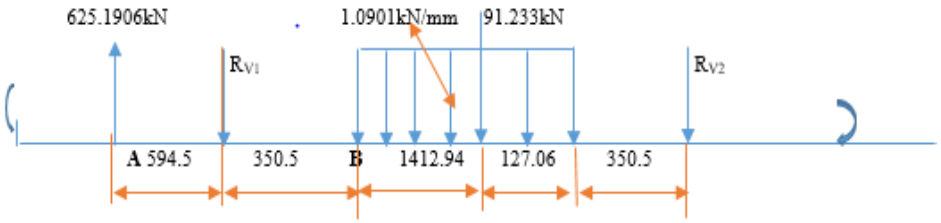

Taking moment about Rv_2

$$625.1906 \times 2835.5 = R_{V1} \times 2240.5 + 91.233 \times 477.56 + 1678.754(1120.5)$$

$$R_{V1} = -67.79\ kN$$

$$625.1906 = -67.791 + 91.223 + R_{V2} + 1678.754$$

$$R_{V2} = -1077.0054\ kN$$

Horizontal loading force diagram for the top roller mill 3

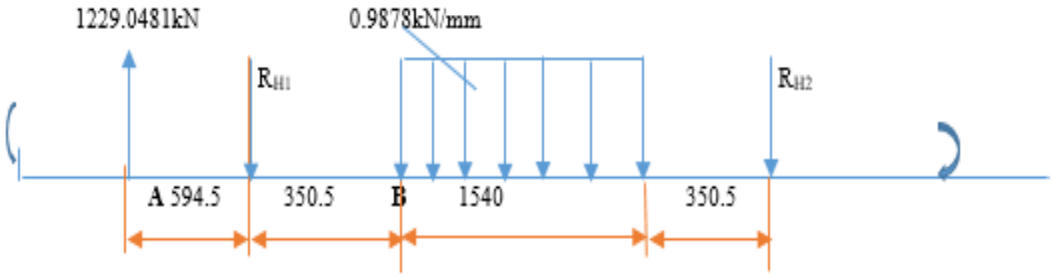

Taking moments about R_{H2}

$$129.0481 \times 2835.5 = R_{H1} \times 2240.5 + 1521.212 \times 1120.5$$

$$R_{H1} = 794.665\ kN$$

$$1229.0481 = 794.665 + 1521.212 + R_{H2}$$

$$R_{H2} = -1{,}086.8289\ kN$$

iv) Top Roller Mill No. 4

Vertical loading force diagram for Top Roller mill 4

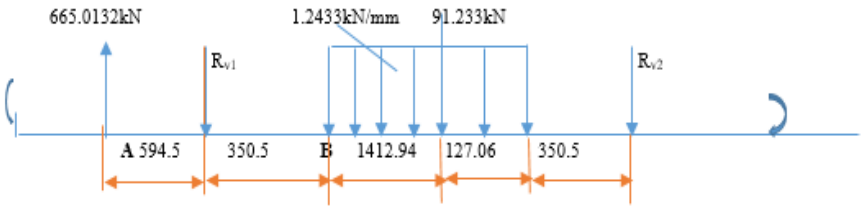

Taking moment about Rv_2

$$665.0132 \times 2835.5 = R_{V1} \times 2240.5 + 91.233 \times 477.56 + 1914.682 \times 1120.5$$

$$R_{V1} = -135.3829\ kN$$

$$665.0132 = -135.3829 + 1914.682 + 91.233 + R_{V2}$$

$$R_{v2} = -1{,}205.5189\ kN$$

Horizontal loading on top roller mill 4

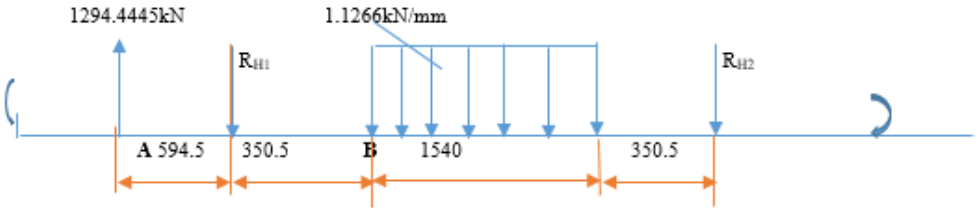

Taking moments about R_{H2}

$$1294.4445 \times 2835.5 = R_{H1} \times 2240.5 + 1734.964 \times 1120.5$$

$$R_{H1} = 770.529\ kN$$

$$1294.4445 = 770.529 + 1734.964 + R_{H2}$$

$$R_{H2} = -1211.0485\ kN$$

e) Summary of bearing reactions at the top rollers 1 through 4

Top Roller	Vertical reaction on the bearing, R_v (kN)		Horizontal reaction on the bearing, R_H (kN)	
	Drive end (1)	Pintle end (2)	Drive end (1)	Pintle end (2)
1	-0.4913	-930.9299	776.1972	-937.6492
2	-139.3146	-1178.0546	740.91	-1180.614
3	-67.791	-1077.0054	794.665	-1086.8289
4	-135.3829	-1205.5189	770.529	-1211.0485

f) Summary of the vertical and horizontal loadings on the top rollers

Parameter of the Top Roller	Top Roller 1 (Mill 1)	Top Roller 2 (Mill 2)	Top Roller 3 (Mill 3)	Top Roller 4 (Mill 4)
Resultant horizontal crushing force due to hydraulic pressure, ΣH, kN	-1,280.972	-1,694.924	-1,491.9212	-1,949.64
Resultant horizontal force on the Pinion, ΣH, kN	1,119.52	1,255.22	1229.048	1294.4445
Horizontal Bearing Reaction at the drive end, R_{H1}, kN	776.1972	740.91	794.665	770.529
Horizontal Bearing Reaction at the pintle end, R_{H2}, kN	-937.6492	-1180.614	-1086.8289	-1211.0485
Resultant vertical crushing force due to hydraulic pressure, ΣV, kN	-1,413.72	-1,870.638	-1,678.754	-1,914.682
Weight of the Top Roller, kN (Vertical Concentrated load)	-91.233	-91.233	-91.233	-91.233

Resultant vertical force on the Pinion , ΣV, kN	573.5318	644.5018	625.1906	665.0132
Vertical Bearing Reaction at the drive end, R_{V1}, kN	-0.4913	-139.3146	-67.791	-135.3829
Vertical Bearing Reaction at the drive end, R_{V1}, kN	-930.9299	-1178.0546	-1077.0054	-1205.5189

---

g) Shear Force & Bending Moment diagrams for top rollers mill 1 through 4

i) Vertical loading on Top Roller mill1

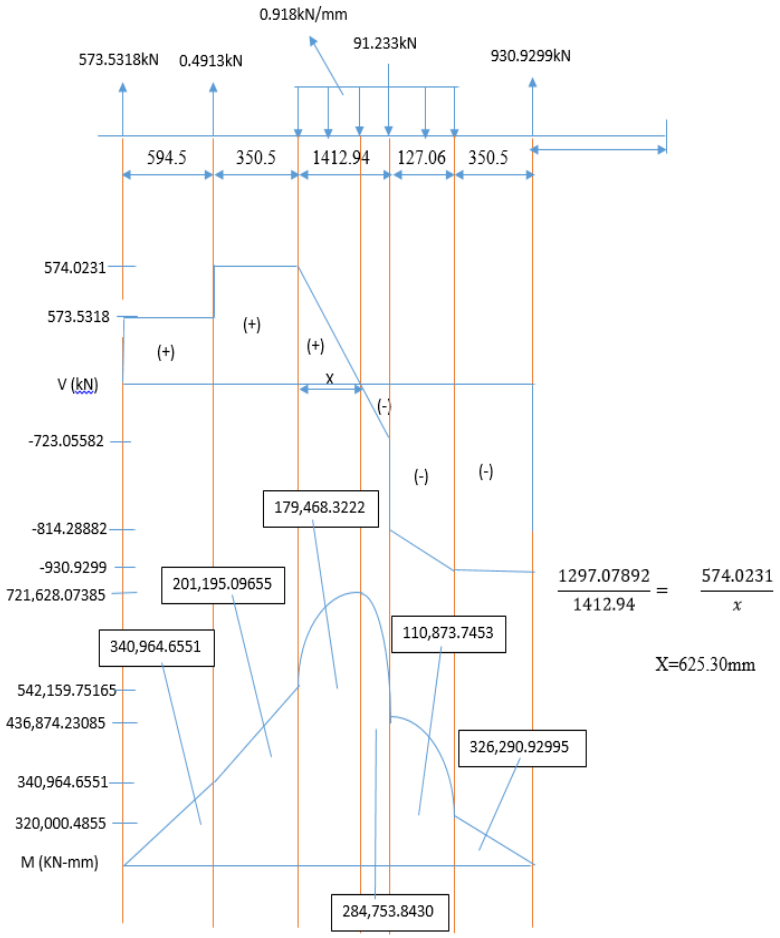

ii) Horizontal loading on top roller mill 1

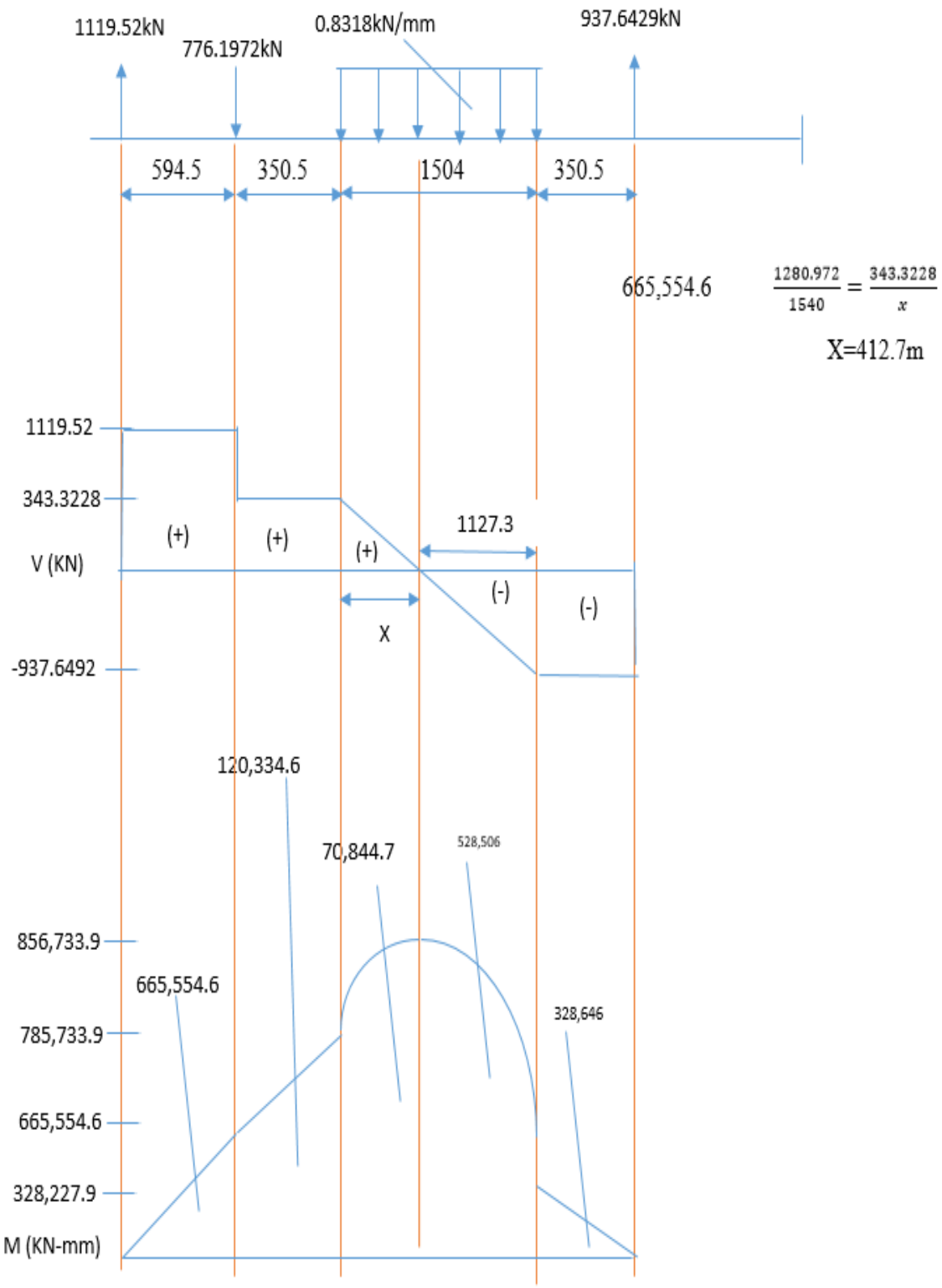

iii) Vertical loading on top roller mill 2

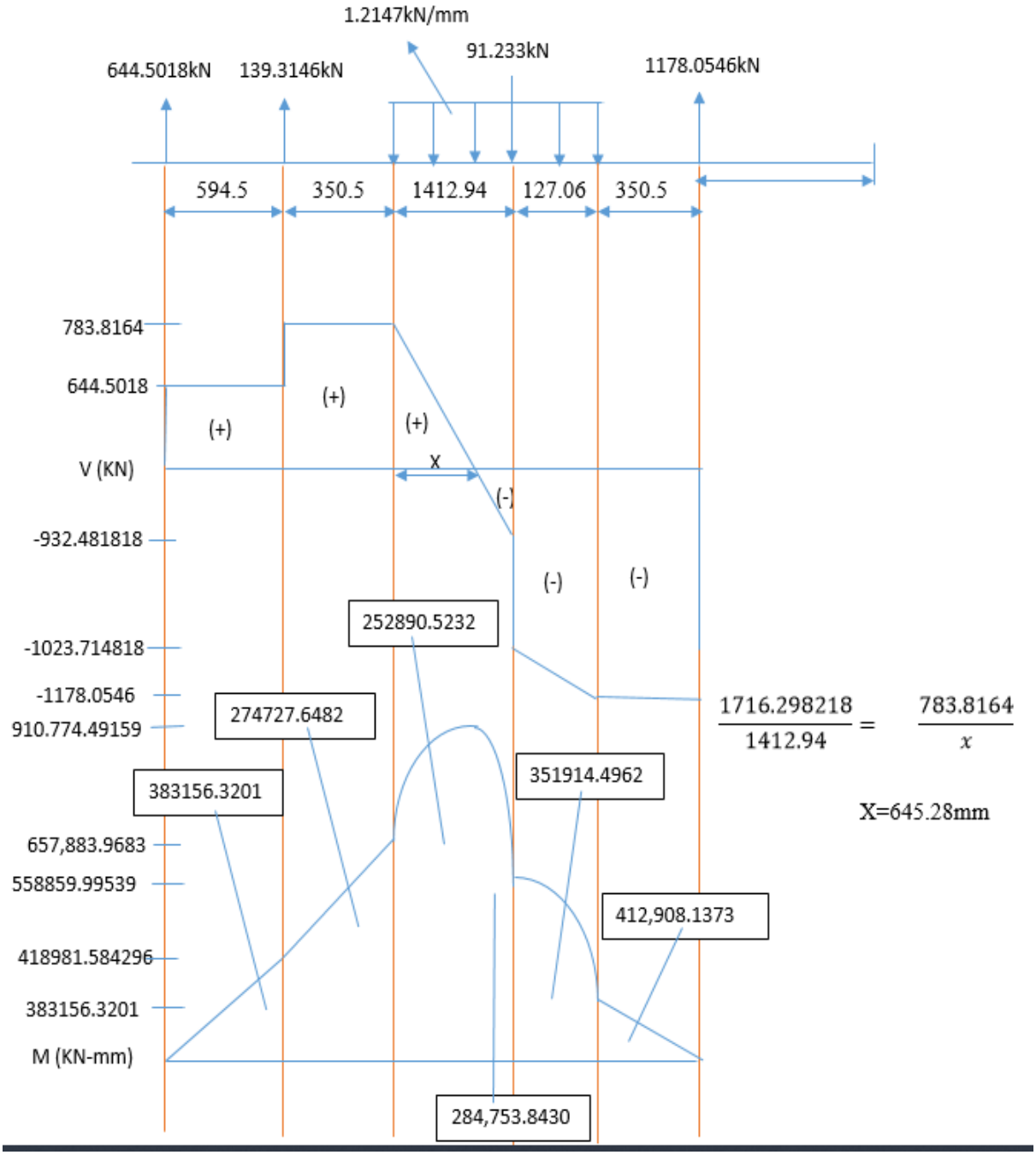

iv) Horizontal loading on top roller mill 2

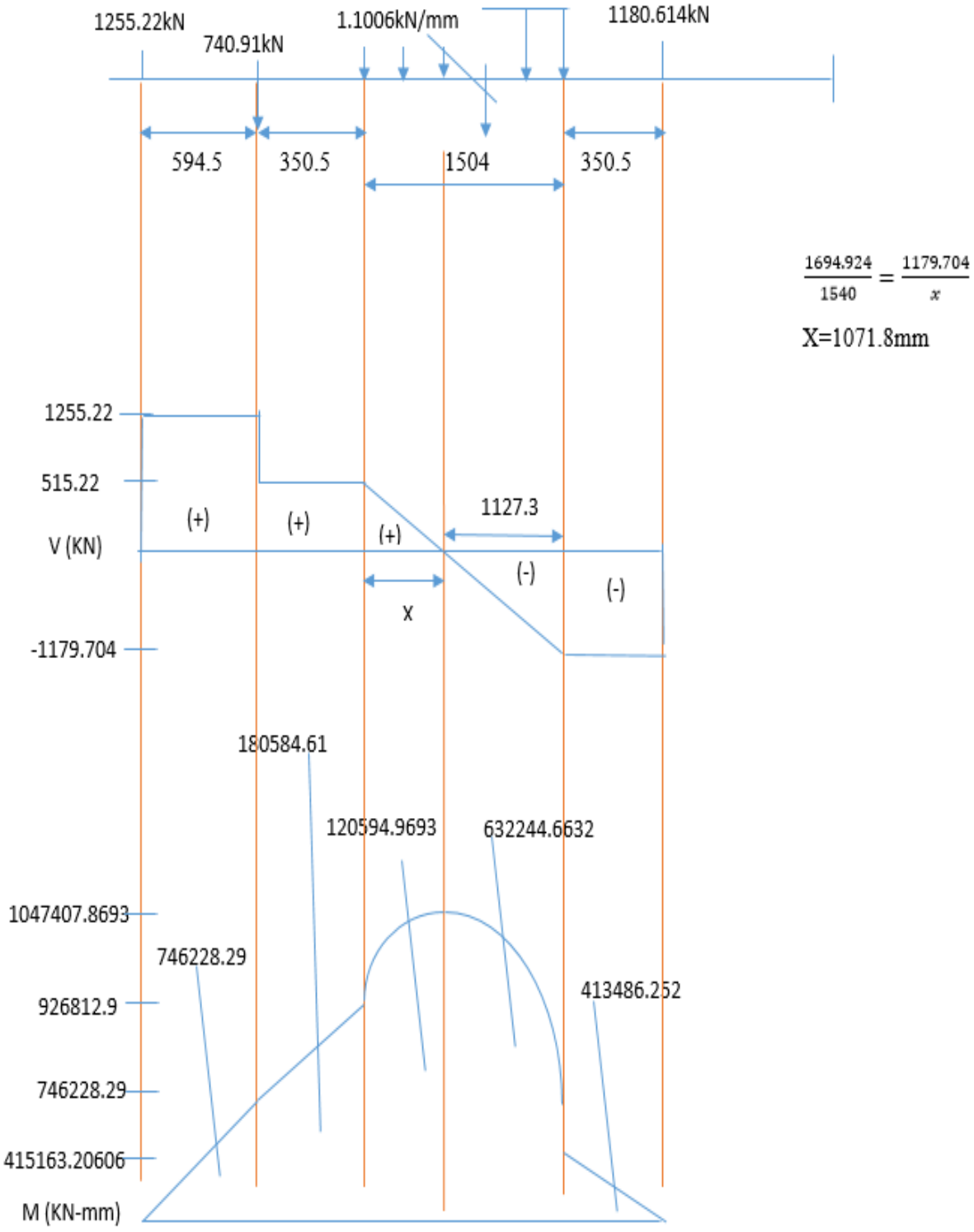

$$\frac{1694.924}{1540} = \frac{1179.704}{x}$$

X=1071.8mm

v) Vertical loading on top roller mill 3

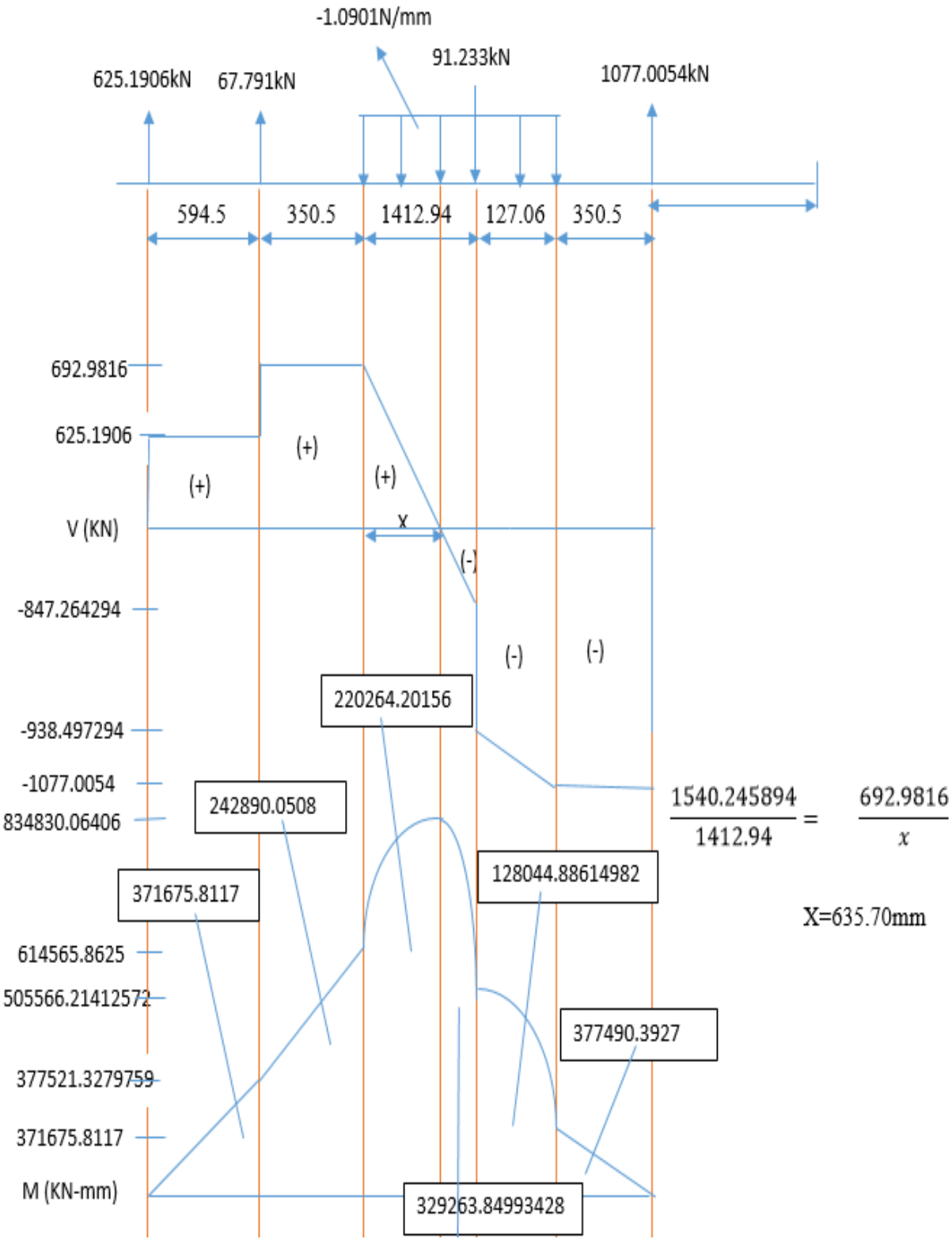

vi) Horizontal loading on the top roller mill 3

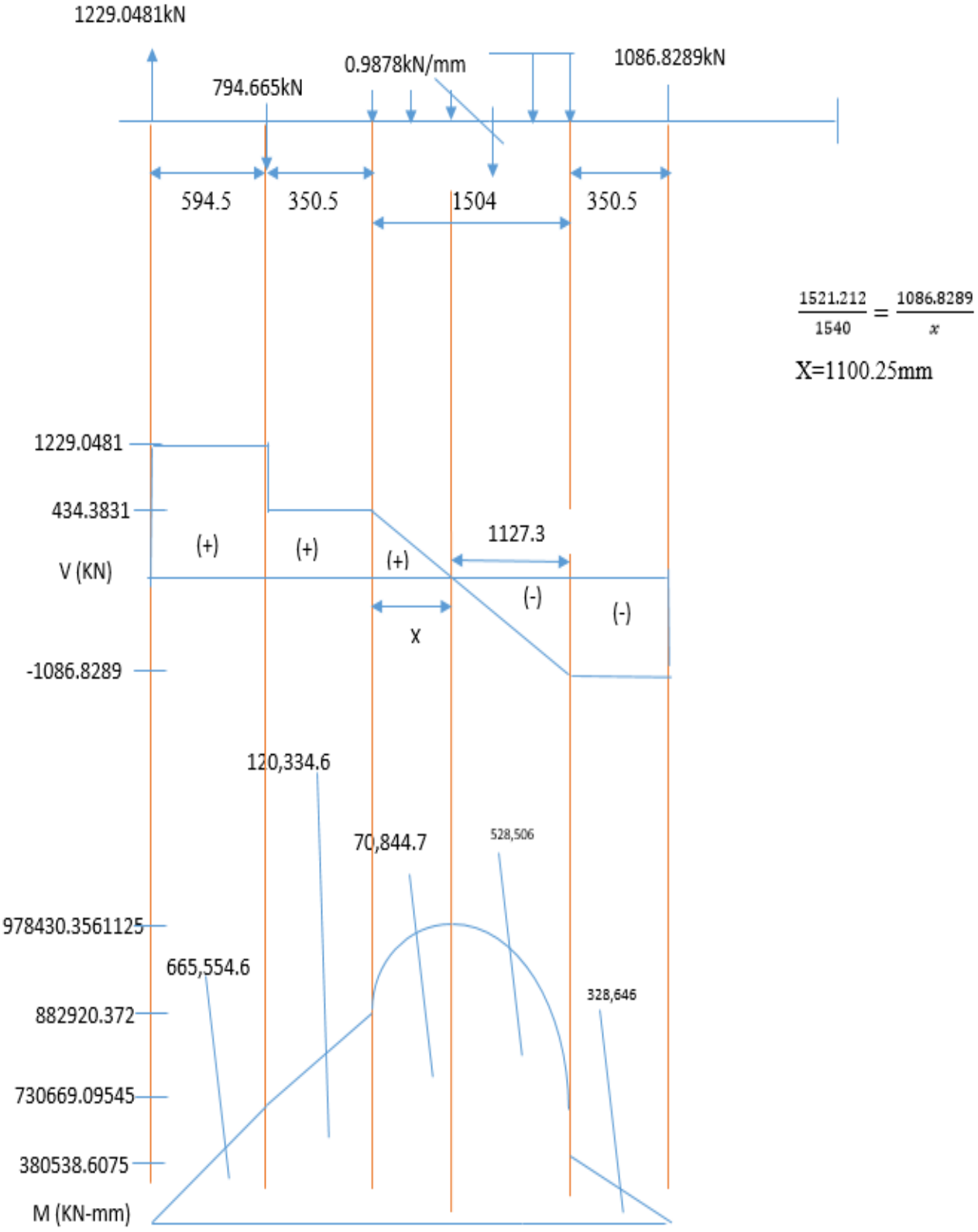

vii) Vertical Loading on top roller mill 4

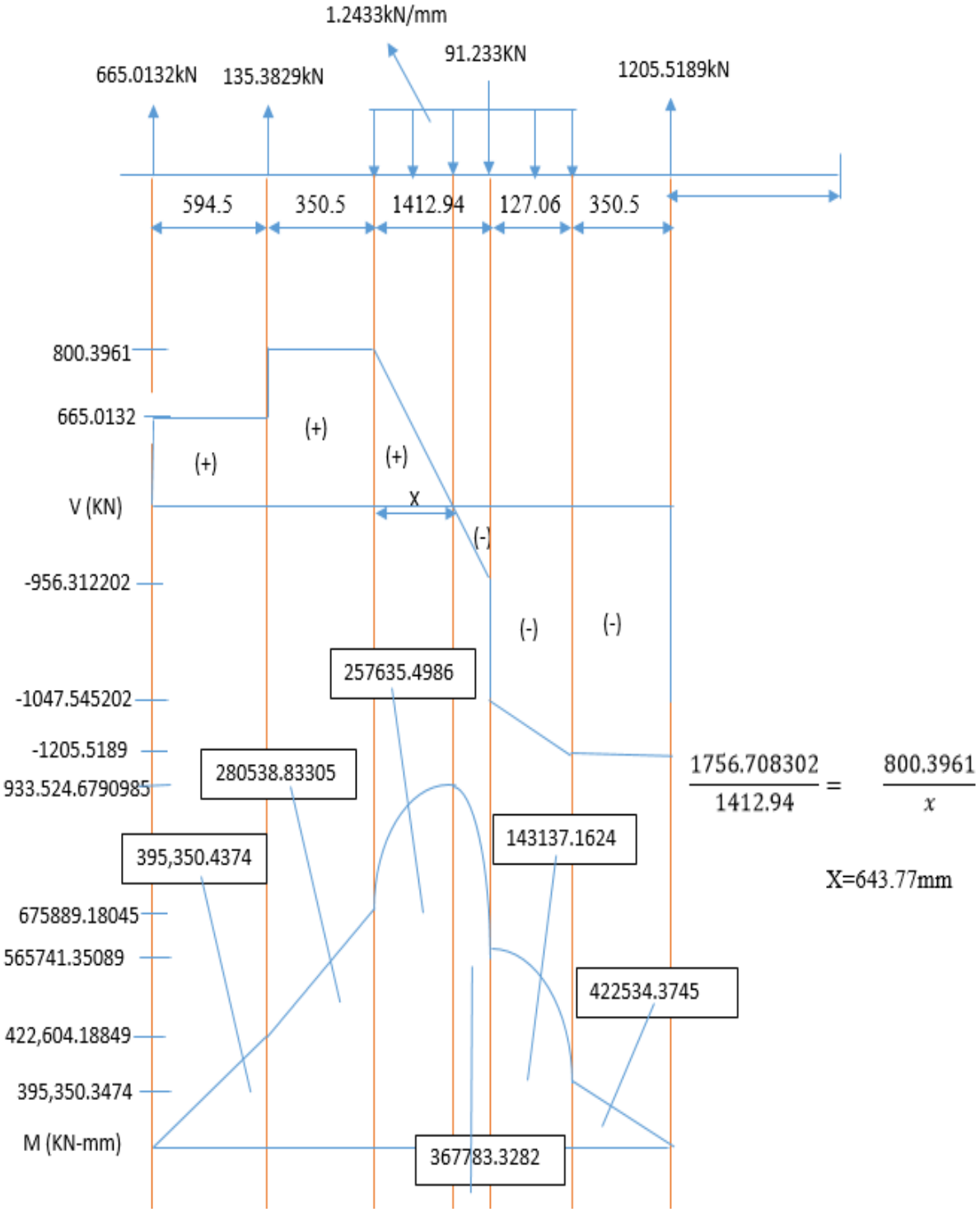

viii) Horizontal loading on top roller mill 4

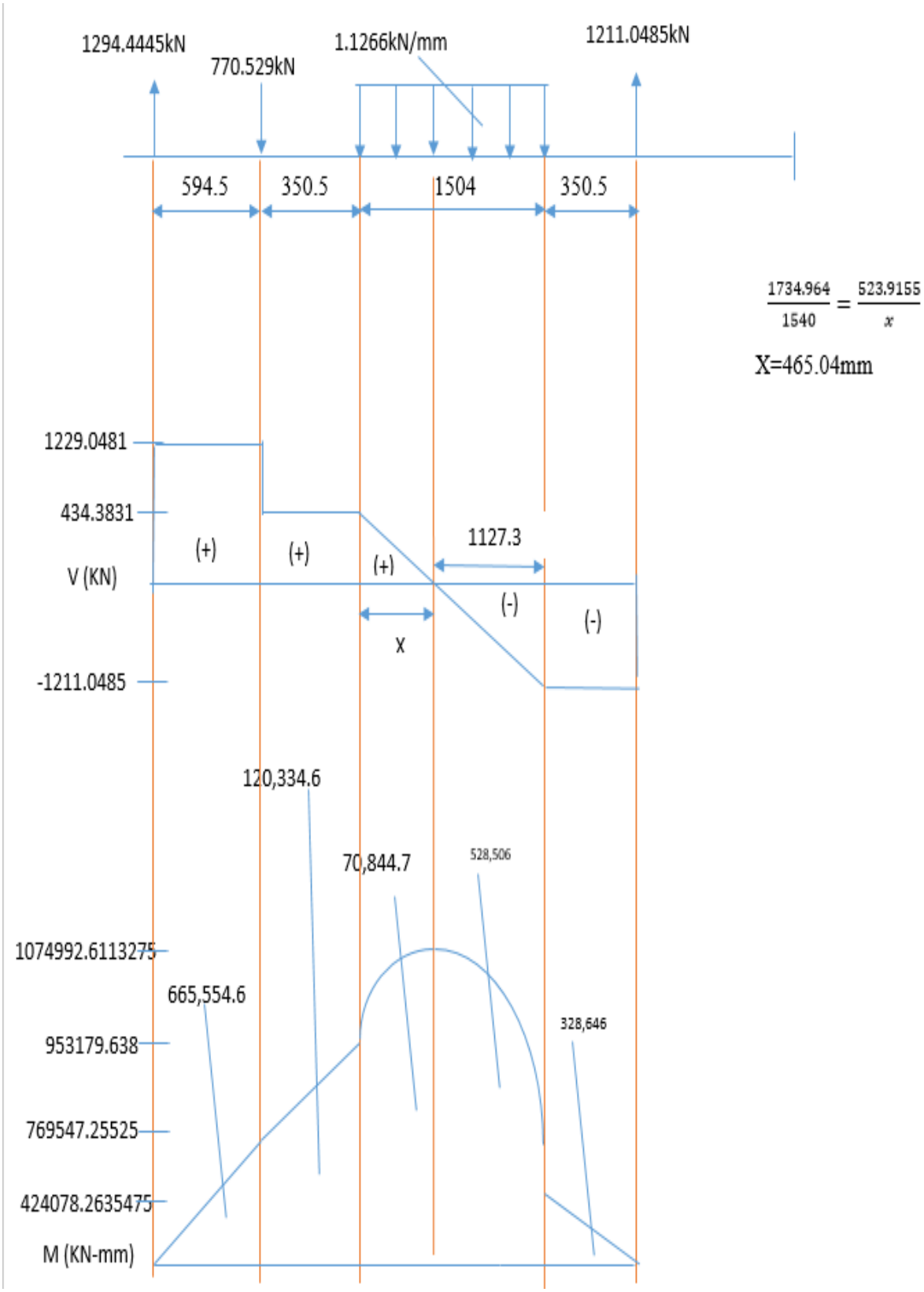

h) Shear stresses on the top rollers 1 through 4

i) Shear stress at the Maximum Bending points

Parameter of the Top Roller	Top Roller 1 (Mill 1)	Top Roller 2 (Mill 2)	Top Roller 3 (Mill 3)	Top Roller 4 (Mill 4)
Maximum vertical component of bending moment, M_v, kN-mm	856,733.9	1047407.8693	978430.3561125	1074992.6113275
Maximum horizontal component of bending moment, M_H, kN-mm	721,628	910774.491596	834830.06406	933524.6790985
Maximum Resultant moment, M_e, kN-mm	1120151.75	1388010.598	1286183	1423754.7
Torque, T, kN-mm	387,134	434,060	421,292	447,623
Maximum Shear Stress, τ_{max}, MPa	77.8	95.5	88.85	98

ii) Stress concentration factors for the Top Roller geometry

Parameter of the Top Roller	Top Roller 1 (Mill 1)			Top Roller 2 (Mill 2)			Top Roller 3 (Mill 3)			Top Roller 4 (Mill 4)		
	A	**B**	**K**	**A**	**B**	**K**	**A**	**B**	**K**	**A**	**B**	**K**
Shoulder at A; D = 426.3mm, d = 386.7mm and r = 10mm												
Shoulder at B; D = 426.5mm, d = 386.7mm and r = 10mm												
Keyway; Equation 3.2 and 3.3 to obtain K_t and K_b												
$\tau_{max} = (\frac{16}{\pi(d)^3}\sqrt{[K_b \times M_e]^2 + [K_t \times T]^2})$												
$\frac{r}{d}$	0.0259	0.0259	-	0.0259	0.0259	-	0.0259	0.0259	-	0.0259	0.0259	-
K_t	1.5	1.5	2.6	1.5	1.5	2.6	1.5	1.5	2.6	1.5	1.5	2.6
$\frac{D}{d}$	1.102	1.1035	-	1.102	1.1035	-	1.102	1.1035	-	1.102	1.1035	-
K_b	2.3	2.31	2.7	2.3	2.31	2.7	2.3	2.31	2.7	2.3	2.31	2.7

Torque, T, kN-mm	387,134			434,060			421,292			447,623		
M_H, kN-mm	362724.48	785889.2	347051.2	406691.28	657883.9683	389118.2	398211.5844	882920.372	381004.911	419400.018	953179.638	401277.795
M_V, kN-mm	185824.3032	542159.75165	177794.858	208818.5832	926812.9	199795.558	202561.7544	614565.8625	193809.086	215464.2768	675889.18045	206154
M_e, kN-mm	407553.334	954756	389943.005	457168.4568	1136570.92	437414.2642	446770.3328	1075750.7	427465.442	471509.522	1168493.7	451135.612
τ_{max}, MPa	97.1	200	191.5	108.9	237	204	106.2	245	191.5	112.3	244	207.75

Appendix 2: Mass properties of the Gear Pinion

Configuration: Default

Coordinate system: -- default –

Material: Alloy Cast steel

Density = 0.01 grams per cubic millimetre

Mass = 1223884.57 grams

Volume = 167655420.33 cubic millimetres

Surface area = 2916367.88 square millimetres

Centre of mass: (millimetres)

= -0.42

= 0.42

= 200.00

Principal axes of inertia and principal moments of inertia: (grams * square millimetres) taken at the centre of mass.

Ix = (0.71, 0.71, 0.00) Px = 85078696767.44

Iy = (-0.71, 0.71, 0.00) Py = 85157484827.92

Iz = (0.00, 0.00, 1.00) Pz = 137599259771.03

Moments of inertia: (grams * square millimetres) taken at the centre of mass and aligned with the output coordinate system.

Lxx = 85 8090797.68 Lxy = 39394030.25 Lxz = 0.00

Lyx = 39394030.25 Lyy = 85 8090797.68 Lyz = 0.00

Lzx = 0.00Lzy = 0.00Lzz = 137599259771.03

Moments of inertia: (grams * square millimetres) taken at the output coordinate system.

Ixx = 134073688262.95 Ixy = 39179301.48 Ixz = -102528675.22

Iyx = 39179301.48 Iyy = 134073688262.95 Iyz = 102528675.22

Izx = -102528675.22 Izy = 102528675.22 Izz = 137599689228.58

Appendix 3: Mass properties of the Top Roller

Configuration: Default

Coordinate system: -- default --

Material: Bare shaft-Forged steel, Roller shell- Malleable cast iron

Mass = 9288262.28 grams

Volume = 1240707026.26 cubic millimetres

Surface area = 18517970.92 square millimetres

Centre of mass: (millimetres)

= 1730.77

= 2148.42

= 3217.06

Principal axes of inertia and principal moments of inertia: (grams * square millimetres) taken at the centre of mass.

Ix = (0.00, 0.00, 1.00) Px = 778497149093.64

Iy = (1.00, -0.09, 0.00) Py = 5474558761307.14

Iz = (0.09, 1.00, 0.00) Pz = 5475796333971.81

Moments of inertia: (grams * square millimetres) taken at the centre of mass and aligned with the output coordinate system.

Lxx = 5474569137203.96 Lxy = - 4949385.68 Lxz = -1254232621.09

Lyx = - 4949385.68 Lyy = 5475785324691.57 Lyz = 83893965.83

Lzx = -1254232621.09 Lzy = 83893965.83 Lzz = 778497782477.07

Moments of inertia: (grams * square millimetres) taken at the output coordinate system.

Ixx = 144474895163853.09 Ixy = 34537518797496.50 Ixz= 1715693399012.09

Iyx = 34537518797496.50 Iyy = 129427924081019.77 Iyz= 4197778662301.70

Izx = 51715693399012.09 Izy = 64197778662301.70 Izz= 71473904418677.63

Appendix 4: Dimensions of the Top roller

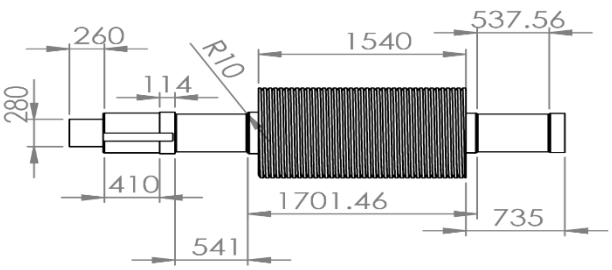

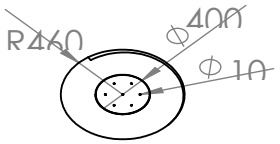

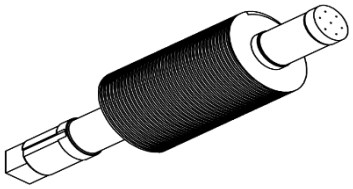

UNLESS OTHERWISE SPECIFIED: DIMENSIONS ARE IN MILLIMETERS SURFACE FINISH: TOLERANCES: LINEAR: ANGULAR:	FINISH: nil		DEBURR AND BREAK SHARP EDGES	DO NOT SCALE DRAWING	REVISION	

	NAME	SIGNATURE	DATE				TITLE:
DRAWN	Kasambula Vicent		3/05/21				MODEL TOP ROLLER 1-4 "Performance Analysis of the top roller in a Sugar mill."
CHK'D	Dr. Catherine Wandera						
APPV'D	Dr. Titus Watmon Bitek						
MFG	nil						
Q.A	nil			MATERIAL: Shell-Cast iron Bare Shaft-Forged steel			DWG NO. TOP ROLLER A4
WEIGHT: 9.3 tons				SCALE:1:50		SHEET 1 OF 1	

Appendix 5: Charts of Theoretical Stress concentration factors

Figure A–15–8

Round shaft with shoulder fillet in torsion. $\tau_0 = Tc/J$, where $c = d/2$ and $J = \pi d^4/32$.

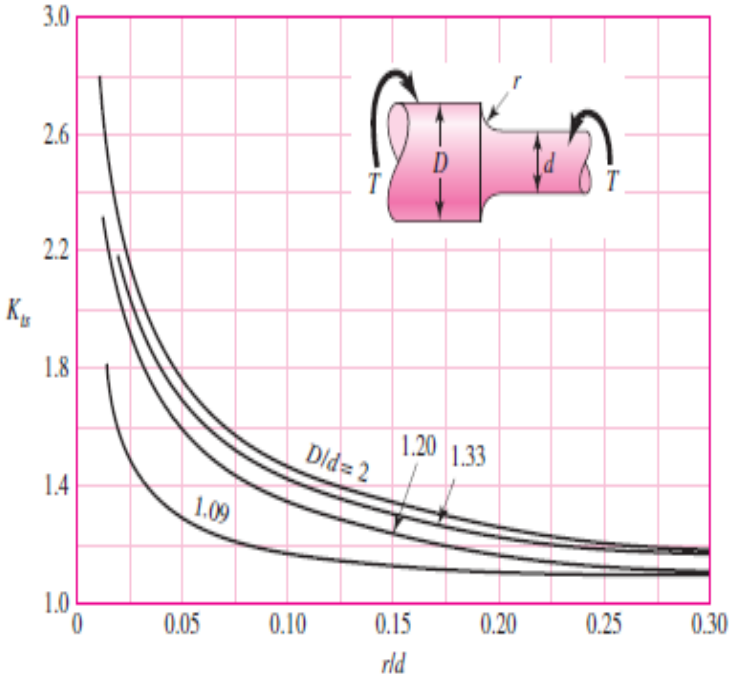

Figure A–15–9

Round shaft with shoulder fillet in bending. $\sigma_0 = Mc/I$, where $c = d/2$ and $I = \pi d^4/64$.

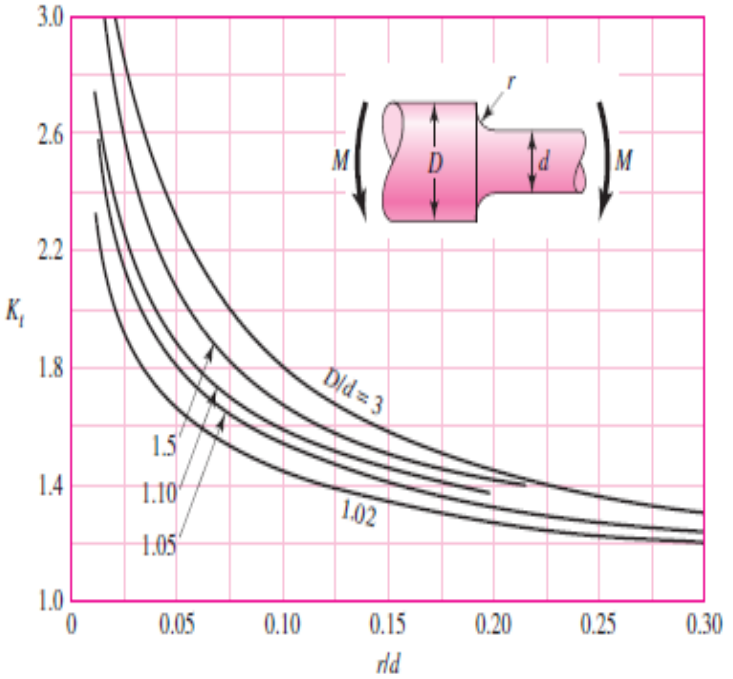

Appendix 6: Chemical composition test results

thermo scientific

Sample Analysis Report

Sample Identity: BIG **Analysed:** 3/1/2021 10:38:59 AM

Method: FELAST **Type Standard:** **Grade:**

Instrument: Thermo Scientific ARL OES Spectrometer

	B %	C %	Al %	Si %	P %	S %	Ca %	Ti %	V %	Cr %	Mn %	Co %	Ni %
Run 1	0.0039	0.3427	0.0172	0.4310	0.0046	0.0358	0.0034	0.0188	0.0039	0.0698	1.0055	0.0008	0.0380
Run 2	0.0035	0.3165	0.0070	0.4240	0.0020	0.0093	0.0010	0.0123	0.0035	0.0675	0.9708	0.0013	0.0386
Run 3	0.0040	0.2927	0.0133	0.4122	0.0017	0.0065	0.0022	0.0134	0.0032	0.0603	0.8995	0.0017	0.0384
Run 4	0.0048	0.3061	0.0191	0.4197	0.0027	0.0048	0.0046	0.0204	0.0032	0.0549	0.8890	0.0017	0.0392
Run 5	0.0040	0.3076	0.0212	0.4226	0.0029	0.0117	) 0.0069	0.0274	0.0035	0.0589	0.9264	0.0016	0.0394
Run 6	0.0046	0.3239	0.0147	0.4214	0.0015	0.0083	0.0050	0.0134	0.0029	0.0532	0.8771	0.0020	0.0389
Run 7	0.0042	0.2956	0.0067	0.4226	0.0009	0.0031	0.0006	0.0158	0.0032	0.0548	0.8827	0.0025	0.0396
Run 8	0.0041	0.2829	0.0069	0.4144	0.0009	0.0034	0.0007	0.0094	0.0030	0.0532	0.8477	0.0030	0.0398
Run 9	0.0052	0.2868	0.0138	0.3896	0.0011	0.0050	0.0035	0.0103	0.0029	0.0510	0.8209	0.0029	0.0398
Run 10	0.0040	0.3032	0.0065	0.4315	0.0027	0.0038	0.0010	0.0121	0.0031	0.0523	0.8438	0.0029	0.0406
Average	**0.0042**	**0.3058**	**0.0126**	**0.4189**	**0.0021**	**0.0092**	) 0.0029	**0.0153**	**0.0032**	**0.0576**	**0.8963**	**0.0021**	**0.0392**
SD	0.00049	0.01818	0.00558	0.01197	0.00114	0.00977	0.00216	0.00548	0.00033	0.00651	0.05753	0.00076	0.00077
RSD%	11.61	5.94	44.18	2.86	54.29	106.61	74.31	35.75	10.12	11.30	6.42	37.01	1.97

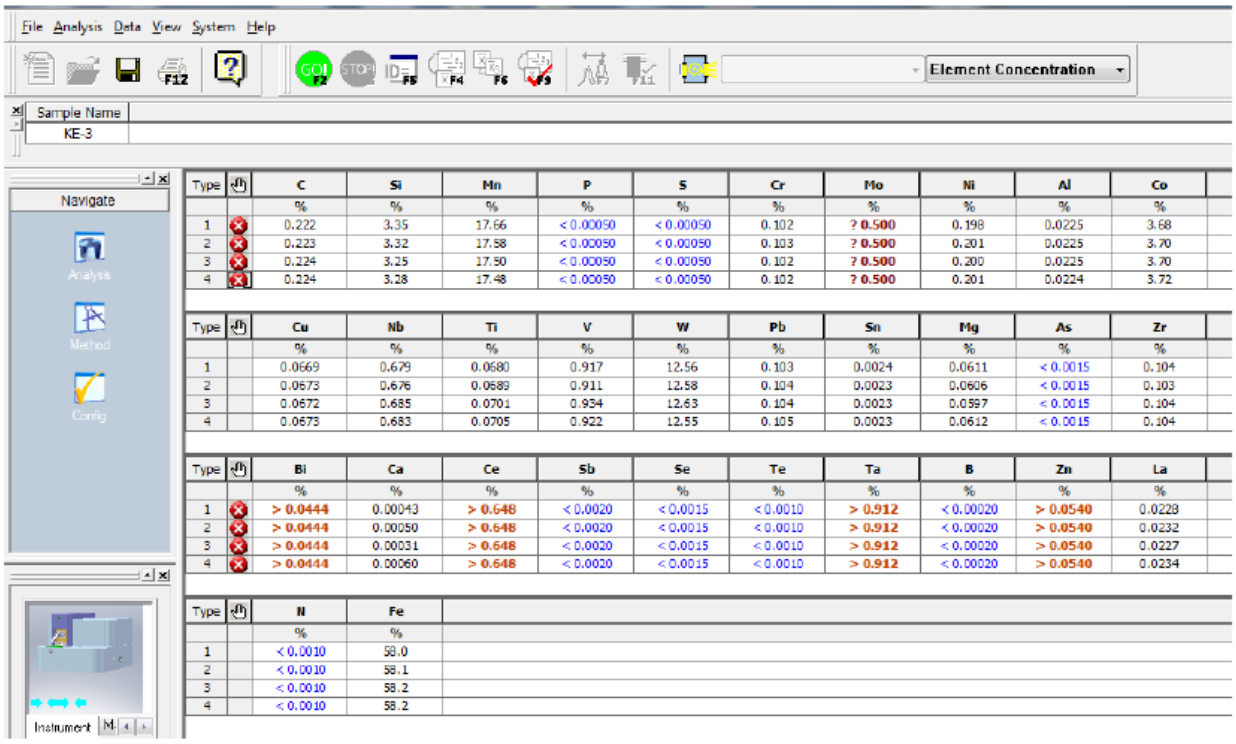

Type	C %	Si %	Mn %	P %	S %	Cr %	Mo %	Ni %	Al %	Co %
1	0.222	3.35	17.66	< 0.00050	< 0.00050	0.102	? 0.500	0.198	0.0225	3.68
2	0.223	3.32	17.58	< 0.00050	< 0.00050	0.103	? 0.500	0.201	0.0225	3.70
3	0.224	3.25	17.50	< 0.00050	< 0.00050	0.102	? 0.500	0.200	0.0225	3.70
4	0.224	3.28	17.48	< 0.00050	< 0.00050	0.102	? 0.500	0.201	0.0224	3.72

Type	Cu %	Nb %	Ti %	V %	W %	Pb %	Sn %	Mg %	As %	Zr %
1	0.0669	0.679	0.0680	0.917	12.56	0.103	0.0024	0.0611	< 0.0015	0.104
2	0.0673	0.676	0.0689	0.911	12.58	0.104	0.0023	0.0606	< 0.0015	0.103
3	0.0672	0.685	0.0701	0.934	12.63	0.104	0.0023	0.0597	< 0.0015	0.104
4	0.0673	0.683	0.0705	0.922	12.55	0.105	0.0023	0.0612	< 0.0015	0.104

Type	Bi %	Ca %	Ce %	Sb %	Se %	Te %	Ta %	B %	Zn %	La %
1	> 0.0444	0.00043	> 0.648	< 0.0020	< 0.0015	< 0.0010	> 0.912	< 0.00020	> 0.0540	0.0228
2	> 0.0444	0.00050	> 0.648	< 0.0020	< 0.0015	< 0.0010	> 0.912	< 0.00020	> 0.0540	0.0232
3	> 0.0444	0.00031	> 0.648	< 0.0020	< 0.0015	< 0.0010	> 0.912	< 0.00020	> 0.0540	0.0227
4	> 0.0444	0.00060	> 0.648	< 0.0020	< 0.0015	< 0.0010	> 0.912	< 0.00020	> 0.0540	0.0234

Type	N %	Fe %
1	< 0.0010	58.0
2	< 0.0010	58.1
3	< 0.0010	58.2
4	< 0.0010	58.2

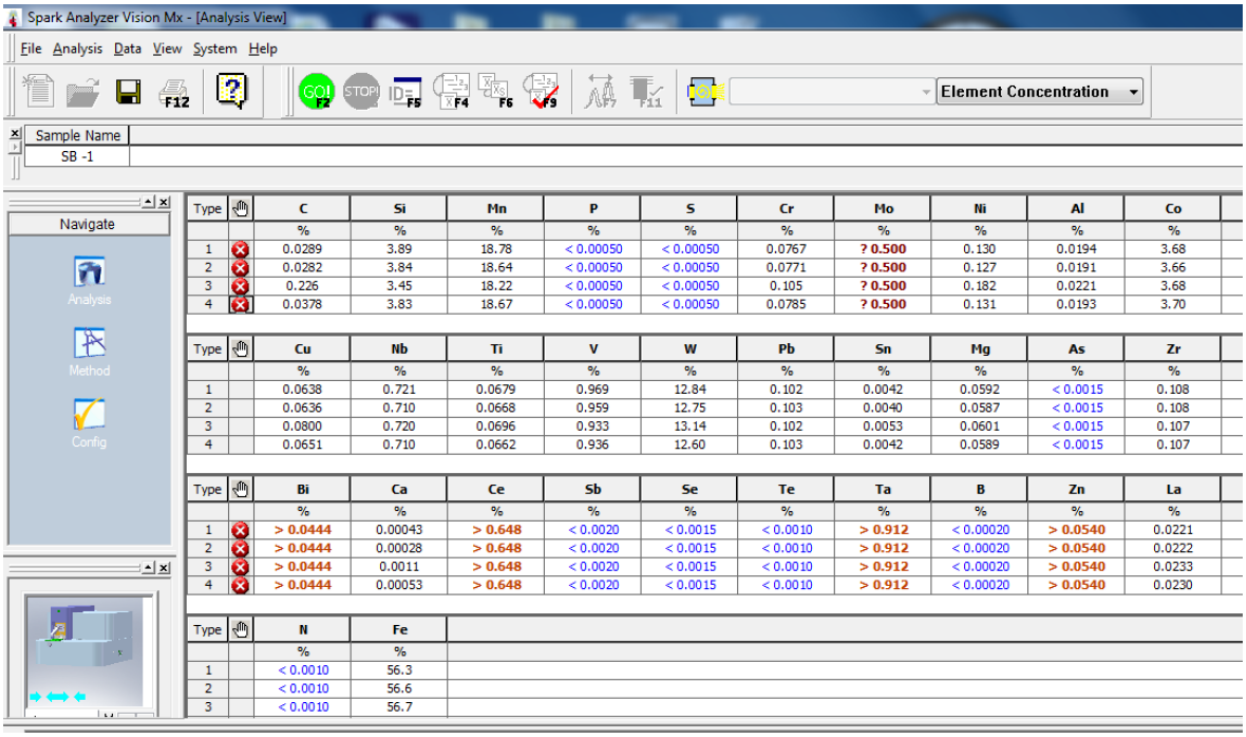

Type		C	Si	Mn	P	S	Cr	Mo	Ni	Al	Co
		%	%	%	%	%	%	%	%	%	%
1	✗	0.0289	3.89	18.78	< 0.00050	< 0.00050	0.0767	? 0.500	0.130	0.0194	3.68
2	✗	0.0282	3.84	18.64	< 0.00050	< 0.00050	0.0771	? 0.500	0.127	0.0191	3.66
3	✗	0.226	3.45	18.22	< 0.00050	< 0.00050	0.105	? 0.500	0.182	0.0221	3.68
4	✗	0.0378	3.83	18.67	< 0.00050	< 0.00050	0.0785	? 0.500	0.131	0.0193	3.70

Type		Cu	Nb	Ti	V	W	Pb	Sn	Mg	As	Zr
		%	%	%	%	%	%	%	%	%	%
1		0.0638	0.721	0.0679	0.969	12.84	0.102	0.0042	0.0592	< 0.0015	0.108
2		0.0636	0.710	0.0668	0.959	12.75	0.103	0.0040	0.0587	< 0.0015	0.108
3		0.0800	0.720	0.0696	0.933	13.14	0.102	0.0053	0.0601	< 0.0015	0.107
4		0.0651	0.710	0.0662	0.936	12.60	0.103	0.0042	0.0589	< 0.0015	0.107

Type		Bi	Ca	Ce	Sb	Se	Te	Ta	B	Zn	La
		%	%	%	%	%	%	%	%	%	%
1	✗	> 0.0444	0.00043	> 0.648	< 0.0020	< 0.0015	< 0.0010	> 0.912	< 0.00020	> 0.0540	0.0221
2	✗	> 0.0444	0.00028	> 0.648	< 0.0020	< 0.0015	< 0.0010	> 0.912	< 0.00020	> 0.0540	0.0222
3	✗	> 0.0444	0.0011	> 0.648	< 0.0020	< 0.0015	< 0.0010	> 0.912	< 0.00020	> 0.0540	0.0233
4	✗	> 0.0444	0.00053	> 0.648	< 0.0020	< 0.0015	< 0.0010	> 0.912	< 0.00020	> 0.0540	0.0230

Type		N	Fe
		%	%
1		< 0.0010	56.3
2		< 0.0010	56.6
3		< 0.0010	56.7

ANALYSED SAMPLE –BROKEN KE 8 SHAFT

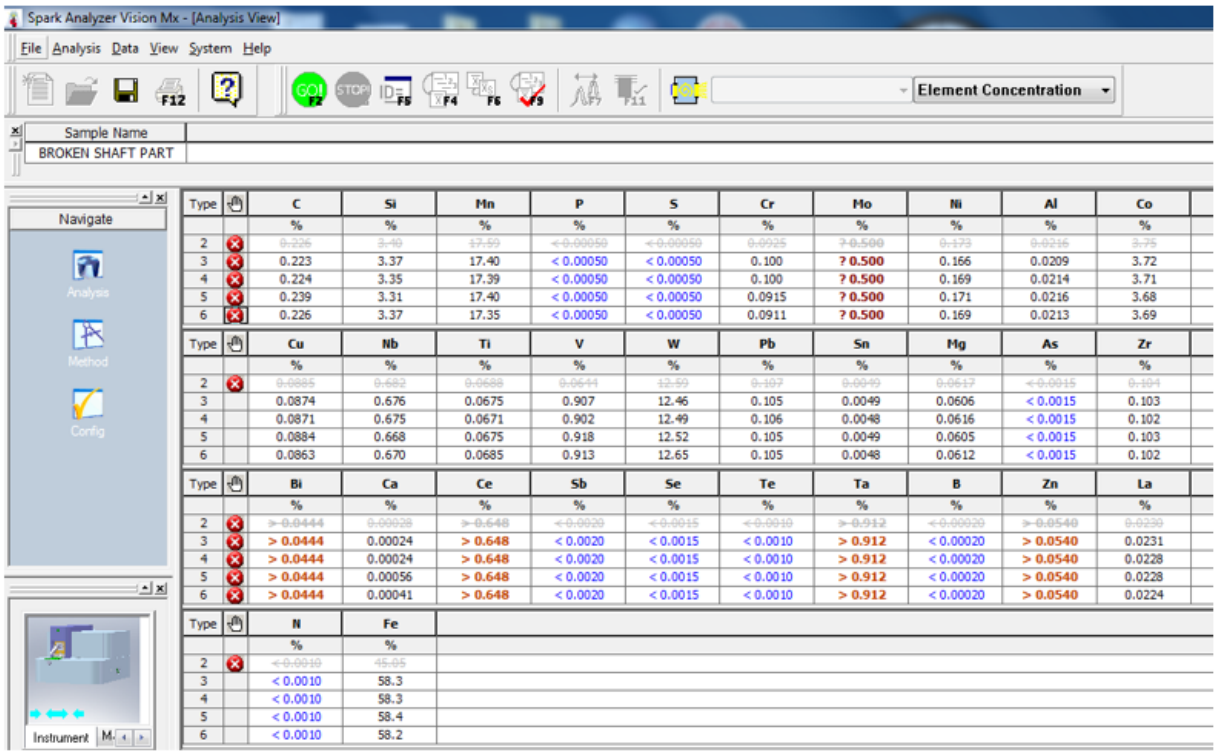

Type		C	Si	Mn	P	S	Cr	Mo	Ni	Al	Co
		%	%	%	%	%	%	%	%	%	%
2	✗	~~0.226~~	~~3.40~~	~~17.59~~	~~< 0.00050~~	~~< 0.00050~~	~~0.0925~~	~~? 0.500~~	~~0.173~~	~~0.0216~~	~~3.75~~
3	✗	0.223	3.37	17.40	< 0.00050	< 0.00050	0.100	? 0.500	0.166	0.0209	3.72
4	✗	0.224	3.35	17.39	< 0.00050	< 0.00050	0.100	? 0.500	0.169	0.0214	3.71
5	✗	0.239	3.31	17.40	< 0.00050	< 0.00050	0.0915	? 0.500	0.171	0.0216	3.68
6	✗	0.226	3.37	17.35	< 0.00050	< 0.00050	0.0911	? 0.500	0.169	0.0213	3.69

Type		Cu	Nb	Ti	V	W	Pb	Sn	Mg	As	Zr
		%	%	%	%	%	%	%	%	%	%
2	✗	~~0.0885~~	~~0.682~~	~~0.0688~~	~~0.0644~~	~~12.59~~	~~0.107~~	~~0.0049~~	~~0.0617~~	~~< 0.0015~~	~~0.104~~
3		0.0874	0.676	0.0675	0.907	12.46	0.105	0.0049	0.0606	< 0.0015	0.103
4		0.0871	0.675	0.0671	0.902	12.49	0.106	0.0048	0.0616	< 0.0015	0.102
5		0.0884	0.668	0.0675	0.918	12.52	0.105	0.0049	0.0605	< 0.0015	0.103
6		0.0863	0.670	0.0685	0.913	12.65	0.105	0.0048	0.0612	< 0.0015	0.102

Type		Bi	Ca	Ce	Sb	Se	Te	Ta	B	Zn	La
		%	%	%	%	%	%	%	%	%	%
2	✗	~~> 0.0444~~	~~0.00028~~	~~> 0.648~~	~~< 0.0020~~	~~< 0.0015~~	~~< 0.0010~~	~~> 0.912~~	~~< 0.00020~~	~~> 0.0540~~	~~0.0230~~
3	✗	> 0.0444	0.00024	> 0.648	< 0.0020	< 0.0015	< 0.0010	> 0.912	< 0.00020	> 0.0540	0.0231
4	✗	> 0.0444	0.00024	> 0.648	< 0.0020	< 0.0015	< 0.0010	> 0.912	< 0.00020	> 0.0540	0.0228
5	✗	> 0.0444	0.00056	> 0.648	< 0.0020	< 0.0015	< 0.0010	> 0.912	< 0.00020	> 0.0540	0.0228
6	✗	> 0.0444	0.00041	> 0.648	< 0.0020	< 0.0015	< 0.0010	> 0.912	< 0.00020	> 0.0540	0.0224

Type		N	Fe
		%	%
2	✗	~~< 0.0010~~	~~45.05~~
3		< 0.0010	58.3
4		< 0.0010	58.3
5		< 0.0010	58.4
6		< 0.0010	58.2

Appendix 7: Acceptance letters

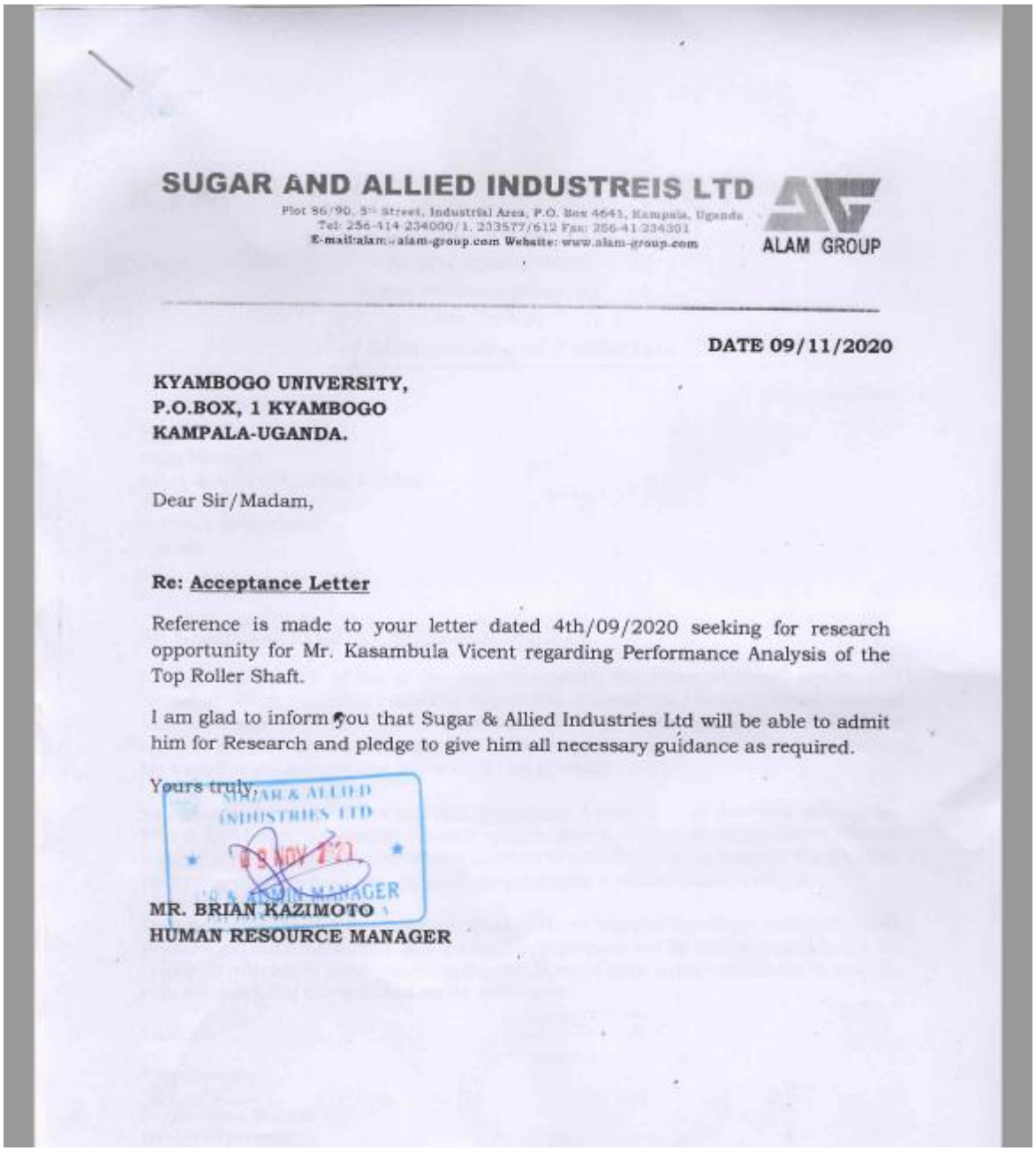

SUGAR AND ALLIED INDUSTREIS LTD

Plot 96/90, 5th Street, Industrial Area, P.O. Box 4641, Kampala, Uganda
Tel: 256-414 234000/1, 233577/612 Fax: 256-41-234301
E-mail:alam@alam-group.com Website: www.alam-group.com

ALAM GROUP

DATE 09/11/2020

KYAMBOGO UNIVERSITY,
P.O.BOX, 1 KYAMBOGO
KAMPALA-UGANDA.

Dear Sir/Madam,

Re: Acceptance Letter

Reference is made to your letter dated 4th/09/2020 seeking for research opportunity for Mr. Kasambula Vicent regarding Performance Analysis of the Top Roller Shaft.

I am glad to inform you that Sugar & Allied Industries Ltd will be able to admit him for Research and pledge to give him all necessary guidance as required.

Yours truly,

SUGAR & ALLIED INDUSTRIES LTD
05 NOV '20
HR & ADMIN MANAGER

MR. BRIAN KAZIMOTO
HUMAN RESOURCE MANAGER

Sugar Corporation of Uganda Limited

P.O. BOX 1, LUGAZI, UGANDA. Tel: 256-312-55 55 00, Fax: 256-312-55 52 96
Email: scoul@mehtagroup.com Website: www.mehtagroup.com

An ISO 9001 & 14001 Certified Company

REF: SDMHR/ADMIN/HR/TRAIN/21 Date: 5th February 2021

TO: MR. KADAMBULA VICENT
Kyambogo University,
P.O Box 1, Kyambogo,
Kampala - Uganda

Dear Sir/Madam,

RE: RESEARCH STUDY

This is in reference to your application dated 4th September 2020 regarding the above subject.

We wish to inform you of Management's decision to allow you conduct your Research Study with this company, for a period of one (01) month.

Please note that for the period indicated above you will be attached to Works Department Mill Section, with effect from 8th to 20th February 2021.

Privately organize for your accommodation, meals and Management will not pay any form of salary or allowances to you

Wish you a gainful stay.

Yours faithfully,
For and on behalf of:
SUGAR CORPORATION OF UGANDA LIMITED

HEAD OF TRAINING SECTION
HUMAN RESOURCES DEPARTMENT
P O BOX 1, LUGAZI (U)

GEOFFREY
SR. DY. MANAGER HR TRAINING & DEVELOPMENT

CC: DY. GM ENGINEERING
CC: SR. DY. MGR. HR FACTORY

Kampala office: 133/135, 6th Street Industrial Area, P.O. Box 1185, Kampala UGANDA. Tel: 256-414-25 50 36 Fax: 256-414-34 75 97

*A*ppendix 8: Mill Photos

Appendix 9: Technical Reports and Mill Maintenance Records

28.04.2019

TECHNICAL REPORT FOR THE FAILURE OF 4TH MILL TOP ROLLER

I would like to state that on 26th April 2019, around 1.20 PM, we have noticed some abnormal sound in the 4rd Mill and mill is not taking load and Donnelly chute is getting filled with bagasse. We came to know that the drive is rotating and there is no motion of discharge roller .

While inspection we found that the discharge roller **(Shaft No KE-8)** shaft got broken in crown side square end.

We have by passed the 4th mill and resumed the crushing operation around 2.50PM..

The spare discharge roller is available and replacing work is under progress.

This shaft can't be repaired it has to be replaced by new one.

The cause of failure may be due to the following reasons…

1. Due to sudden impact load cause of any foreign martial passes.
2. Undue stress formation due to cyclic load.

Details of discharge roller.

Roller Number: -KE-8
Position worked: - 4TH Mill top.

28/4/19

R.Eswaramurthy,
Engineering manager.

ad Office & Factory
nyara Sugar Ltd
O.Box No.179, Plot 31, Block 9&10
ujenje, Masindi,Uganda.
l: (256) 0362600200 Fax: (256) 0362600211

www.kinyara.co.ug

Kampala Office
Address for Correspondence
Kinyara Sugar Ltd
P. O. Box 7474
2nd Street, Industrial Area
Kampala, Uganda
Tel: (256) 0772 221520

16th April 2019

MILLS MAINTENANCE

1. Replace Coupling box mill #1 – **Masaba James**
2. Replace mill #3 C/S mono bearing-**Barry**
3. Inspect mill #1 and 4 discharge plus #2 feed roller all o/s bearings for grease line blockage-**Oil man**
4. Open mill #3 bottom scrapper clean and re-set it back-**Namukwa**
5. Realign inter carrier #1 and 2 V-Belt-**Masaba**
6. Arc mill #2, 4 and 5 top and bottom rollers-**Draku**
7. General mill cleaning setting mash chart knife blades and flush rotary screen with hot water mixed with caustic soda-**Bapangana**
8. Check all mill trash plate long bolts, fulcrum holding down bolts, u bolts and mill head stock foundation bolts- **Namakwa**
9. Check all top and bottom scrapper bracket bolts plus all bull gear bearing foundation and cover bolts-**Namakwa**
10. Check oil level on inter carrier gear bolts, fluid coupling boxes and maceration pump gear boxes plus imbibitions pump gear boxes- **Oil man**
11. Repair damaged side plates on bagasse elevator at the tail-**Ainea contractor**
12. Replace inter carrier #4 head shaft bush bearing to be reversed-**Agondua**
13. Replace inter carrier #4 gear box sprocket - **Agondua**
14. Inter carrier no-4 Tail loose sprocket (Off side)bush to be replaced-**Agondua**
15. No-3 Mill Bull gear mill side Plummer block bottom support to be weld-**Work shop**
16. Mill no-1Donally chute hole to be patched-**Work shop**
17. Provide plates at the side ends of mill #5 juice trough to stop juice from dropping down- **Work shop**
18. Weld leakage on maceration pump #1 delivery pipe line at the elbow- **Work shop**
19. Replace worn out suction pipe on maceration pump #3- **Work shop**
20. Weld a leakage on mill No.5 return juice pipe line-**Work shop**
21. Inspect all mill tang plates- **Work shop**
22. Weld leakages at the bottom of mill juice trough, mill #1, 3 and 4- **Work shop**
23. Weld crack on mill#3 head stock foundation brackets on c/s and tighten the loose bolts-**Work shop**
24. Mill no- 3 Spreader pipe leak to be weld-**Work sop**
25. Mills roller lubrication point to be check and mill drive gear box inspection Parts and lubrication-**Odaga**
26. All mills setting to be check and adjusted as per setting reading-**Alsan**

29th April 2019

Mini MILLS MAINTENANCE

1. Replace Coupling box mill #2 & 4 – **Byamaiso**
2. Replace Mill no-4 Broken top roller-**Shift foreman**
3. Arc mill #1, and 2 top and bottom rollers - **Draku**
4. Inspect all mill top and bottom scrapper bracket bolts - **Namukwa**
5. Check all mill trash plate long bolts, fulcrum holding down bolts, U bolts and mill head stock foundation bolts proved washers if required - **Namukwa**
6. Inspect all tang plates – **w/shop**
7. Lubricate all inter carrier head drive bearings plus baggase elevator - **Oil men**
8. General mill cleaning, resetting of mash chart knives and flushing rotary screen with hot water mixed with caustic soda - **Bapangana**
9. Check maceration pump oil levels – **Oil men**
10. Macerations pump no- 3 suction leak to welded-**Work shop**
11. Unscreened I juice pump no-2 Suction leak to be arrest-**Work shop**
12. Check mill drive gear box internals and lubrication points-**Odaga**
13. Check all mill roller lubrication points-**Odaga**

Pre Mills

1,Check knive no-1,2 and 3 knive bolts-**Contractor**

2,Check fibrizer hammer and tip-**Eberu**

3, Damaged slate to be replaced in cane carrier no-1 and 2-**Olwata**

4,Fibrizer bearing oil tank filter to be cleaned -**Odaga**

Appendix 10: Top Roller Purchase and Reconditioning Invoice

iNVOICE

EXPORTER : KRISTNA ENGINEERING WORKS TATAPURAM,ENIKEPADU, VIJAYAWADA - 521 108 A.P. INDIA.	INV NO. EXP/12/2009-10, Dt. 11.06.2009 EXPORTER'S REF: Buyer's Order No: KS41894 Dt.29.12.2008
CONSIGNEE : STANBIC BANK UGANDA LIMITED P.O. Box 7131, KAMPALA UGANDA.	Other Reference(s) : LC. No. 090227SM1499UG Dt. 27.02.09
NOTIFY: KINYARA SUGAR LIMITED P O BOX 7474 KAMPALA UGANDA.	Country of origin of goods : INDIA Country of Final Destination : UGANDA
Carriaged by : SEA FREIGHT Place of Receipt/by Pre-Carriage : MUMBAI Vessel/Flight No. Port of Loading : JNPT/NHAVA SHEVA Port of Discharge: MOMBASA Final Destination : UGANDA	Payment Terms : 25% Advance by TT and balance by LC. LC. No. 090227SM1499UG Dt. 27.02.09

Marks & Nos	Kind of Packing	Description of Goods	Quantity	PRICE/No US $	Amount US $
KEW/12/2009-10 Case Nos. 1/2 to 2/2 From : kristna Engineering works,Tatapuram Enikepadu, Vijayawada - 521 108 A.P. INDIA. To : KINYARA SUGAR LIMITED P O Box 7474 Kampala UGANDA.	Packed with export worthy woodn pallets by wrapping with HDPE sheet as cylindrical cases and mounted on MS Frame.	Top Lotus Roller with shaft 36MM Pitch Quantity 2 No. as per purchase order no. kS41894 dtd. 29.12.2008. (Roller dia 910X1680MM long duly grooved to 36MM pitch with 45degrees as Top Roller Fitted with juice protection ring as per drawing no. 02-20-32 R2)	2 Nos.	31,300.00	62,600.00
				Total CIF Mombasa Port, Kenya	62,600.00
				Less : 25% Advance recived by TT	15,650.00
				Total Amount due against this invoice	46,950.00
Amount Chargeable (In Words) :	US Dollars Forty Six Thousand Nine Hundred Fifty Only. - CIF Mombasa- Kenya				

GROSS WT	:	21.30 MT.	RBI CODE NO.	HK-000277, Dt. 04-01-94
NET WT.	:	20.74 MT.	I.E. CODE NO.	0991020189
Volume	:	11.76 CBM	SDF FORM Dt.	

Declaration:
We declare that this Invoice shows the actual price of the goods described and that particulars are true and correct.

for KRISTNA ENGINEERING WORKS

AUTHORISED SIGNATORY

EXPORT INVOICE

EXPORTER : S.B. RESHELLERS PVT. LTD., D-5 & D-15, MIDC - SHIROLI, KOLHAPUR - 416122 MAHARASHTRA - INDIA	Invoice No. & Date : 6104 / 28.07.2018	Our Reference No. and Date : 150253/ 16.03.2018
	Buyers Reference No. & Date : PO.KSL 17002856 DT. 19.02.2018 & PO. 1834/11.05.2018 Cont. 304	Parts for Sugar Mill Machinery Country of Origin of Goods : India
Consignee : KINYARA SUGAR LIMITED, PLOT NO.35, BLOCK 9 & 10, PO BOX 179, BUTENDE, MASINDI - UGANDA	Notify Party :	Terms of Payment : 20% advance along with Purchase order & balance against dispatch documents. HS CODE NO. 8438 90 10
Carriage by : Sea or Air or Multimodal Transport By Sea	Place of receipt by pre-carrier : Port of Loading : JNPT PORT - MUMBAI	CWP 1135
Port of Discharge : MOMBASA PORT - KENYA	Final Destination : MASINDI - UGANDA	Delivery : MONTH OF JULY-2018

Marks & Nos Container No.	No. of Kind of Pkgs.	P.O.Line Item No.	Description of Goods	Qty.	Rate Each USD	Total Amt. USD
KINYARA SUGAR LIMITED,	Case No. 1	000010	**RE-EXPORT AFTER REPAIRS:** GROOVED SHELL FOR MILL 1 & 2 TOP LOTUS ROLLER Shaft No. KE-2 70MM PITCH AS PER DRAWING NO. DRG NO.2-21-31-P1	1.00	12,800.00	12,800.00
	Case No. 2	000011	GROOVED SHELL FOR MILL 1 & 2 TOP LOTUS ROLLER Shaft No. KE-5 70MM PITCH AS PER DRAWING NO. DRG NO.2-21-31-P1	1.00	12,800.00	12,800.00
	Case No. 3	000020	GROOVED SHELL FOR MILL 4 TOP LOTUS ROLLER Shaft No. KE-8 SIZE : OD 905MM X 1680MM L X36MM PITCH AS PER DRAWING NO. DRG NO.2-20-37-P1	1.00	12,800.00	12,800.00
	Case No. 4	000030	GROOVED SHELL FOR MILL 3 TOP LOTUS ROLLER Shaft No. KE-9 SIZE: OD 905MM X 1680MM L X 50MM PITCH, AS PER DRAWING NO. DRG NO.2-20-36-P1 **Bill of Entry No.: 5707704/23.03.2018** **Bill of Lading No. : AYD0106600/12.03.2018** SHAFT REPAIR CHARGES (KE-5, KE-8 & KE-9)	1.00 1.00	12,800.00 2,796.00	12,800.00 2,796.00
			Total	**4.00**		**53,996.00**
Less Advance Received :						10,240.00
Net Payable amount in Words :	FORTY-THREE THOUSAND SEVEN HUNDRED FIFTY-SIX DOLLARS ZERO CENTS					43,756.00

Declaration:
We declare that this invoice shows the actual price of the Goods described and the all particulars are true & correct.

"Export under LUT ARN-AD270518000148T"

Incoterm 2010: FOB JNPT PORT MUMBAI

S. B. Reshellers Pvt. Ltd.

Deepen Sahnis
AGM-Export and BD